

**Testing the ability of ASTER (Advanced Spaceborne Thermal Emission and Reflection Radiometer) to map hydrothermal alteration zones. A case study of the Haib Porphyry Copper-Molybdenum Deposit, Namibia.**

**Paidamwoyo Mhangara**

Thesis presented in partial fulfilment for the requirements of the degree of Master of Natural Science at the University of Stellenbosch.



Supervisors: Professor HL Zietsman and Professor R Scheepers.  
Department of Geography and Environmental Studies.

April 2005

## **AUTHORS' DECLARATION**

I, the undersigned, hereby declare that the work contained in this thesis is my own original work and that I have not previously submitted it, in its entirety or in part, at any university for a degree.

Date

## **Abstract**

The availability of multispectral data from the satellite-borne ASTER (Advanced Space borne Thermal Emission Reflection Radiometer) sensor with 14 spectral bands, launched on 18 December 1999, ushers in a new dimension in large-scale mineral exploration. The ASTER bands are strategically positioned to map distinctive absorptive features for mapping alteration mineralogy, which has increased the potential to map hydrothermal alteration zones as compared to the conventional Landsat TM satellite and aerial photographs.

This research tests the ability of ASTER to map hydrothermal alteration zones by applying various image enhancement techniques and comparing them. The study area is the Haib copper prospect in Namibia. The Crosta technique, standard colour composites, spectral band ratioing, the software defoliant technique, log residuals and spectral linear unmixing were applied and compared against results from the previous detailed geophysical and geochemical exploration. The results from all the techniques corresponded with published geological maps from previous work and indicated ASTER's ability to detect alteration zonations.

Comparison of the methods applied showed that choice of technique is usually dependent of the level of detail which one seeks to achieve. Standard colour composite and log residuals are more useful for a generalized overview of the alteration mineralogy, whilst uniquely defining mineral end members is achieved by application of the Crosta technique, ratioing and spectral linear unmixing. Application of the software defoliant techniques involved ratioing results, which are affected by spectral interferences from other minerals.

The presence of a highly fractured system has been established by application of Sobel filtering. A spatial association of the extracted fracture system with alteration areas suggest mineralization at the Haib is fracture controlled. The results support the presence of argillic-phyllitic and prophylic alteration zones on a regional scale, a scenario which can be equated to the Lowell-Guilbert model. The potassic-phyllitic zone boundary could not be spectrally detected which also supports previous studies which suggest the potassic zone is non-definitive and is over-printed by the phyllic zone. The results demonstrate that ASTER is an effective tool to map hydrothermal alteration systems in arid areas.

## Opsomming

Multispektrale data van die ASTER ('Advanced Space Borne Thermal Emmission Reflection Radiometer') sensors bestaande uit 14 spektrale bande, afkomstig van 'n satelliet gelanseer op 18 Desember 1999 lui 'n nuwe era in vir grootskaalse minerale eksplorasië. Die ASTER bande is strategies sodanig op die spektrum geposisioneer om onderskeidende absorberende verskynsels van veranderde mineralisasië te identifiseer. Hierdie data het die potensiaal verhoog om hidrotermale veranderingstelsels meer suksesvol te karteer as met konvensionele Landsat TM beelde en lugfotos.

Hierdie navorsing toets die vermoëns van ASTER om hidrotermale veranderingstelsels te karteer deur 'n wye reeks beeldverrykings tegnieke toe te pas en te vergelyk. Die studiegebied is die Haib koperafsetting in Namibië. Die Crosta tegniek, standaard kleursamestellings ('colour composites'), ratio-tegnieke, plantegroei-stroeping ('software defoilant'), log residuele ('log residual'), en spektrale lineêre ontmenging ('spectral linear unmixing') is toegepas en die resultate met vorige gedetailleerde geofisiese en geo-chemiese veldopnames te vergelyk.

Die verkreeë resultate van al die verskillende tegnieke het grootliks met gepubliseerde geologiese kaarte van die gebied ooreengestem en bevestig dat ASTER data geskik is om sulke mineralogies veranderde gebiede te karteer.

Vergelykings tussen die tegnieke het getoon dat die keuse van tegniek bepaal word deur die vlak en tipe detail wat verlang word. Standaard kleursamestellings en die log residuele tegnieke lewer goeie resultate om veralgemeende oorsigte van mineralogies veranderde sones te verskaf, terwyl die Crosta-, ratio- en spektrale lineêre ontmengingstegnieke meer suksesvol is om spesifieke minerale te identifiseer. Die plantegroei-stroeping-tegniek is nodig in gevalle waar spektrale ratios deur plantegroei-respons geaffekteer word.

Die aanwesigheid van 'n intensief gefrakteerde sisteem is bepaal deur 'n Sobel filter toe te pas. Ruimtelike assosiasies tussen die voorkoms van die gefrakteerde sone met en die mineralogies gewysigde sones dui aan dat mineralogiese wysiging in die Haib gebied deur frakturering beheer is. Die resultate steun die aanwesigheid van argillities-fillitiese en

propolities gewysigde sones op 'n streekskaal, 'n scenario wat deur die Lowell-Guilbert-model voorgehou word. Die grense van die kalium-fillitiese sone kon nie spektraal waargeneem word nie. Dit steun ook vorige studies wat suggereer dat die kaliumsones nie-afbakenbaar is en waarskynlik deur die fillitiese sone oorlê word. Die resultate bevestig onomwonde dat ASTER data benut kan word om hidrotermaal veranderde sones in semi-ariëde gebiede effektief te karteer.

## **Acknowledgements**

I am greatly indebted to the Canon Collins Educational Trust for Southern Africa for awarding me the Special Diana Collins Scholarship; this generous financial contribution has allowed to me complete this Masters degree.

Special honour goes to Professor Larry Zietsman, my supervisor and principal lecturer, for his supportive hand throughout my entire Masters degree course; he provided us with an environment conducive to learning and was willing to share his vast knowledge and experience all the time. I am forever grateful for his accessibility and guidance during my research.

Many thanks go to Professor Reyno Scheepers, my co-supervisor, for his sound geological advice which added value to this study.

My sincere gratitude is expressed to Wolfgang Lück for providing technical advice during his own busy schedule. I owe deep gratitude to Mr Gordon Koll for his valuable contributions and initial encouragements to embark on this research. I am also greatly indebted to Caryll Tyson for ushering me into the world of remote sensing.

I am much obliged to my entire family for their moral and financial support. My deep appreciation goes to Sophia Mahoya for her constant spiritual encouragement.

Finally, I would like thank all my colleagues in the Geography Department for creating an academically friendly atmosphere, which made the department my second home.

**TABLE OF CONTENTS**

<b>CHAPTER 1 RATIONALE OF THE STUDY AND THE HAIB STUDY AREA.....</b>	<b>1</b>
1.0 Introduction.....	1
1.1 Problem Statement.....	1
1.2 Research Aim.....	1
1.3 Research Objectives and Sub-objectives.....	1
1.4 Motivation of the study.....	2
1.5 Delimitation of the study.....	3
1.6 Regional geological setting of the study area.....	3
1.7 Distribution of economic mineralization.....	6
1.8 Previous mineral exploration work on the Haib copper prospect.....	6
1.9 Data and materials available.....	6
1.10 Conclusion.....	7
<b>CHAPTER 2 HYDROTHERMAL ALTERATION MAPPING USING ASTER.....</b>	<b>7</b>
2.0 Introduction.....	8
2.1 Application of multispectral remote sensing in mineral exploration.....	8
2.2 Alteration zone analysis.....	9
2.3 Spectral characteristics of alteration zones.....	10
2.4 Utility of ASTER in alteration mapping.....	13
2.5 Alteration mineral assemblages at the Haib copper prospect.....	15
2.5.1 Introduction.....	15
2.5.2 Potassium-silicate alteration.....	16
2.5.3 Chlorite-sericite alteration.....	16
2.5.4 Phyllic alteration.....	16
2.5.5 Regional distribution of alteration assemblages.....	17
2.5.6 Local distribution of alteration assemblages.....	17
2.5.7 Structures surrounding the Haib porphyry stock.....	20
2.6 Conclusion.....	21
<b>CHAPTER 3 METHODOLOGY: GENERATION AND ANALYSIS OF SIMULATED ASTER IMAGES.....</b>	<b>22</b>
3.0 Introduction.....	22
3.0.1 Selection of mineral end members to be subjected to image enhancement.....	22
3.1 Standard false colour composites-RGB band combinations.....	22
3.1.1 Application of standard false colour composites.....	24
3.2 Absorptive feature mapping of phyllic and prophylic minerals.....	28
3.2.1 Application of absorptive feature mapping technique.....	28

3.3 Spectral band ratioing.....	31
3.3.1 Application of Spectral band ratios.....	31
3.3.2 The software defoliant technique for the improvement of band ratios.....	37
3.4 Log residual technique.....	39
3.4.1 Selection of bands for the log residual technique.....	40
3.4.2 Log residual results.....	40
3.5 Crosta technique (Feature Orientated Principal Component Analysis).....	40
3.5.1 Band selection and criterion for the identification of PC carrying the target mineral...49	
3.5.2 Application and selection of minerals to be subjected to the Crosta Technique.....	50
3.5.3 Crosta Technique results.....	52
3.5.4 Discussion of the Crosta Technique results.....	56
3.6 Spectral Linear Unmixing.....	68
3.6.1 Application and selection of minerals for spectral linear unmixing.....	68
3.6.2 Results for spectral linear unmixing.....	69
3.7 Structural Feature Extraction .....	69
3.8 Conclusion.....	73
<b>CHAPTER 4 COMPARISON OF TECHNIQUES AND DISTRIBUTION OF SIMULATED ALTERATION ZONES.....</b>	<b>77</b>
4.0 Introduction.....	77
4.1 Comparison of techniques used to map hydrothermal alteration deposits.....	77
4.2 The Lowell-Guilbert Model.....	81
4.3 Distribution of alteration assemblages in the main mineralized zone.....	89
4.4 Association of sericite alteration with sulphide mineralization.....	89
4.5 Accuracy assessment.....	89
4.6 Conclusion.....	90
<b>CHAPTER 5 CONCLUSIONS AND RECOMMENDATIONS.....</b>	<b>94</b>
5.0 Introduction.....	94
5.1 Conclusions.....	94
5.2 Recommendations.....	95
<b>REFERENCES.....</b>	<b>97</b>

## List of Figures

Figure 1.1 Location of the study area.....	3
Figure 1.2 Geological map of the Haib copper prospect.....	4
Figure 2.0 Spectral Signatures for Alteration Minerals.....	12
Figure 2.1 ASTER bands superimposed on model atmosphere.....	14
Figure 2.2 Regional distribution of alteration assemblages.....	18
Figure 2.3 Spatial distribution of alteration similar to the Lowel-Guibert model.....	18
Figure 2.4 Spatial distribution of alteration assemblages in the mineralized zone.....	19
Figure 2.5 Rose diagram.....	20
Figure 2.6 Distribution, length and orientation of fractures and shears.....	21

## Spectral Graphs

Figure 3a Spectral signature of sericite-muscovite positioned on the ASTER bands.....	31
Figure 3b Spectral signatures of hydroxyl-bearing clays positioned on the ASTER bands....	32
Figure 3c Spectral signatures of carbonates positioned on the ASTER bands.....	33
Figure 3d Spectral signatures of chlorite, epidote and quartz positioned on the ASTER bands.....	34
Figure 3e Spectral signatures of potassic zone minerals positioned on the ASTER bands.....	35
Figure 3f Spectral signatures of ferrigenous minerals positioned on the ASTER bands.....	36

## Flowcharts

Figure 3.0 Process flowchart for mapping alteration mineralogy using ASTER.....	23
---	----

## Layouts

Figure 3.1: True colour composite RGB 3-2-1.....	25
Figure 3.2: Normalized RGB 4-6-8.....	27
Figure 3.3: Absorptive feature mapping of the phyllic and prophylic alteration zones.....	29
Figure 3.4: Sericite alteration ratio image.....	40
Figure 3.5: Argillic alteration ratio image.....	41

Figure 3.6 Prophyllitic alteration ratio image.....	42
Figure 3.7: Chlorite alteration ratio image.....	44
Figure 3.8: Quartz ratio image subjected to the software defoliant technique.....	45
Figure 3.9: Biotite ratio image subjected to the software defoliant technique.....	46
Figure 3.9: Iron oxide ratio image subjected to the software defoliant technique.....	47
Figure 3.11: Log residual image for general alteration mapping.....	48
Figure 3.12: Hydroxyl bearing clay mineral: Crosta Technique.....	58
Figure 3.13 Iron oxides-Ferrigenous alteration: Crosta Technique.....	59
Figure 3.14: Sericite alteration: Crosta Technique.....	60
Figure 3.15: Chlorite alteration: Crosta Technique.....	61
Figure 3.16 Calcite (carbonate): Crosta Technique.....	62
Figure 3.17: Biotite: Crosta Technique.....	63
Figure 3.18 Illite-sericite group: Crosta Technique.....	64
Figure 3.19: Alunite: Crosta Technique.....	65
Figure 3.20: Kaolinite: Crosta Technique.....	66
Figure 3.21: Kaolinite-smectite: Crosta Technique.....	67
Figure 3.22: Sericite alteration: Spectral linear unmixing.....	70
Figure 3.23: Argillic alteration (Indicator kaolinite): Spectral linear unmixing.....	71
Figure 3.24: Distribution and orientation of basement fractures and shears Sobel Filtering...74	
Figure 3.25: Sericite-Argillic alteration spatial association with fractures.....	75
Figure 3.26: Structural and phyllic mineralization spatial association.....	76
Figure 4.1: Modelling the phyllic-prophyllitic alteration zones: Crosta Technique.....	83
Figure 4.2: Modelling the potassic-phyllic-prophyllitic zones: Crosta Technique.....	84
Figure 4.3 Modelling the phyllic-prophyllitic alteration zones: Absorptive feature mapping..85	
Figure 4.4: Modelling the potassic-phyllic-prophyllitic alteration zones:Ratioing Technique.86	
Figure 4.5: Modelling the potassic-phyllic-prophyllitic zones using biotite as potassic zone zone indicator: Spectral Linear Unmixing.....	87

Figure 4.6: Modelling the potassic-phyllitic-prophylic zones using orthoclase as potassic zone indicator: Spectral Linear Unmixing.....88

Figure 4.7: Surface distribution of alteration assemblages in the main mineralized zone: Ratioing Technique.....91

Figure 4.8: Surface distribution of alteration assemblages in the main mineralized zone: Spectral Linear Unmixing.....92

Figure 4.9 Spatial co-occurrence of pyrites with sericite alterations: Spectral Linear Unmixing.....93

**List of Tables**

Table 3.1 Directed principal component analysis of the quartz and kaolinite band ratios for quartz detection by the software defoliant technique.....	38
Table 3.2 Directed principal component analysis of the biotite and kaolinite band ratios for potassic-biotite alteration detection by the software defoliant technique.....	38
Table 3.3 Directed principal component analysis of the iron oxide and kaolinite band ratios for ferrigenous alteration detection by the software defoliant technique.....	39
Table 3.4: Eigenvector statistics for mapping hydroxyl-bearing minerals.....	52
Table 3.5: Eigenvector statistics for mapping ferrigenous alteration minerals.....	52
Table 3.6: Eigenvector statistics for mapping sericite-muscovite.....	53
Table 3.7: Eigenvector statistics for mapping chlorite-epidote.....	53
Table 3.8: Eigenvector statistics for mapping calcite.....	54
Table 3.9: Eigenvector statistics for mapping biotite:-potassic zone indicator.....	54
Table 3.10: Eigenvector statistics for mapping illite-sericite.....	54
Table 3.11: Eigenvector statistics for mapping alunite-argillic alteration zone.....	55
Table 3.12: Eigenvector statistics for mapping kaolinite-indicator argillic alteration zone....	55
Table 3.13: Eigenvector statistics for mapping kaolin-smectite.....	56

## **CHAPTER 1 RATIONALE FOR THE STUDY AND THE HAIB STUDY AREA**

### **1. 0 Introduction**

This chapter presents the rationale for the study and a brief overview of the study area. The datasets and materials used in the research are also listed.

### **1.1 Problem statement**

Remote sensing has become an indispensable tool in modern scientific mineral exploration. Conventional mapping was restricted to the use of aerial photographs and Landsat TM for large-scale alteration mapping. Landsat TM has limited spectral and spatial resolution for effective use in mineral exploration because it has fewer spectral bands and a larger pixel size. Human visual interpretation of aerial photographs is subjective and cannot detect the subtle differences in mineralogy, which are usually diagnostic. The availability of multispectral data from a satellite-borne ASTER sensor with 14 spectral bands, launched on 18 December 1999, provides a new dimension in large-scale alteration mapping. ASTER was launched as a result of the cooperative efforts between NASA and Japan's Ministry of Economy, Trade and Industry (METI) and the Earth Remote Sensing Data Analysis Center (ERSDAC). Several image-enhancement techniques are available for identifying and discriminating the subtle differences in alteration mineralogy. This research seeks to test the ability of the high spectral resolution ASTER imagery to map alteration mineralogy by comparing various image-enhancement techniques used in alteration mapping for identifying mineralized zones, which might be of economic value.

### **1.2 Research aim**

The overall aim of this research is to test the ability of ASTER imagery for mapping alteration mineralogy, which is associated with economic base metals, mostly copper, by comparing various digital image enhancement techniques.

### **1.3 Research objectives and sub-objectives**

#### **1.3.1 Objective 1.**

To map alteration mineralogy with ASTER imagery by utilizing suitable image enhancement techniques, which have shown potential for the identification and discrimination of subtle diagnostic differences in mineralogy.

#### **Sub-objectives:**

- (i). To compare the following image processing techniques, with the aim of testing their efficiency in highlighting the mineralized zones:

Standard Colour Composites, Relative Band Depth Mapping, Ratioing, Crosta Technique (Feature Orientated Principal Component Analysis), and the Log Residual Method.

- (ii). Use standard spectral signatures to do spectral linear unmixing.
- (iii). Determine the presence of fractures through the application of Sobel filtering (edge detection filter) and establish the spatial relationships between fracturing and mineralization.
- (iv). To classify the main mineral types and alteration zones.

### **1.3.2 Objective 2.**

Validate and assess the accuracy of the alteration mapping utilizing ground and field data.

#### **Sub-objectives:**

- (i) To spatially associate the mineralized zones with the Lowel-Guilbert porphyry copper deposit model. (Evaluate the spatial relationship of mineral occurrences to the Lowel-Guilbert model.)
- (ii) To validate and assess the mineral alteration mapping results by overlaying alteration zones digitized from existing geological maps.

### **1.3.3 Objective 3.**

Integrate the results of the various image processing techniques.

### **1.4 Motivation for the study**

Remote sensing techniques may assist mineral exploration in several ways, different individual image enhancement techniques being appropriate to specific problems and to particular areas. The potential of remote sensing techniques in mineral exploration programmes using satellite imagery must be assessed in combination with information from field studies concerned with ground truth reconnaissance and with detailed follow-up investigations. In the more accessible parts of the world most, if not all, of the mineral deposits with surface or near-surface expressions have been found. In the search for new deposits, exploration must be conducted, therefore, both in the inaccessible terrain and in the areas where transport cover, fossil weathering horizons and barren geological formations overlie bedrock, which is structurally favourable for mineralization. Modern remote sensing techniques now offer the possibility of detecting hydrothermal alteration zones and thermal

anomalies from space-borne platforms. The different image enhancement techniques are useful in highlighting the mineralized zones in an area, which drastically reduces the amount of fieldwork to be carried out. This also yields significant economic dividends and has several attractive mineral exploration ramifications.

Determining mineralogy during an exploration programme aids rapid evaluation and therefore increases efficiency. The economic benefits of identifying a mineral deposit are immense. The ability to use several image-enhancement techniques is therefore invaluable in any effective and economic mineral exploration programme.

### **1.5 Delimitation of the study**

The purpose of this research is to demonstrate specific image-enhancement techniques used in detecting alteration zones using ASTER for information extraction. Remote sensing is a regional reconnaissance method that indicates target areas for follow-up surveys by more detailed and costly methods. In mineral exploration the reconnaissance surveys are followed by field mapping and by geophysical and geochemical surveys that eventually define a prospect suitable for drilling. Mineral discovery results from a combination of exploration methods and no single method is responsible for the discovery. This research shall, however, be restricted to the demonstration of specific information extraction techniques using high spectral resolution ASTER imagery and comparing the results with previous work done on the Haib copper prospect.

### **1.6 Regional geological setting of study area**

The Haib Porphyry copper-molybdenum prospect is situated in the rugged Richtersveld terrain of southern Namibia, approximately 5 km from the Haib-Orange River confluence. The prospect lies between latitude 17°-18° and longitude 28°-29° within the Richtersveld province which consists of genetically related volcanic and plutonic rocks. A map showing the geographical location of the Haib prospect is shown on Figure 1.1.

The rocks constituting the Richtersveld province are characterized by weak deformation and low metamorphic grades, and are surrounded by the highly deformed, high-grade metamorphites of the Namaqua Province. In the west the Richtersveld province is partially overlain by younger geosynclinal sediments and volcanics of the Gariiep Group (Minnitt, 1986). A map showing the geology of the Haib is shown on Figure 1.2.

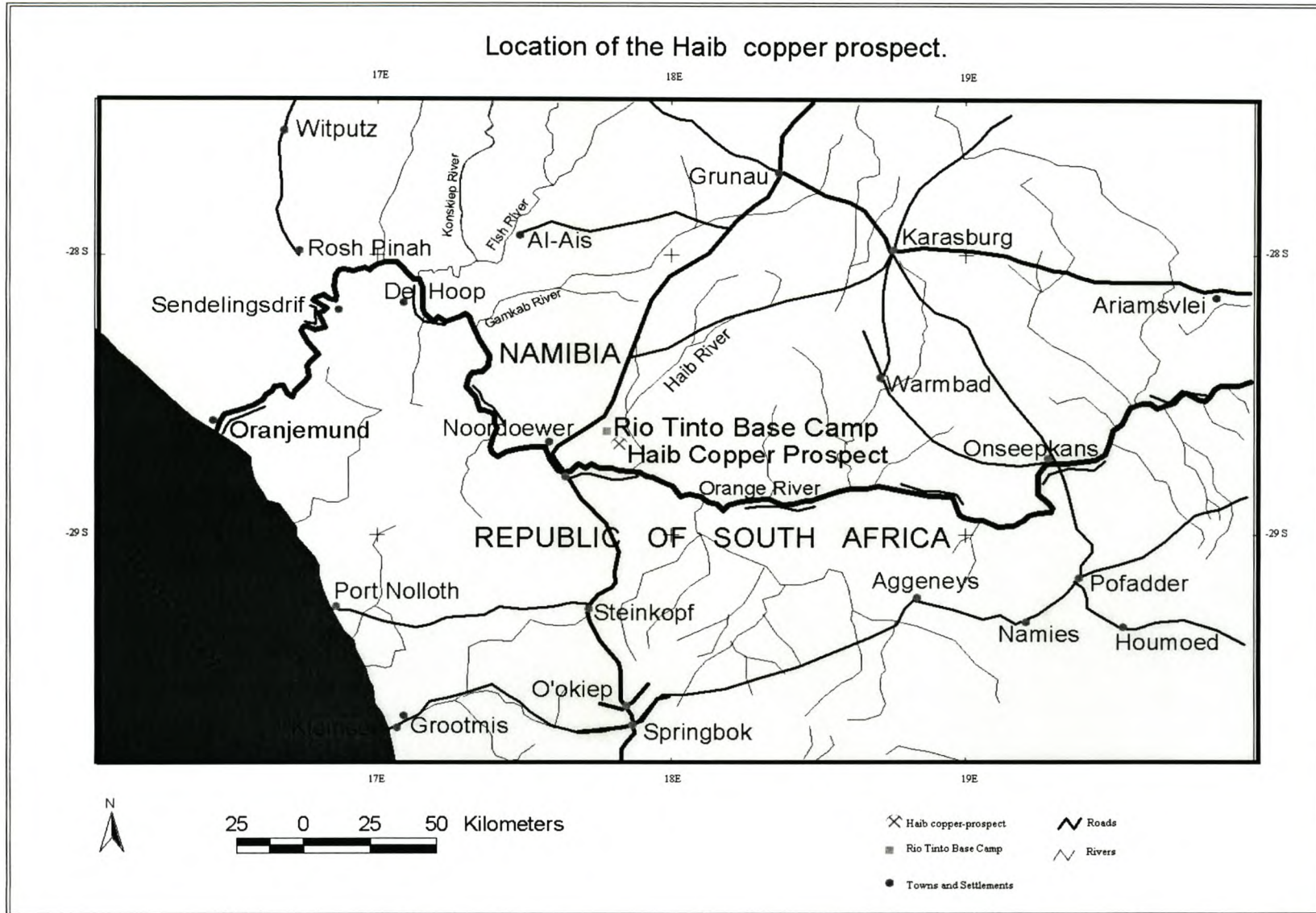


Figure 1.1 Location of the study area.

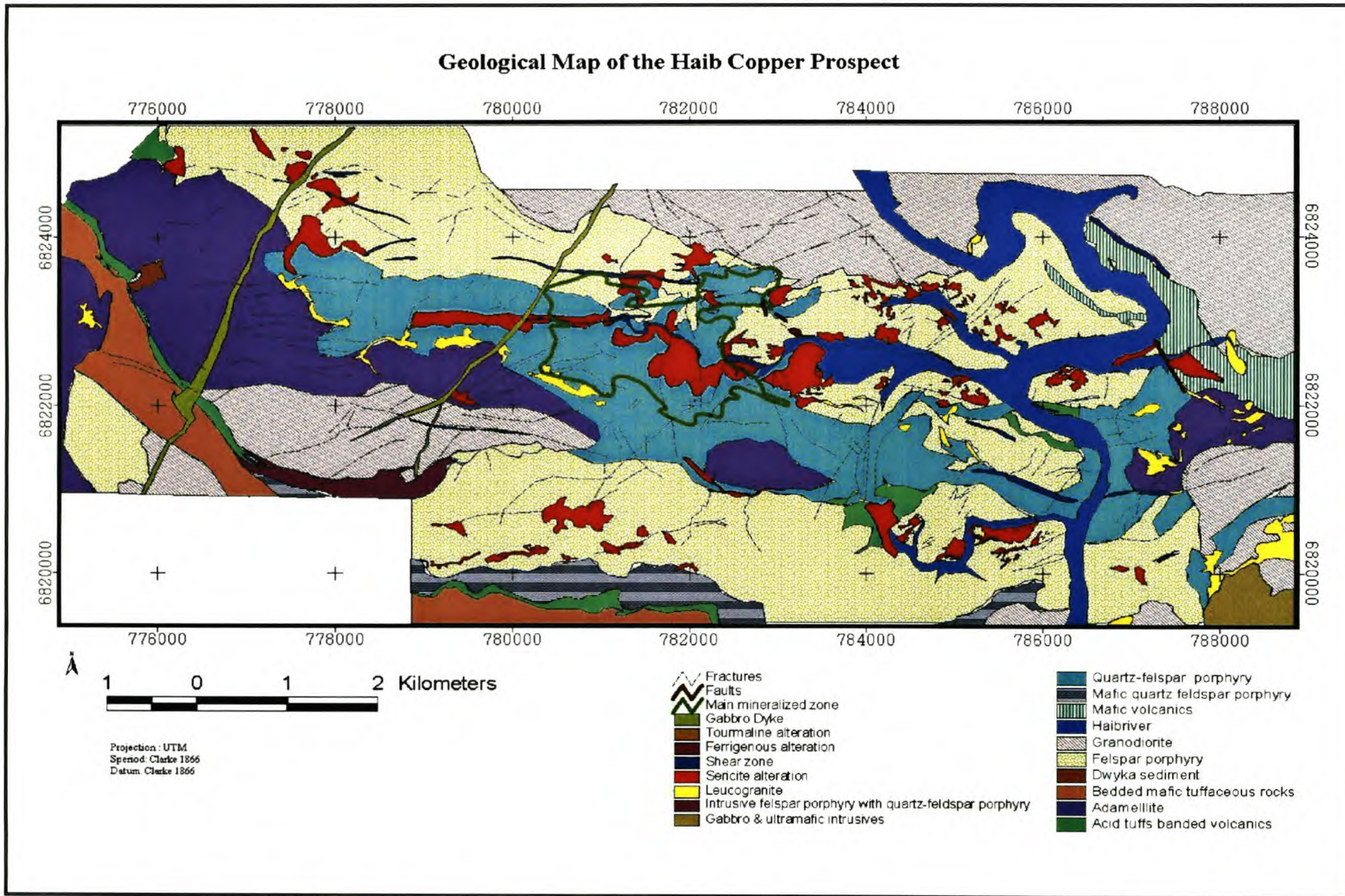


Figure 1.2 Geological map of the Haib copper prospect.

### **1.7 Distribution of economic mineralization**

The economic metals found within the Haib prospect are copper, molybdenum and silver. Concentration of metal mineralization occurs in the sulphide zones which trend north-west-south-west with superimposition of copper, molybdenum, silver and pyrites in the central portions (Minnit, 1986). The main zone of mineralization occurs within the Haib porphyry stock, where a zone of moderate to intense phyllic alteration overprints and is superimposed on the earlier potassic alteration, which affected the entire Haib porphyry stock (Minnit, 1986).

### **1.8 Previous mineral exploration work on the Haib copper prospect**

Detailed mineral exploration to assess the economic mineral potential of the Haib copper prospect was done by Rio Tinto in the 1970s. Research efforts to understand the character of this deposit, which involved radiometric age dating of rocks, was done by Reid (1977). Blignault (1977), Reid (1977) and Minnit (1979) chemically and mineralogically investigated the genetic link between the six phases comprising the Vioolsdrif Suit (Minnit, 1986). Advanced exploration initiatives by Rio Tinto culminated in the publication of detailed geological maps and assessments of the exact metallurgical content of the economic mineralization (Minnit, 1986). The evaluation was done through a combination of mineral exploration techniques, which include geochemical sampling and drilling. Productive mining activities at the Haib are erratic and currently abandoned. Miningtek, a South African research organisation, is currently involved in the development of a metallurgical technique which will optimize the recovery of the metal.

### **1.9 Data and materials available**

The following datasets and materials were available for the study.

- ASTER 1D:AST07 Level 2 surface reflectance VNIR and SWIR imagery.

Date of image acquisition: 9 March 2003.

Source: Earth Observing System Data Gateway for the Land Processes Distributed Archive Centre.

- General geological map of the Haib prospect.

Date: 1986

Scale: 1: 2000

Source: Mineral Deposits of Southern Africa Volume 2: Minnit 1986:1568-1569

- Map for the regional distribution of alteration assemblages.

Date: 1986

Scale: 1: 5000

Source: Mineral Deposits of Southern Africa Volume 2: Minnit 1986:1573

- Map of the surface distribution of alteration assemblages in the main mineralized zone.

Date: 1986

Scale: 1: 500

Source: Mineral Deposits of Southern Africa Volume 2: Minnit 1986:1574

- Fracture distribution map of the area .

Date: 1986

Scale: 1: 5000

Source: Mineral Deposits of Southern Africa Volume 2: Minnit 1986:1571

- Mineral occurrence data.

Date: 1986

Scale: 1: 500

Source: Mineral Deposits of Southern Africa Volume 2: Minnit 1986:1575

- Geological report from previous detailed mineral exploration by Rio Tinto (Minnit, 1986).

- USGS spectral library ( TNT Mips 6.4 software).

### **1.10 Conclusion**

The Haib hydrothermal alteration copper deposit has been sufficiently investigated using geochemical and geophysical methods to provide adequate information, which can be used for comparisons when testing ASTER's ability to map hydrothermal alteration zones. The available datasets are adequate to meet the objectives of the study.

## CHAPTER 2 HYDROTHERMAL ALTERATION MAPPING USING ASTER.

### 2.0 Introduction

This chapter gives a detailed review of hydrothermal alteration detection using multispectral remote sensing. A brief exposition of ASTER's capabilities to map alteration mineralogy is followed by a concise overview of the Haib alteration system.

### 2.1 Application of multispectral remote sensing to mineral exploration.

The ability of multispectral remote sensing to identify and map concentrations of key minerals can be used to survey large regions for new exploration targets rapidly and effectively (Drury, 2001). Mineral exploration is the scientific investigation of the Earth's crust to determine if there are mineral deposits present that may be commercially exploited (Peters, 1978). Hydrothermal alteration zones are of considerable research interest due their potential economic implications and favourable spectral properties for remote identification (Rowan, Hook, Abrams, Mars, 2003). Economic Mineralization of potential economic value is often produced by fluid processes that substantially alter the mineralogy and chemistry of the host rocks. This alteration can produce distinctive assemblages of minerals that vary according to the location, degree and longevity of those flow processes (Ferrier, White, Griffiths, Bryant & Stefouli, 2001). Alteration areas usually occur in zones which are concentrically shaped with a core of high-grade alteration, which is usually of the greatest economic interest. The recognition of such spatial patterns of alteration is one of the objectives of mineral exploration (Ferrier *et al.*, 2001). Spectral identification of potential areas of hydrothermal alteration minerals is a common application of remote sensing (Crosta, De Souza, Filho, Azevedo & Brodie, 2003).

Remote sensing has become an indispensable tool in the systematic search for mineral targets due to the surface expression of alteration mineralogy, which can easily be detected by satellites (Sabins, 1999). Spectral remote sensing data are of invaluable use in mapping hydrothermally altered rocks, because many alteration minerals produced have distinctive absorptive features caused by the presence of OH and other hydroxyl bonds: Mg-OH and Al-OH, particularly in the short-wave infrared (SWIR) part of the spectrum (2000-2400  $\mu\text{m}$ ) (Hunt, 1977). Geological remote sensing can be defined as the science of remotely acquiring, processing and interpreting spectral information about the earth's surface. Sensors record interaction between matter and the electromagnetic energy (Richards, Robinove, Wiesnet, Salomonson & Maxwell, 1983). Orbital remote sensing at visible and near-infrared (VNIR)

and short-wave infrared (SWIR) wavelengths is based on the spectral reflectance of objects on the Earth's surface (Drury, 2001).

Reflectance is defined as the ratio of the intensity of light reflected from a surface to the intensity of the light incident upon it (Mustard & Sunshine, 1999). Rocks are a collection of minerals and their reflectance spectra are composites of the individual spectra of the constituent minerals (Hook, Abbott, Grove, Kahle & Palluconi, 1999). Mineral spectra exhibit diagnostic features at various wavelengths, which provide a means for their remote discrimination and identification. These features are produced by electronic or vibrational-rotational processes resulting from the interaction of electromagnetic energy with the atoms and molecules which comprise the minerals that make up a rock (Clark, 1999; Hook *et al.*, 1999). Remote sensing data can be used to recognize gossans and hydrothermally altered rocks by their spectral signatures (Sabins, 1999). Subtle differences in the reflectance spectra can indicate major differences in chemistry or some physical parameters (Drury, 2001).

## 2.2 Alteration zone analysis

The objective of an alteration zone analysis is to define areas of anomalous spectral composition associated with areas of mineralization (Sabins, 1999). Hydrothermally altered rocks are a lithologic anomaly, which results from the chemical attack of pre-existing rocks by hydrothermal fluids (Coumoul, Abdulhay & Roubichou, 1989). The spatial distribution of hydrothermally altered rocks is a key to locating the main outflow zones of hydrothermal systems, which may lead to the recognition of mineral deposits, because areas of known surface alteration are often associated with underground base and precious metal deposits. Digital spectral analysis and image classifications can be performed, which can pinpoint alteration anomalies as small as 15 m using ASTER (Drury, 2001). Target alteration zones in a satellite image can be classified and subdivided according to relative amounts of hydroxyl. Various hydrothermal alteration assemblages are developed according to ambient temperature and pressure regimes during mineralization. Mapping the assemblages at the surface allows the geologist to understand the mineralization system and to detect areas of mineralization.

The key mineral assemblages, in particular the clay minerals, appear very similar in the field and as such are difficult to discriminate (Coumoul *et al.*, 1989). However, they all have specific spectral features, in particular in the short-wave infrared (SWIR) part of the spectrum. Remote sensing data can be used to recognize gossans and hydrothermally altered rocks by their spectral signatures (Sabins, 1999). Zonation in an alteration halo reflects chemical and

temperature gradients in a hydrothermal system (Sabine, 1999). Five distinct alteration types are widely recognized: potassic; phyllic; advanced argillic; argillic and propylitic (Sabins, 1999).

Minerals commonly found in the phyllic zone are quartz, sericite and pyrite. The propylitic zone commonly contains the minerals chlorite, epidote and calcite. The argillic zone is characterised by the minerals quartz, kaolinite, and montmorillonite. Other key minerals discriminated by ASTER are chlorite, kaolinite, sericite, alunite, jarosite and silica (Crosta *et al.*, 2003). Initially broad alteration types such as argillic and propylitic assemblages can be discriminated simply by using the relative position of absorption bands in key minerals. Simple band difference imaging can localize broad alteration zones (Peters, 1978).

### **2.3 Spectral characteristics of alteration zones**

Spectral signatures have been widely used to directly identify hydrothermally altered rock, for example, at Nevada (Rockwell, 1989), Chile, Peru and Bolivia (Eiswerth & Rowan, 1993; Kneeper & Simpson, 1992). Spectral properties, which are derived from the satellite multispectral scanner data, serve as the basis for lithologic mapping, because they allow the geologist to discriminate and perhaps even identify geological units that are on the image using photo-interpretative techniques.

The ability to distinguish units implies recognising differences in spectral or spatial information on the image. Several physical properties of geologic materials such as texture, roughness and particle size can be derived from remote sensing data (Kaufmann, 1988). Ferric-bearing oxides and oxyhydroxides, such as goethite, hematite, lepidocrocite, and other ferric minerals such as jarosite, have distinctive broad absorption bands centred in the ultraviolet, visible and near-infrared portions of the electromagnetic spectrum. These minerals are often referred to by the field term “limonite” (Blanchard, 1968). The absorption bands associated with limonitic minerals are caused by electronic vibration processes associated with ferric-iron cation in the lattice structures of the minerals (Hunt, Salisbury & Lenhoff, 1971; Hunt & Ashley, 1979).

The overall depression in the spectral response curves of limonitic materials below 500 nm is caused by an intense ferric iron absorption band centred in the ultraviolet region. A non-limonitic rock lacks this absorption. Other spectral features attributable to the presence of ferric iron occur as an inflection in the curve at 650 nm and broad, shallow absorption bands in the 850-950 nm region. The depth and position of the absorption band in the last region

will depend upon the species of ferric-bearing limonitic mineral present (Miyake, 2002). The identification of limonitic rocks utilising satellite imagery is done routinely as an exploration method for delineating potential areas of hydrothermally altered rocks (Rowan, Wetlaufer & Goetz, 1974; Podwysoki and Segal, 1980; Podwysoki, Segal & Abrams, 1982) because of these minerals or secondary weathering products in hydrothermally altered rocks.

Hydrothermally altered rocks commonly contain pyrite formed as part of the alteration process, which weathers to form limonitic materials. However, not all limonitic rocks are hydrothermally altered; limonite may also result from diagenetic processes or secondary weathering of iron-bearing minerals in unaltered rocks. Additionally, some hydrothermally altered rocks are bright and non-limonitic. Minerals containing Al-O-H, Mg-O-H (Hunt *et al.*, 1971) or the carbonate radical (Hunt & Salisbury, 1970), and their mineral lattice structures have narrow and often distinctive absorption bands which are centred in the mid-infrared (Hunt & Salisbury, 1970). Carbonate, clay minerals such as kaolinite, montmorillonite, talc and other minerals such as jarosite, alunite, prophyllite and sericite have such diagnostic bands. The exact positions and intensities of the absorption bands can often be diagnostic of specific minerals, but can only be determined with spectroradiometers capable of 0.01 $\mu\text{m}$  spectral resolution. *In situ* field spectra for some representative types of rocks are represented in Figure 2.0.

In the reflected region detectable minerals are restricted mainly to those carrying ferric, hydroxyl and carbonate components, together with differences in overall reflectivity that stem from a multitude of factors (Drury, 2001). The thermally emitted region is more diagnostic because of the shifts in spectral features associated with variations in silicon and aluminium co-ordination with oxygen and other molecular features, which gives more information on rock-forming minerals (Drury, 2001). Because of the unique spectral characteristics of many alteration and rock-forming minerals, multispectral remote sensing can make a significant contribution to the field of exploration geology (Sabins, 1999).

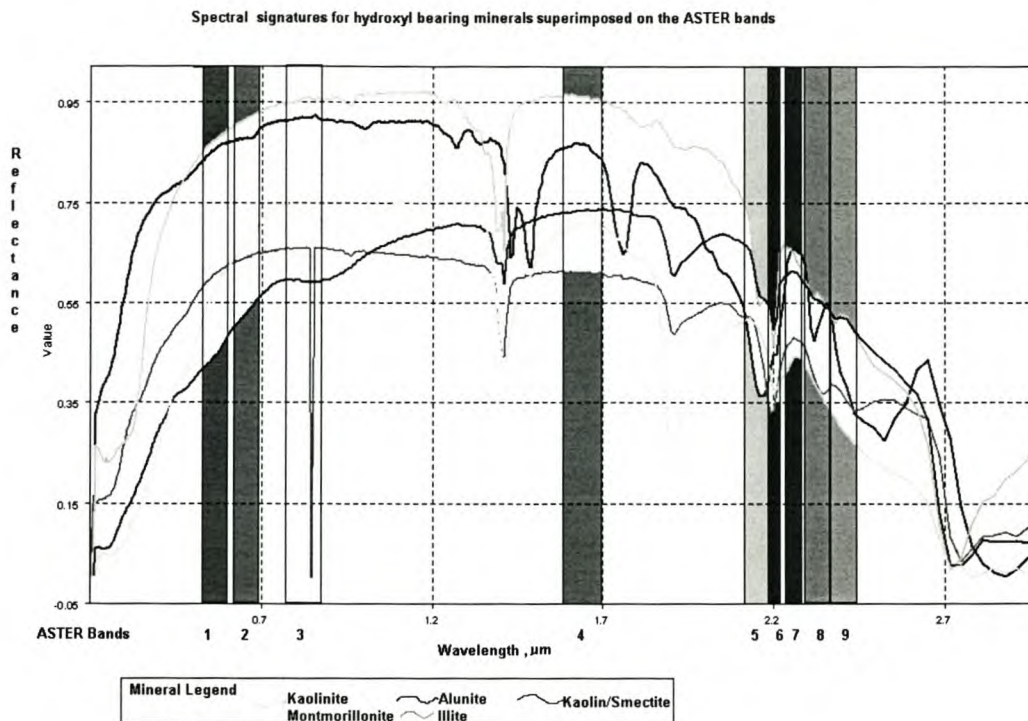


Figure 2.0 Spectral signatures for alteration minerals

Source: Adopted from the USGS spectral library.

Geological remote sensing is performed through atmospheric windows, where electromagnetic radiation is allowed to pass without significant attenuation. The five atmospheric windows available for remote mineral mapping are the visible to near-infrared (VNIR), the short-wave infrared (SWIR), the mid-infrared (MIR), the thermal infrared (TIR) and the microwave regions. The VNIR, SWIR and TIR regions are the most useful for mapping surface mineralogy because these wavelengths are sensitive to a wide range of diagnostic surface mineral electromagnetic-radiation material interactions (Drury, 2001). Remote sensing images yield distinct spectral signatures for different minerals. Each group of minerals has different spectral characteristics. Two examples of common mineral groups with their spectral characteristics are listed below.

1. Tectosilicates (quartz +feldspars):

- No absorption features in solar reflection region,
- Increased reflectance in the VNIR+SWIR;
- Absorption features in the TIR region;
- Multispectral data in the TIR region can distinguish between different types of silicates.

2. Limonite (iron oxide):

- Leads to strong absorption in the blue-end region of the visible spectrum;

-Compound or double ratio of ASTER is developed to map limonite-bearing zones.

#### 2.4 Utilization of ASTER in Alteration Mapping

Lithology and hydrothermal alteration can be inferred and mapped from imagery in a variety of ways (Starling, 2003). ASTER data allow the discrimination of sulphates (alunite, andyrite and jarosite), carbonates (calcite, dolomite and ankerite), montmorillonite clays, kaolinite clays and quartz/silification. Colour aerial photographs, and to a lesser extent black and white photos, can be useful in more detailed mapping of hydrothermal alteration. In areas of moderate to good exposure they are used to differentiate argillic/advanced argillic alteration, propylitisation and areas of iron oxides, such as leached caps often seen in porphyry copper deposits (Starling, 2003).

In order to prioritise mineralization anomalies derived from the imagery, even a rapid, first-pass structural interpretation performed in the field can help to define the best initial targets for field checking (Starling, 2003). Another important factor in the field analysis of areas of potential mineralization is the recognition of alteration signatures. This involves the field checking of alteration signatures produced from ASTER image processing and includes definition of alteration types related to known deposits. An understanding of the alteration types is essential for elucidating the hydrothermal system and determining the location of the outcrop in both lateral and vertical alteration profiles relative to fluid sources (Starling, 2003).

The main factors for consideration when selecting the satellite imagery to use for mineral exploration are (1) application definition, (2) resolution and scale, (3) spectral coverages and data processing. ASTER is a high spatial resolution, multispectral imaging radiometer on NASA's Earth Observing System TERRA platform launched on December 18, 1999 (Yamaguchi, Kahle, Tsu, Fujisada, Sato, Kudoh, Watanabe, Kato & Pniel, 2001). ASTER bands superimposed on model atmosphere are shown on Figure 2.1.

ASTER detects electromagnetic energy in the VNIR, SWIR and TIR regions of the electromagnetic spectrum with fourteen spectral bands (Jensen, 2000). The spatial resolution ranges from 15 metres for the three VNIR bands to 30 metres for six SWIR bands and 90 metres for five TIR bands. The ASTER image swath is 60 km (Yamaguchi *et al.*, 2001). ASTER was actually designed by geologists for geological purposes. It is useful for mapping geological alteration and the key mineral groups, which include: iron oxide (VNIR), OH-

bearing minerals (SWIR), and silicates (TIR) and carbonates (SWIR and TIR). ASTER is a unique breakthrough for space-borne geological mapping.

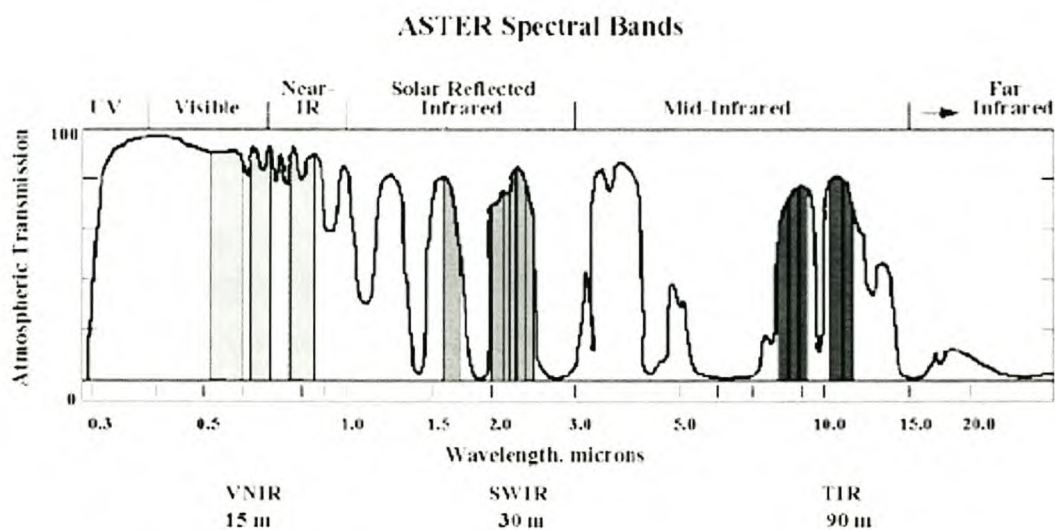


Figure 2.1 ASTER bands superimposed on model atmosphere

Source: Adopted from <http://asterweb.jpl.nasa.gov/instrument/band.htm>

Five ASTER bands (#5-9) cover the SWIR range. Band 6 is centred on the clay absorption feature (often associated with hydrothermal alteration and improved mineral potential). Band 8 is centred on carbonate features, allowing global discrimination of limestones and dolomites from other rocks. Information contained within the 5 bands can be enhanced through band ratioing, principal components and other image processing manipulations. Five ASTER bands (#10-14) cover the TIR range. Bands 10, 11 and 12 are designed for detection of sulphates and silica spectral features. Evaluating reflectance patterns seen in SWIR band 6 with TIR band 10 will allow discrimination between common minerals such as alunite, a sulphate common in arid regions. Band 14 is centred on carbonate spectral features, complementing information in SWIR band 8. Together the TIR bands are capable of discriminating lithologies, compositional variations among rock types and areas of hydrothermal alteration. ASTER, unlike Landsat TM, is available for night-time TIR acquisitions that would markedly improve interpretations. The VNIR data at 15 meters resolution is currently the best resolution multispectral data available commercially from satellites, with the exception of the 4-meter resolution IKONOS data. Comparison with the 10 meters resolution SPOT Panchromatic band shows that it has much better resolution than the ASTER data, while a comparison with

the Panchromatic 15 band on the Landsat 7 ETM+ shows that ASTER is better both spectrally and spatially.

The SWIR data consist of 6 bands designated bands 4 to 9. Band 4 has a similar wavelength to Landsat band 5 and is located where most cover types have maximum reflectivity. Bands 5 to 9 cover an area of the short-wave infrared where many OH-bearing minerals and carbonate minerals have absorption features. Bands 5 to 8 approximately cover the wavelength limits of Landsat 6 and 7. Minerals which may be of interest to exploration geologists and which will produce absorption features in this region are alunite and pyrophyllite, and which are significant for mineral exploration, are easily detected by ASTER, whilst Landsat TM has no such capability. It defines acidic environments typical of advanced argillic-style alteration. The Kaolin group, which is significant for mineral exploration, is useful for defining argillic-style alteration and mapping regoliths deposits. Illite-muscovite-smectite is a common mineral in the surficial environment and is useful for geological mapping. Landsat TM is incapable of detecting these minerals directly. ASTER VNIR and SWIR have enhanced capability in the discrimination of mineral assemblages relative to the existing Landsat Thematic Mapper data. ASTER TIR data are the only available multispectral thermal imaging data, apart from airborne systems and, although it only has a resolution of 90 m, it is useful for defining surface silification (Yamaguchi *et al.*, 2001).

## **2.5 Alteration mineral assemblages at the Haib Copper Deposit**

### **2.5.1 Introduction**

The distribution of silicate alteration assemblages on a regional and local scale has been examined by Rio Tinto exploration company. Silicate alteration assemblages in the Haib prospect are related to the mineralized areas within the deposit. Hydrothermal processes dominated by early potassic alteration were overprinted by a late phase of phyllic alteration. These ore-forming processes gave rise to three silicate assemblages, namely, potassium silicate, chlorite-sericite, and quartz-sericite  $\pm$  pyrite. In addition, a late stage of hydrothermal activity gave rise to vein-controlled epidote-chlorite-calcite assemblages (prophylic alteration) and clay-mineral assemblages (argillic alteration) (Minnit, 1986).

Anhydrite and Fe-Ti-oxide phases also constitute important alteration minerals within the main zone of mineralization. Most of the alteration within the porphyry is restricted to envelopes of varying width, which are centred around veins. Whereas the early potassium

alteration is pervasive, the latter chlorite-sericite and quartz-sericite  $\pm$  pyrite alteration is largely fracture controlled and is only pervasive where the vein alteration envelopes merge or overlap. It is concluded that multiple events of tectonism, intrusion, alteration, and mineralization were more or less superimposed on one another to produce the Haib copper prospect, which represents the integrated effect of these processes (Minnit, 1986).

### **2.5.2 Potassium-silicate alteration**

Potassium-silicate alteration assemblages are characterized by hydrothermal K-feldspar, including orthoclase, microcline, and varieties of peristerites, anti-perthites and hydrothermal biotite. Minor amounts of sericite, Na-feldspar, and anhydrite are also associated with this style of alteration. Quartz, plagioclase, chlorite and epidote also occur in K-silicate alteration assemblages. Accessory minerals include carbonate, apatite, urtite and sphene with magnetite, pyrite and chalcopyrite representing opaque minerals. No definitive "potassic core zone" of the type described by Lowell and Guilbert (1970) could be identified. Potassic alteration at the Haib prospect is localized, being predominant at depth and the level of alteration is moderate to intense. Hydrothermal K-feldspar is fracture-controlled, occurring mostly in veinlets in the affected rocks (Minnit, 1986).

### **2.5.3 Chlorite-sericite alteration**

The widespread chlorite-sericite alteration is developed under hydrothermal conditions intermediately between those giving rise to potassium-silicate and phyllic alteration. During alteration, biotite is progressively replaced along the traces by chlorite. Continued alteration, after complete replacement of biotite by chlorite, gives rise to sericite. Plagioclase is more intensely sericitized under chlorite-sericite alteration than potassic alteration. Minerals present in minor amounts include anhydrite, carbonate, apatite, sphene, magnetite, pyrite and chalcopyrite (Minnit, 1986).

### **2.5.4 Phyllic alteration (quartz-sericite $\pm$ pyrite)**

Phyllic alteration is the most common characteristic of porphyry copper deposits and reflects the action of potassium-rich, acidic, hydrothermal solutions on the rocks. Because of the completeness of this alteration style and the simplicity of the mineral assemblages, there is little difference between phyllic alteration in the quartz-feldspar porphyry and the feldspar porphyry.

Quartz and sericite are the predominate minerals, but pyrite may or may not constitute a major rock-forming mineral. Biotite, chlorite, epidote, tourmaline, and clay minerals are usually present in minor amounts (Minnit, 1986).

### **2.5.5 Distribution and Zonation of the Alteration Assemblages**

Hydrothermal alteration zones in and around the Haib stock are developed on two different scales, regional and local distribution.

#### **2.5.5.1 Regional distribution**

On a regional scale the Haib stock can be equated to the potassic core of the classic Lowell-Guilbert model, with concentrically arranged zones of phyllic and propylitic alteration surrounding the core. The spatial distribution of the regional alteration zones, relative to the Haib porphyry stock, is schematically shown in Figure 2.2 .

In a regional context the central K-feldspar biotite Haib porphyry stock is surrounded by zones of intense phyllic alteration in the volcanic rocks, which the Haib stock intrudes. On a regional scale these patches of phyllic alteration constitute the phyllic zone normally associated with porphyry deposits in the United States. The phyllic zone is, in turn, surrounded by a diffuse zone of propylitic alteration (Minnit, 1986). The spatial distribution of the alteration zones typical of the Lowell Guilbert model is schematically shown below, where (A) indicates the scenario shortly after the intrusion of the stock, and (B) at a later stage when fractures, alteration and mineralization were superimposed on the stock. Figure 2.3 depicts the scenario schematically.

#### **2.5.6 Local Distribution**

**Horizontal Zoning:** Potassic alteration of the Haib stock is partially camouflaged by the unaltered K-feldspar-biotite mineralogy and, although this style of alteration is weak, it is, nevertheless, a pervasive zone of phyllic alteration, which is almost coincident with the zone of high-grade mineralization which is superimposed on the potassic alteration. This zone of phyllic alteration is surrounded by a wide and irregular halo of chlorite-sericite assemblages, which cross-cut and dissect the surrounding K-feldspar-biotite assemblages. Silicate alteration on a local scale within the main mineralized area displays a weakly annular geometry with an inner sericite zone being separated from the outer K-feldspar-biotite zone by a chlorite-sericite alteration assemblage (Minnit, 1986). The distribution of alteration assemblages on surface in the vicinity of the mineralized zone is shown in Figure 2.4 .

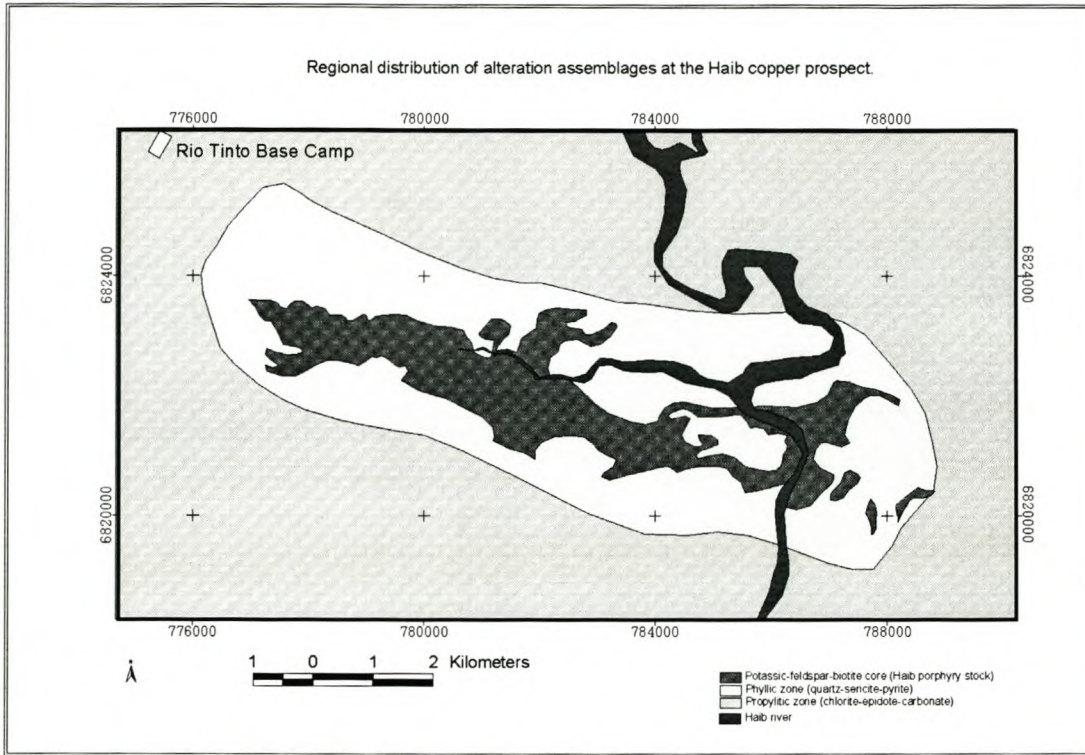


Figure 2.2 Regional distribution of alteration assemblages.

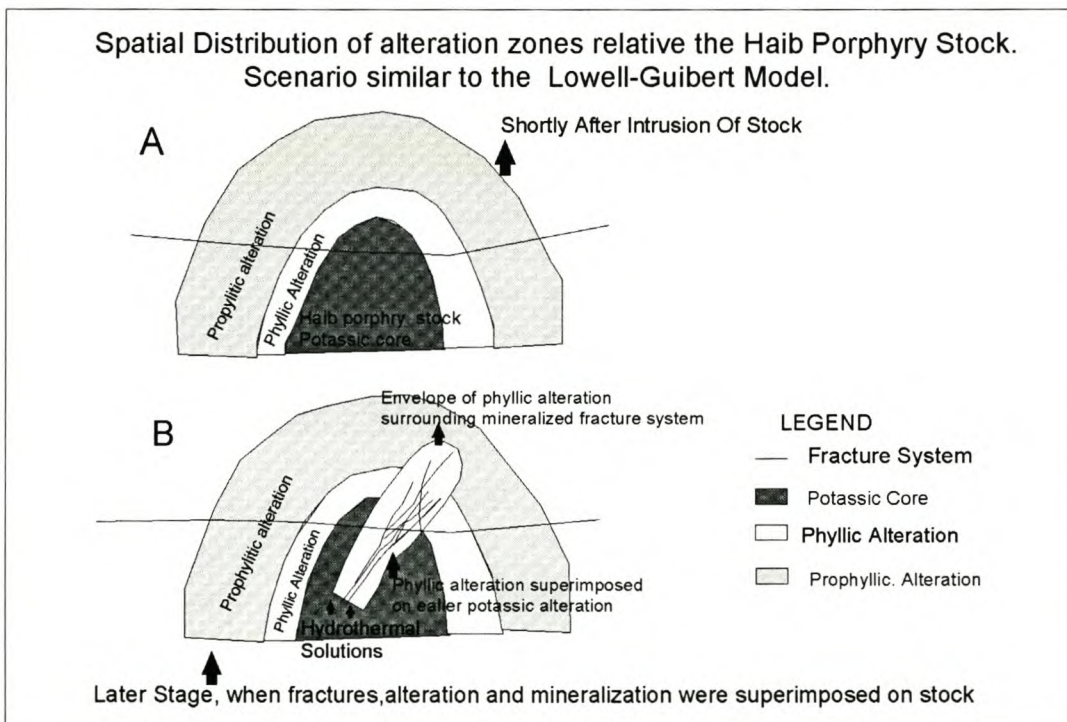


Figure 2.3 Spatial distribution of alteration similar to the Lowell-Guibert model.

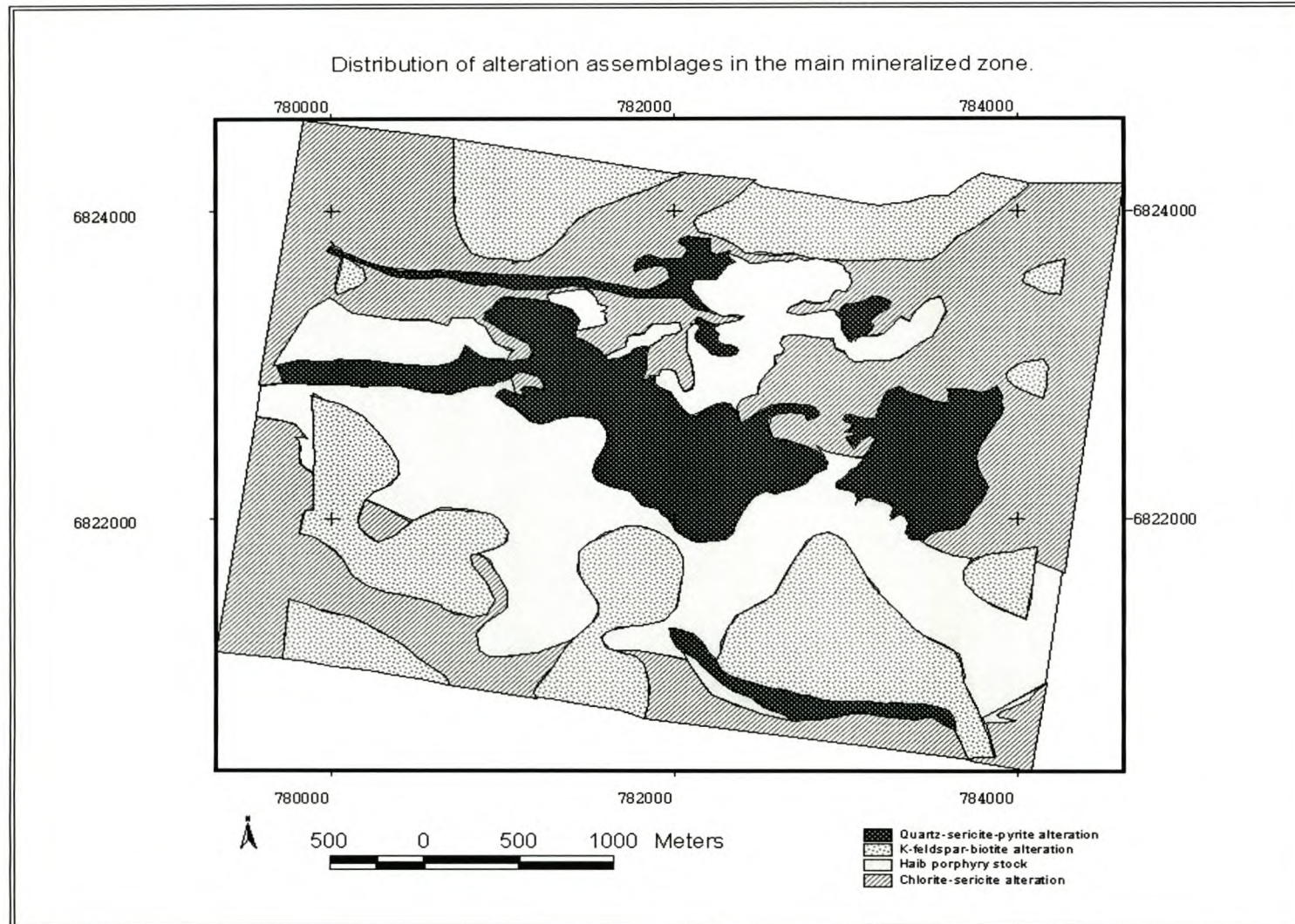


Figure 2.4 Spatial distribution of alteration assemblages in the mineralized zone

### 2.5.7 Structures surrounding the Haib porphyry stock

The zone of the high-grade mineralization within the main mineralized area is parallel to the regionally developed set of fractures, the orientation of which is between N140° and E150°. This latter set of fractures possibly formed prior to, or at the same time as, the mineralization and was responsible for producing the conduits along which the hydrothermal solutions moved. The rose diagram below (Figure 2.5) indicates the general orientations of the fractures.

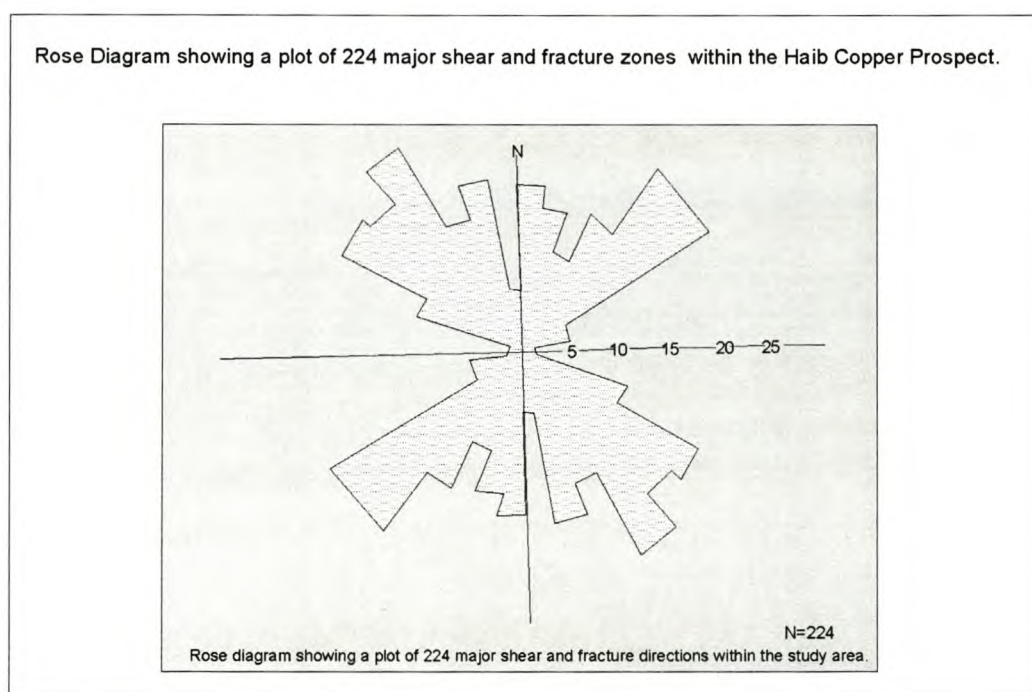


Figure 2.5 Rose diagram.

Source: Mineral Deposits of Southern Africa : Minnit 1986: 1571

The east-west trending fracture zones along the northern and southern flanks of the Haib porphyry stock represent graben faults (Minnitt, 1986), flanking a zone of subsidence, approximately 15 km long and 4 km wide, which is intruded by the Haib porphyry stock. Sericite alteration tends to be restricted to, or is in close proximity to, the flanks of the Haib porphyry stock and graben faults, suggesting that the faults flanking the stock were conduits for hydrothermal solutions (Minnitt, 1986). The distribution, length and orientations of the major basement fractures and shears in the study area, showing the position of the Haib porphyry stock and the distribution of the main zones of sericite alteration, is shown in Figure 2.6.

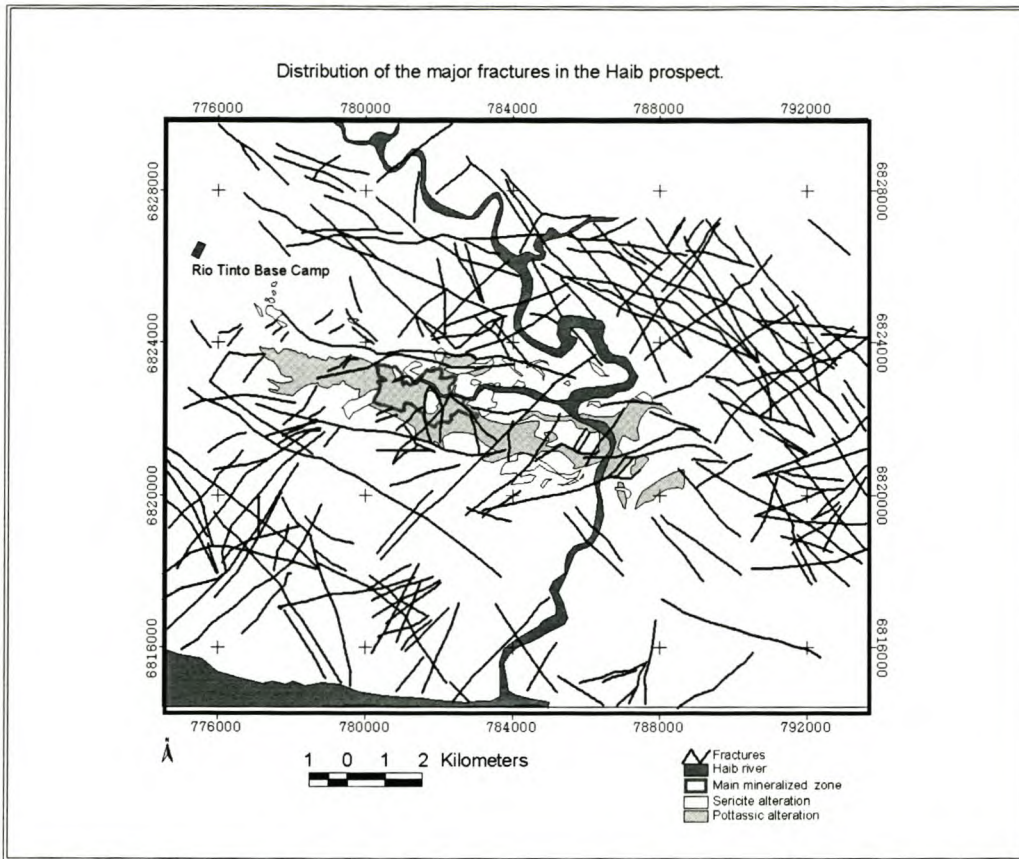


Figure 2.6 Distribution, length and orientation of fractures and shears.

Source: Mineral Deposits of Southern Africa : Minnit 1986: 1571

## 2.6 Conclusion

The alteration mineral assemblages examined at the Haib have the potential to be detected by the ASTER satellite, since most of the mineral assemblages such as the argillic minerals, sericite, calcite, epidote and chlorite have absorption features strategically placed in the SWIR bands for ASTER. The regional hydrothermal alteration zones, which have been equated to the classic Lowell-Guilbert model, with concentric zones of phyllic and propylitic alteration surrounding the core have potential for spectral detection considering ASTER's capabilities discussed previously.

## **CHAPTER 3 METHODOLOGY: GENERATION AND ANALYSIS OF SIMULATED ASTER IMAGES.**

### **3.0 Introduction**

This chapter details the principles of the techniques applied in this study as well as the generation and analysis of the simulated results. Figure 3.0 shows the process flowchart, which gives a summary of the procedures executed in this research.

The geological maps of the Haib copper prospect were scanned and georeferenced using the Erdas Image software. ASTER images were then georeferenced to the geological map of Haib copper prospect and resampled using the Nearest Neighbor method before the execution of image enhancement techniques. Mineral zones and other geological features were extracted from the Haib copper prospect map through digitizing. The following sections give a more detailed overview of the processes executed and the results generated.

#### **3.0.1 Selection of mineral end members to be subjected to image enhancement .**

The selection of end members to be subjected to the image enhancement techniques is based on choosing minerals, which have been mapped in detail using the traditional geological mapping techniques in the Haib area and are well documented in published geological maps. From this array of proved minerals, the selection was then narrowed to indicator key end members, which are diagnostic to the specific alteration zones and are active in the VNIR and SWIR with diagnostic absorptive and reflective features. It is essential to note that most end members are pervasive, but their concentration increases in particular alteration zones. The selection of minerals to represent a particular zone does not therefore entail their exclusive occurrence in that particular alteration zone, but rather their occurrence in greater concentrations to be diagnostic of that zone.

In the following sections each of the image enhancement techniques is described in greater detail, starting with the standard colour composites, absorptive feature mapping, band ratioing, the software defoliant technique, log residual method, Crosta technique and spectral linear unmixing.

#### **3.1 Standard Colour Composites- RGB Band Combinations**

The standard false colour composites are one of the most common and useful techniques used in multispectral remote sensing (Drury, 2001). A computer colour monitor uses three separate

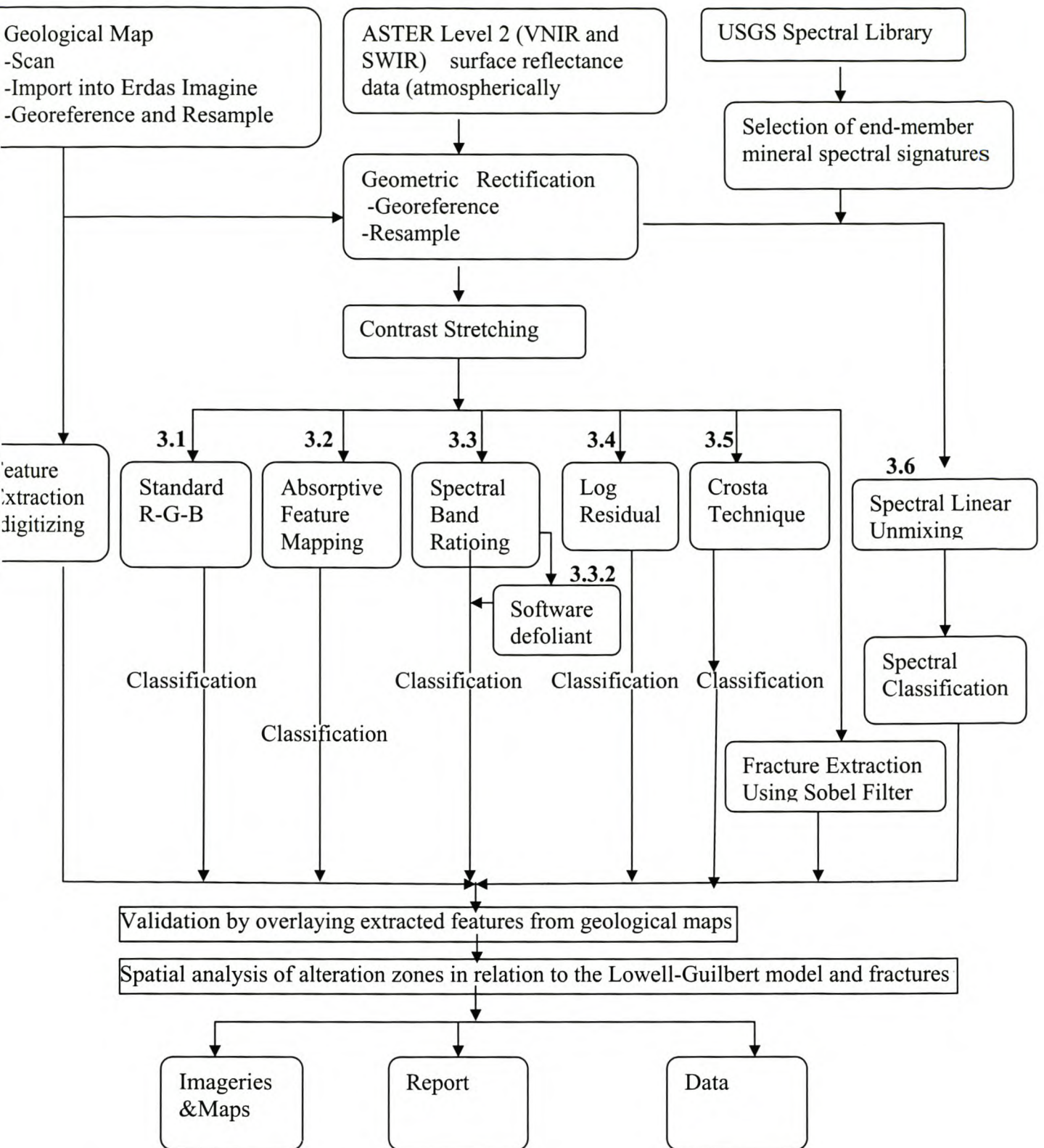


Figure 3.0 Process flowchart for mapping alteration mineralogy using ASTER.

colours to produce an image on the screen ( red, green and blue), and these 3 primary colours can combine to make all other colours of varying hues and intensities (Kowalczyk *et al.*,1991). Standard colour composite use different bands of datasets to specify the intensity of each of these primary colours. This method allows one to view three bands of a dataset at a time, thereby effectively enhancing the visualisation of the multispectral dataset. Colour composites are the basic form of spectral analysis, and a decision on which band combination to use is based on the spectral properties of the target minerals (Drury, 2001). The goal was to define a useful way of manipulating the bands in the image to highlight a ground target of interest based on the spectral properties of the target. Selection of bands for the standard colour composite is based on the understanding of the spectral characteristics of the minerals, which one wishes to analyse. Bands selected for the analysis are restricted to those bands which coincide with the highest reflectance feature or peak of the targeted mineral, in which the pixels tend to shine brightly, accentuating the mineral of interest. The resultant image therefore displays spectral information from different spectral regions and therefore indicates the complementary nature of surface compositional information present as a function of their wavelength (Rowan *et al.*, 2003).

### **3.1.1 Application of standard false colour composites**

#### RGB Combination 3-2-1 True Colour Composite of the Haib

In a reconnaissance survey it essential for one to have a visual impression of the area. In conventional mineral exploration, this usually requires one to visit the area to gain a physical impression of the area. A similar scenario can be simulated in a desktop study using remote sensing by generation of a more or less true colour composite. For this study the ASTER RGB 3-2-1 bands has been used to simulate the natural visual setting at the Haib copper prospect. This is because band 3 represents near infrared and is assigned to the red gun, band 2 is in the visible red and is also assigned to the green gun and band 1 is in the visible green the electromagnetic spectrum and is assigned to the blue gun. The results of this band combination are shown below. The results indicate the primary differences in albedo, topography and the semi-arid environment of the Haib prospect, which makes it favourable for the remote detection of minerals due to sufficient ground exposure. The iron oxide minerals are indicated in shades of browns. The rugged topography of the Haib is evident on the image due to the shadowing effect in most parts of the image. The highly sheared zones have also been highlighted well, where the bedrock deformation can be seen, the sericite alteration zones show up as whitish areas. In this image the undisturbed bedrock and soils are expressed as browns, greens and grey. Vegetation is normally high reflective feature in band

3, so the apparent lack of bright red pixels indicates the aridness of the area and the shades of brown can only be attributed to the iron oxides, which also have a high reflective feature in band 3. The variation in rock colours mainly reflects the presence of iron minerals and variation in albedo. The results from this RGB 3-2-1 image form an essential basis for this study, since the lack of vegetation indicates that the Haib prospect is ideal for the spectral detection of surface minerals using remote sensing. The image inspection equates easily to a physical inspection of the Haib for an initial reconnaissance survey. The results for the RGB 3-2-1 image are shown in Figure 3.1.

#### RGB 4-6-8 Mapping Altered Areas

The selected bands are all found in the SWIR region of the electromagnetic spectrum. In this wavelength region, clays, carbonates and sulphate minerals have diagnostic absorption features, which result in distinct colours on the image. This band combination highlights the areas of alteration, which include epidotization, chlorization and silification. The selection of these bands is based primarily on the need to highlight spectral diagnostic features for ferruginous alteration (iron oxides) band 8, sericite/illite band 6 and carbonates band 4. All hydroxyl-bearing minerals have a high reflectance in band 4, so selection of this band highlights most of the clay minerals as bright red, which are essentially the zones of interest due to their association with economic base minerals. Carbonates also have a high reflectance in band 4, so they also are also highlighted in red. Band 6 is centred on the clay absorption feature, whilst band 8 is centred on a carbonate feature. A range of minerals is highlighted on band 6, which include sericite/illite, smectite and jarosite. Chlorite, biotite and epidote, tourmaline and carbonates are highlighted in band 8. The results for the normalized 4-6-8 band combination are shown in Figure 3.2. The red and orange indicate kaolinite-rich areas, whilst the carbonate, chlorites, epidotes are yellowish green and iron oxides are blue. Reddish areas indicate the sericite and other hydroxyl clay minerals. The red areas are the targeted zones due to their association with the copper ore. A normalization algorithm (Lambert correction) was applied on the 4-6-8 in order to remove albedo variations and topographic effects, which helped enhance visual analysis of the lithological variations and detect the colours related to hydrothermal alteration. This combination proved useful in detecting alteration zones. Pure minerals could not be detected due to the large pixel sizes of 30 meters, and a mixture of minerals could be found in one pixel in most cases. This band combination proved useful for a rapid reconnaissance to highlight areas of alteration.

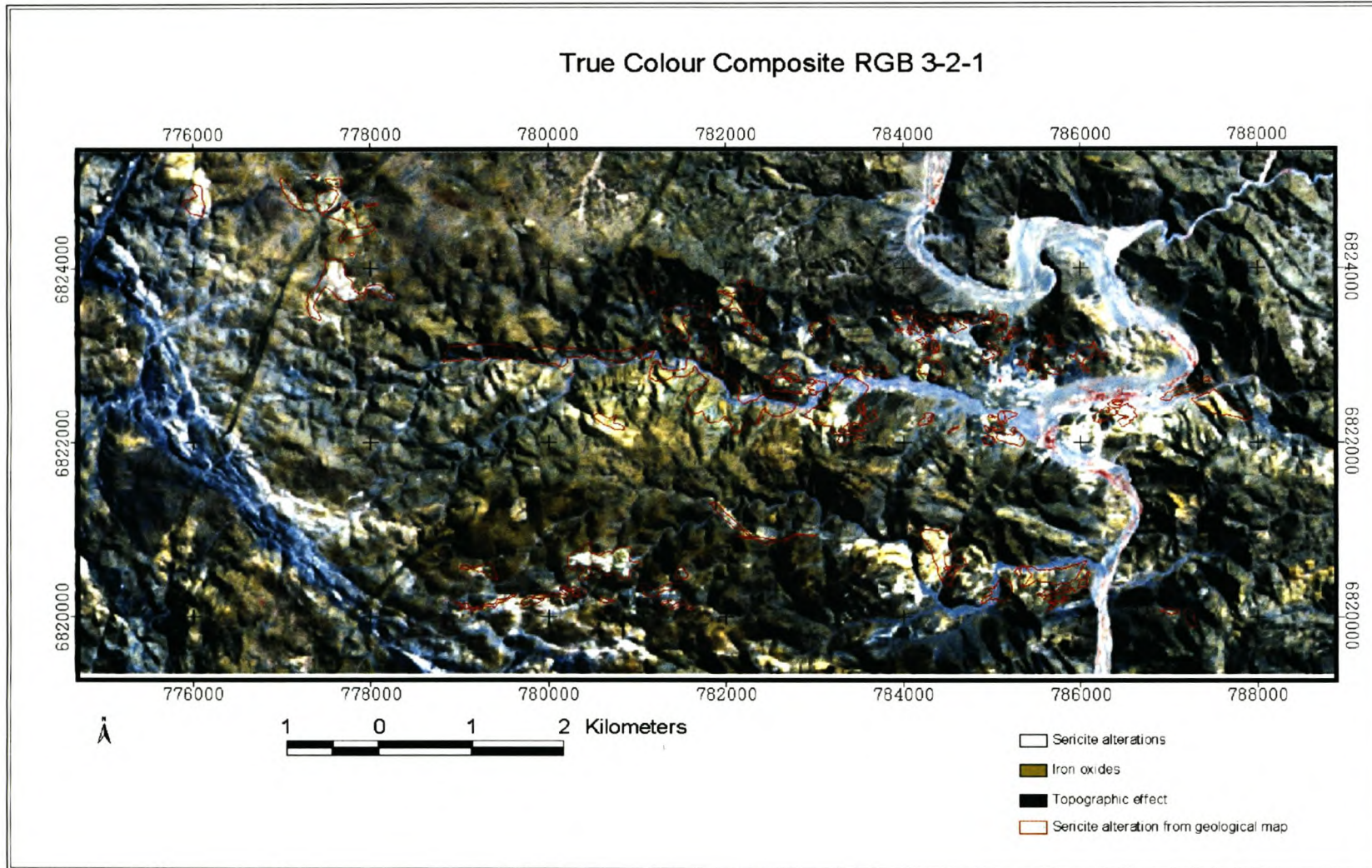


Figure 3.1: True colour composite RGB 3-2-1.

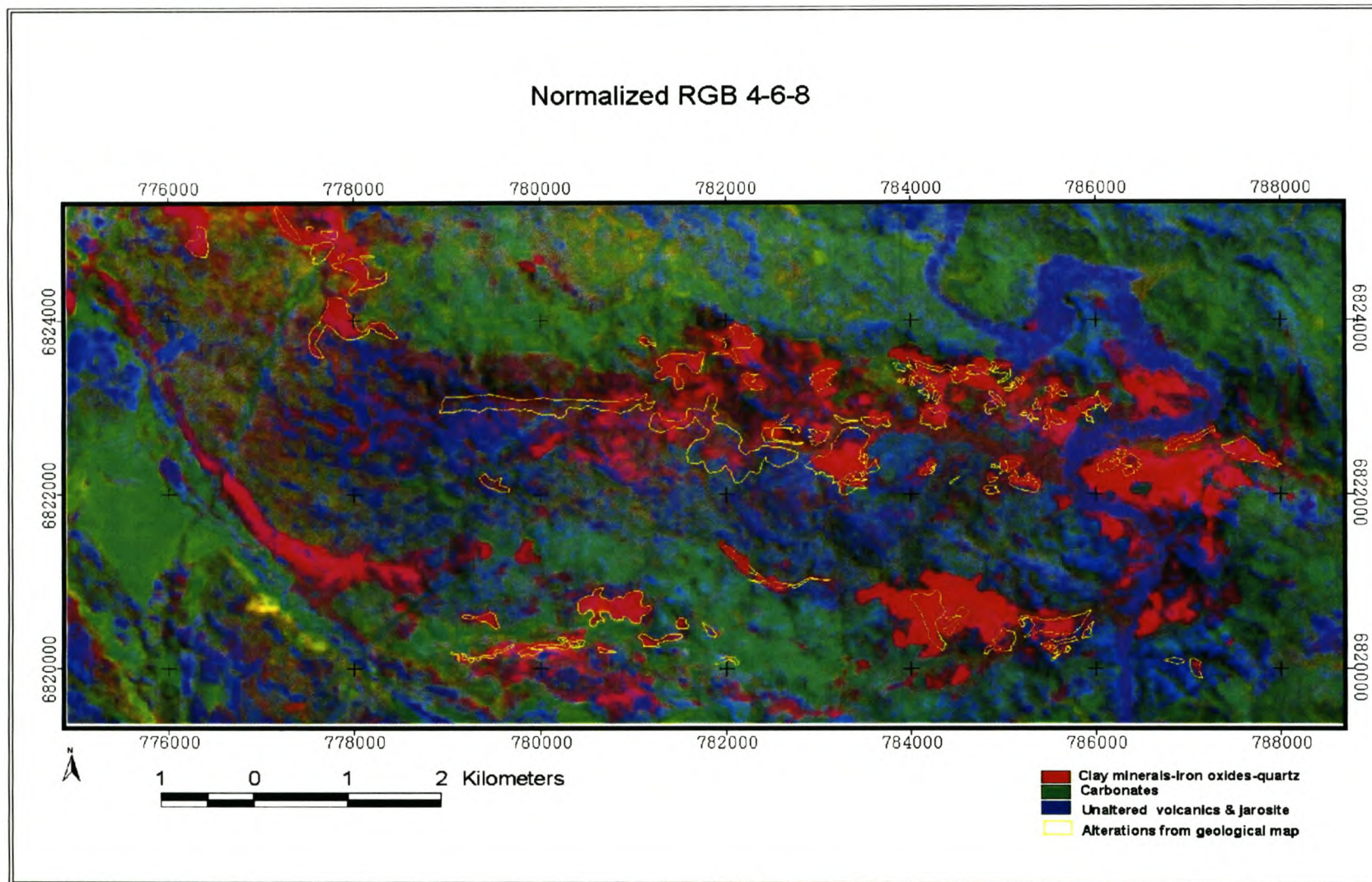


Figure 3.2: Normalized RGB 4-6-8.

### **3.2 Mapping the phyllic and prophylic zone minerals using absorptive features (band depths)**

This technique uses diagnostic absorption features to map specific minerals. The selection of the appropriate band for mapping using the relative band depths is based on the investigation of the mineral spectra. This involves looking for the best diagnostic absorption features in the laboratory spectra of the minerals, which will be able to uniquely define a particular mineral. The band that coincides with the selected diagnostic absorptive feature is negated in order to highlight the mineral of interest as bright pixels.

#### **3.2.1 Application of absorptive feature mapping technique**

A study of the spectral curves for argillic minerals such as alunite and pyrophyllite indicate diagnostic absorptive features near 2.165  $\mu\text{m}$  located in band 5, whilst the sericite group minerals (muscovite-illite-Al smectite) are characterised by a single diagnostic feature around 2.200  $\mu\text{m}$  centred in band 6. The kaolinite mineral species such as kaolinite and dickite have diagnostic absorptive features at 2.175  $\mu\text{m}$  in band 5 and at 2.210  $\mu\text{m}$  in band 6. The ASTER bands are strategically positioned at these wavelength to map out these minerals. The argillic and sericite group minerals are used in this study as indicator end members for the phyllic zone.

Carbonates, chlorite and epidote, which are indicative end members for the prophylic zone, all have a single diagnostic absorption feature around 2.350  $\mu\text{m}$ .

Absorptive minerals will show on the image as dark cells. In order to facilitate visualisation and effectively utilize the diagnostic absorptive features to discriminate the mineral end members and show them as bright pixels, bands 5, 6 and 8 were negated. Carbonates, chlorite and epidote are mapped out in the prophylic zone clearly as bright pixels on the image shown below.

The negated bands 5 and 6 are subjected to a pairwise principal component analysis to have the total effect of both bands in one image. The principal component, in which both loadings on the input images have the same sign, represents the combined phyllic image. A positive sign on both loadings indicates that the pixels are mapped out brightly, whilst a negative sign indicates that pixels are mapped out dark and hence negation of the image is required. PC 2

carries the desired argillic and sericite information necessary to map the phyllic zone. PC 2 is subjected to a histogram equalized transformation to facilitate visual enhancement.

The results are displayed as a false colour composite, which is used to facilitate visualisation. The phyllic image (PC 2) is added to the negated resultant of band 8 to produce an phyllic-prophyllitic image in which pixels carry anomalous concentrations of both phyllic and prophyllitic zone minerals show out brightly. The results were subjected to a histogram equalization transformation. Figure 3.3 shows the final results for absorptive feature mapping. The red marks the phyllic zone and cyan to light blue is indicative of the prophyllitic zone. The darkest green cells indicate the occurrence of all indicator end members. The results compare favourably with the mapped zonations on the distribution of alteration assemblages.

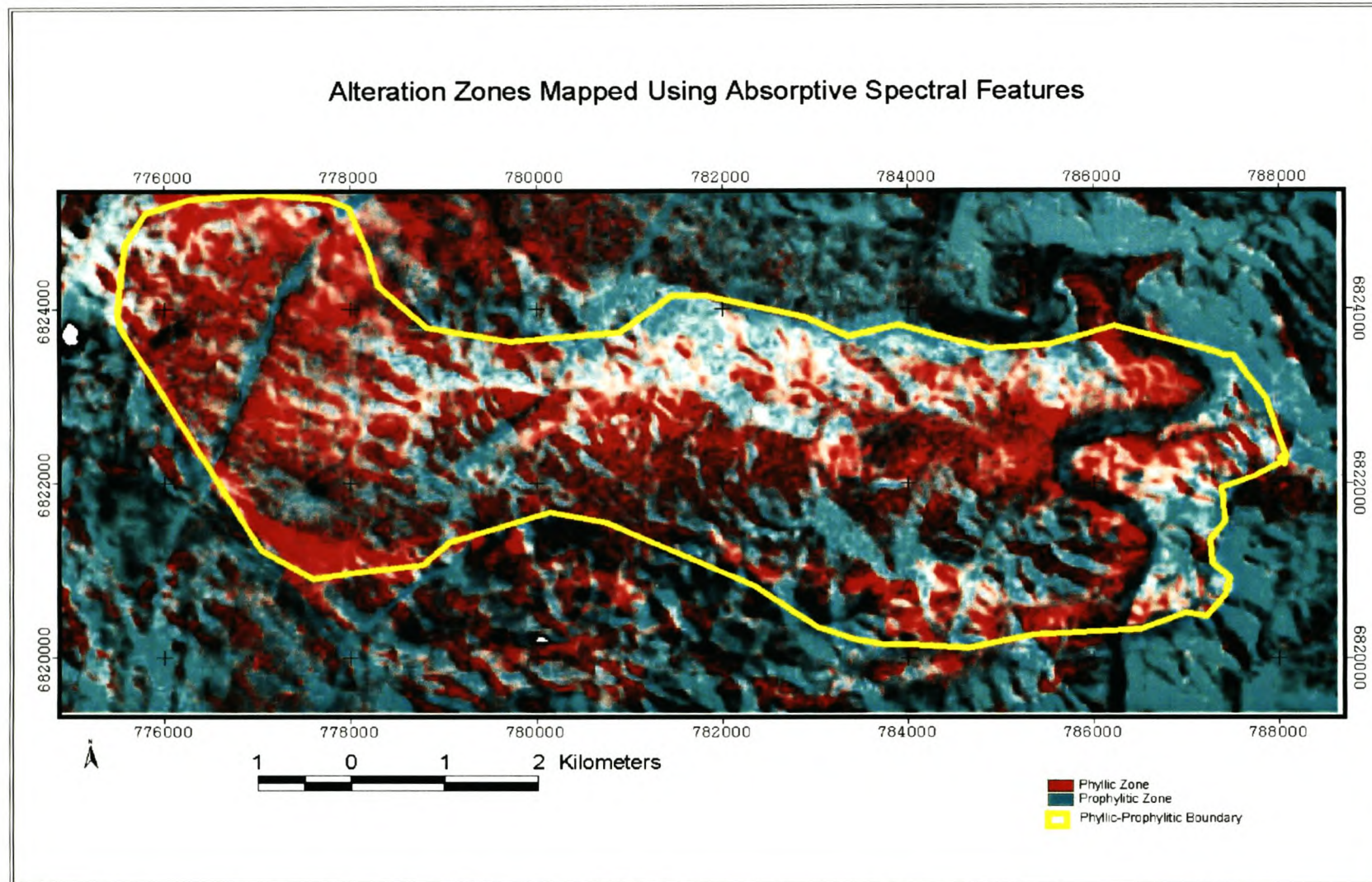


Figure 3.3: Absorptive feature mapping of the phyllic and propylitic alteration zones.

### 3.3 Spectral Band Ratioing

Band ratios accentuate the spectral differences between mineral targets by computing a ratio image (division) using two spectral bands; this cancels out the topographic effect, which is approximately equally constant in all bands (Shibata, 2002). Bands are chosen to accentuate the occurrence of a particular material (Smith, 2001). Band selection is based on analysing the spectral signature of the target mineral and then choosing one wavelength band in which the mineral is highly reflective (appears bright) and the other in which the mineral is strongly absorbing (appears dark). The more reflective band is used as the numerator, so that the occurrence of the target mineral yields a higher ratio value (greater than 1.0) and appears bright in the ratio image (Ninomya *et al.*, 2002). Band ratios enhance compositional information whilst suppressing albedo and topographic slope (Rowan & Kahle, 1982). Ratios were therefore constructed with reference to the spectral properties of the lithologies present in the field in order to differentiate the altered zones from the host rock. To further accentuate the presence of the mineral target, band additions within the highly reflective regions may be computed before the division with the absorption bands, which can also be added before final division. Image addition tends to emphasize information correlated from band to band and give the compounded effect (Mather, 2001). Band ratios are therefore useful data reduction techniques, which highlights the subtle spectral variations that are masked by the brightness variations in the image.

$$\text{Mineral Band Ratio} = \frac{\text{diagnostic reflective band}}{\text{diagnostic absorptive band}}$$

#### 3.3.1 Application of spectral band ratioing

##### Sericite Ratio: (B5+B7)/B6

The sericite band ratio was derived through an analysis of the spectral features of the sericite/muscovite spectral signature shown in Figure 3.1. The spectral curve of sericite above indicates two diagnostic reflective features in bands 5 and 7, and a strongly absorptive feature in band 6. The reflective feature in band 4 has been avoided since it is common to all hydroxyl-bearing minerals. Band 8 was deliberately avoided, since is centred on the carbonate and chlorite absorptive features. The goal is to identify sericite group minerals uniquely without inclusion of the minerals.

Spectral signature for sericite/muscovite superimposed on the ASTER bands

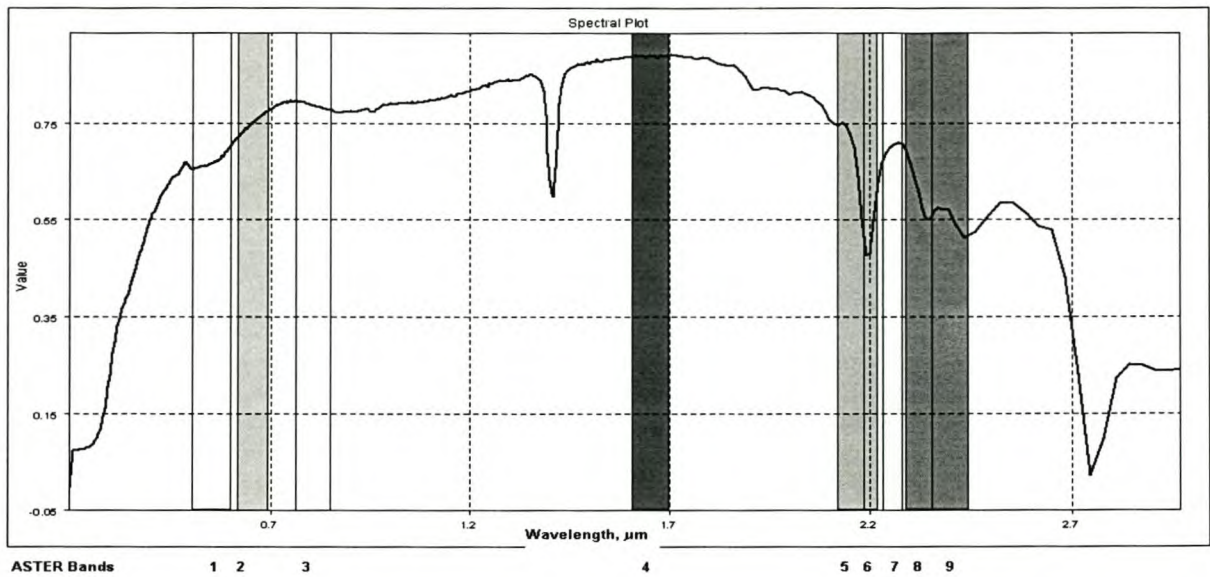


Figure 3a Spectral signature of sericite-muscovite positioned on the ASTER bands.

Band 6 centred at 2.205 µm is critical for high sulfidation alteration cover absorption for sericite, which is associated with the economic copper, silver and molybdenum minerals. An addition of the two diagnostic reflective bands for sericite will emphasize correlated information in band 5 and 7, which when divided by the absorptive band 6 the sericite zones are highlighted. Figure 3.4 show the result of the sericite ratio image. The results of the generated sericite ratio compare favourably with those on the geological map. The results highlighted the sericite zones, which are shown below with an overlay of the digitized sericite zones from the geological map. This ratio has been successful in accentuating the targeted sericite alteration areas.

$$\text{Argillic Ratio} = (B4+B7) / (B5 + B6)$$

The selection of the optimum bands for ratioing to map out the argillic zones was made through the analysis of the spectral features of the kaolinite group minerals and other hydroxyl clay minerals common in the argillic zone. The spectral signatures for the argillic minerals are shown in Figure 3.2 below.

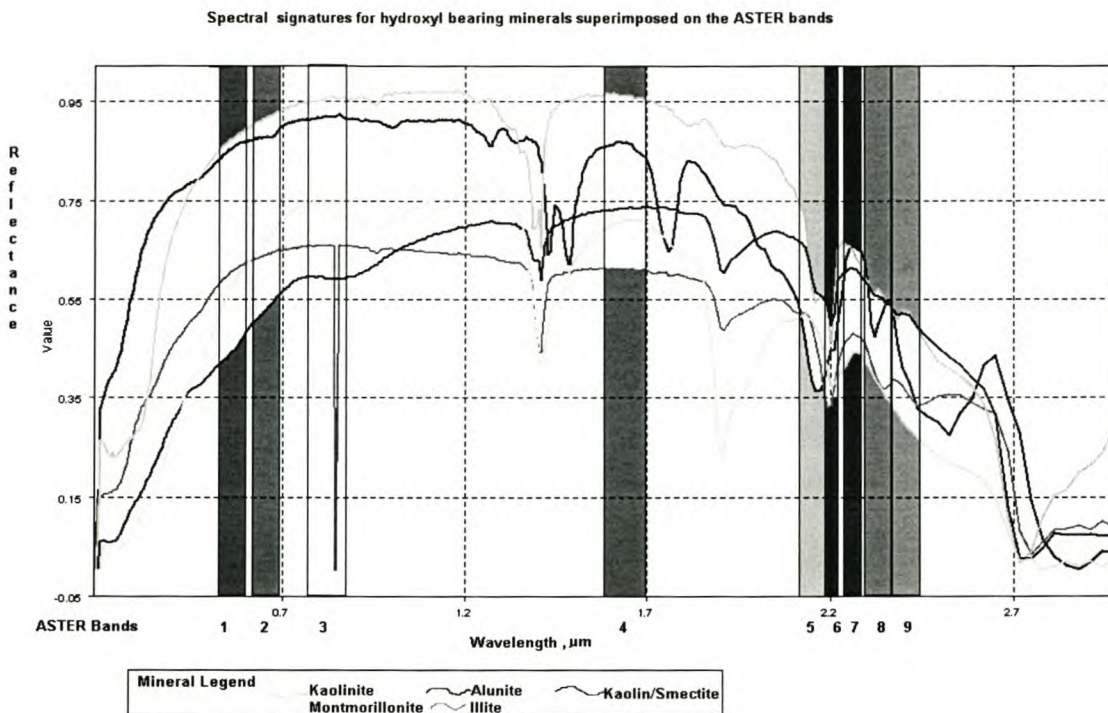


Figure 3b Spectral signatures of hydroxyl-bearing clays positioned on the ASTER bands.

A study of kaolinite, the main indicator mineral for the argillic zone, shows it has a doublet-shaped diagnostic absorption feature near 2.175  $\mu\text{m}$  (band 5) and 2.210  $\mu\text{m}$  (band 6). Kaolinite diagnostic features are depicted by an asymmetric absorption feature centred at 2.205  $\mu\text{m}$  (band 6). The argillic ratio was therefore derived by the addition of the two reflective bands (band 4 and 7) divided by the resultant of the addition of the two absorptive bands. The effective of this computation is to accentuate argillic zones brightly. The resultant highlighted zones compare favourably with alterations from the geological map of the area. The generated results are shown below.

$$\text{Prophylic Ratio} = \frac{(B6+B9)}{(B7+B8)}$$

A ratio of  $(B6+B9)/(B7+B8)$  was derived to map out the prophylic zone minerals, which consist of carbonates, chlorite and epidote from the study of the spectral features of the key end members in the prophylic zone. The standard spectral signatures of carbonates, chlorite and epidote are shown below.

Spectral Signatures for carbonates ( calcite and dolomite) superimposed on the ASTER bands

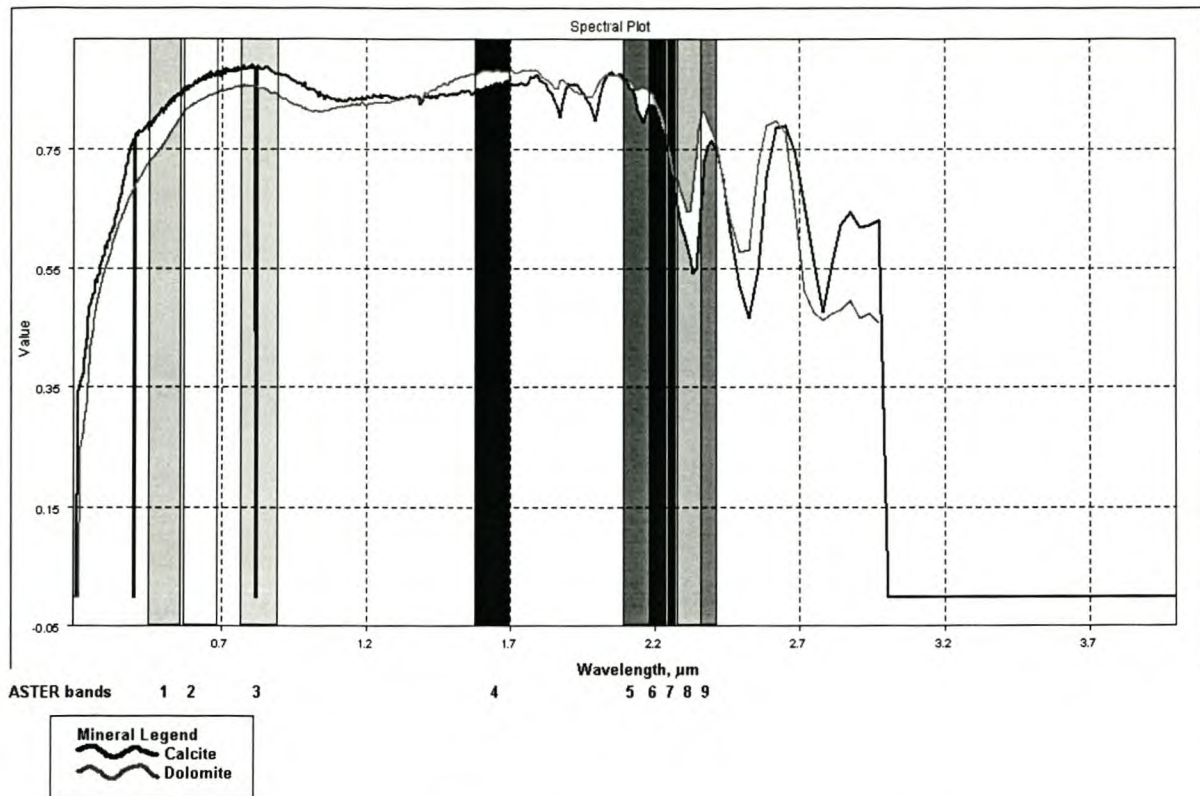


Figure 3c Spectral signatures of carbonates positioned on the ASTER bands.

Carbonate, chlorite and epidote all show a diagnostic absorptive feature in band 8. Carbonates have absorptive features between 2.30 µm (dolomite) and 2.35 µm calcite, chlorite at 2.32 µm and epidote at 2.33 µm. An additional absorptive features located in band 7 is present in all the prophylic indicator minerals. The denominator for the ratio is derived from the addition of the two absorptive bands, which increases the relative band depth. Bands 6 and 9 have reflective diagnostic features and their addition gives the resultant, which is the numerator to this prophylic ratio. Bands 6 and 9 are ideal for this discrimination due to the fact that their reflective nature is in direct contrast to the absorptive nature of the clay minerals in these two bands, which therefore entails that clays minerals will be suppressed effectively. Figure 3.5 shows the prophylic ratio image. The prophylic zone was successfully highlighted and compares favourably with the regional distribution map for the alteration assemblages/zones.

$$\text{Chlorite-Epidote Ratio} = (5+9)/8$$

A ratio of  $(5+9)/8$  was computed to accentuate the occurrence of chlorite in the study area. The basis for this derivation is based on the fact that chlorite and epidote, which have similar spectral features, show high reflectance in bands 5 and 9, so an addition of these two

reflective features with the resultant divided by the strongly absorptive feature in band 8, which is diagnostic for chlorite and epidote, will highlight the presence of chlorite and epidote. Clay minerals are effectively suppressed by this ratio, since they are absorptive in bands 5 and 9. A study of the spectral curves for chlorite and epidote below provides a means for the selection of the chosen bands for ratioing. The chlorite-epidote ratio image is shown in Figure 3d.

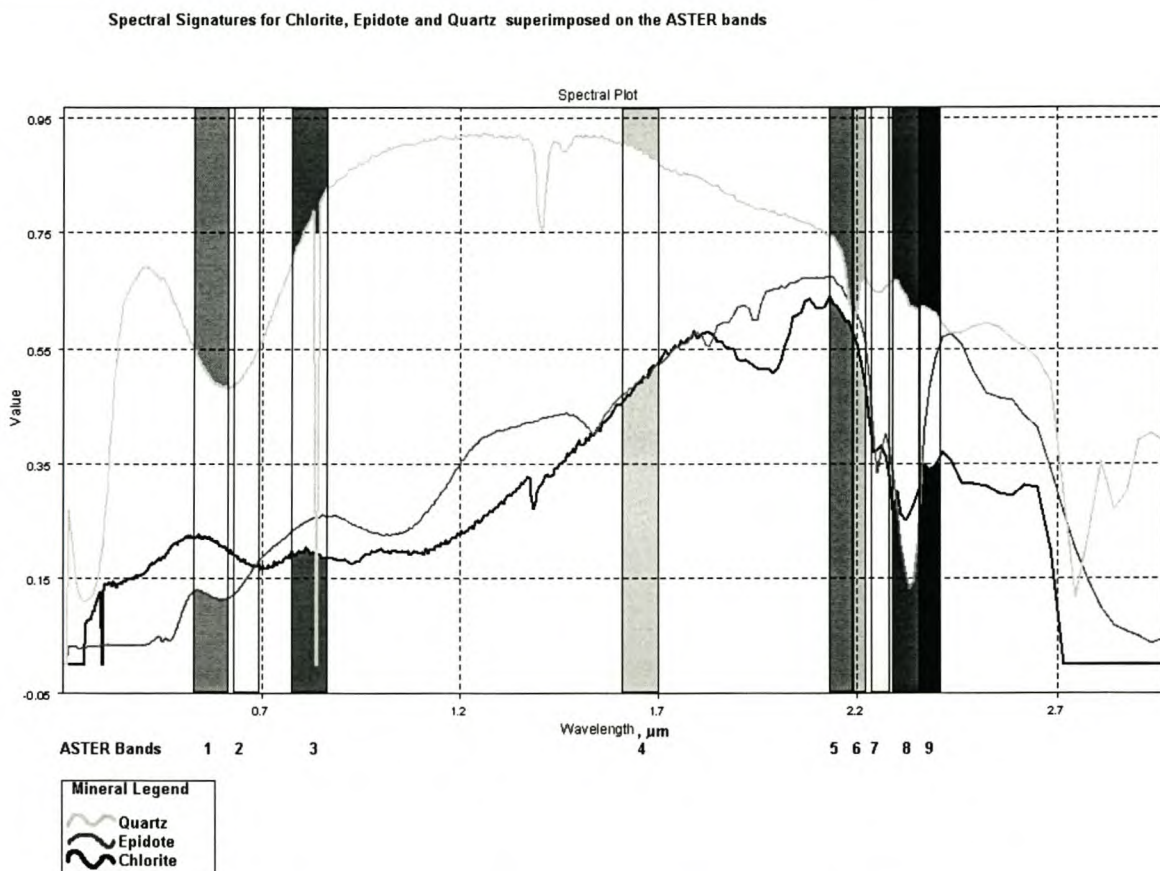


Figure 3d : Spectral signatures of chlorite, epidote and quartz positioned on the ASTER bands.

#### Quartz Ratio = 4/1

The 4/1 is a simple ratio for quartz that has been derived by studying the spectral signature for quartz. Quartz is highly reflective in band 4 and has an absorption feature in band 2. The division of these two bands highlights the presence of quartz as bright pixels. This ratio, however, also highlights the iron-bearing minerals slightly. The spectral signature for quartz is shown in Figure 3d. The quartz image ratio is improved by application of the software defoliant technique in section 3.3.2

Biotite ratio = 7/3

Biotite was chosen as the indicator end member to model the potassic zone. Biotite is active in the VNIR and SWIR regions and its spectral features make its detection easy. Orthoclase and microcline are more difficult to detect in the VNIR and SWIR regions. The selection of bands was based on identification of diagnostic reflective and absorptive features, which also effectively suppress the accentuation of clay minerals, chlorite, epidote and calcites. The biotite ratio is improved by subjecting the biotite image ratio to the software defoliant technique in section 3.3.2. The results are shown on Figure 3.9. The pervasive nature of biotite in both the potassic zone and phyllic zone makes the distinction between the two zones difficult. The results from this computation also indicate that there is no definitive potassic zone as suggested in the Lowell-Guilbert model, which is concentrically shaped on the surface. The potassic zone is probably more developed at depth, which cannot be detected by the satellite. The spectra for the potassic zone minerals are shown below in Figure 3e.

Spectral signatures for potassic zone minerals ( orthoclase , microcline and biotite) superimposed on ASTER bands

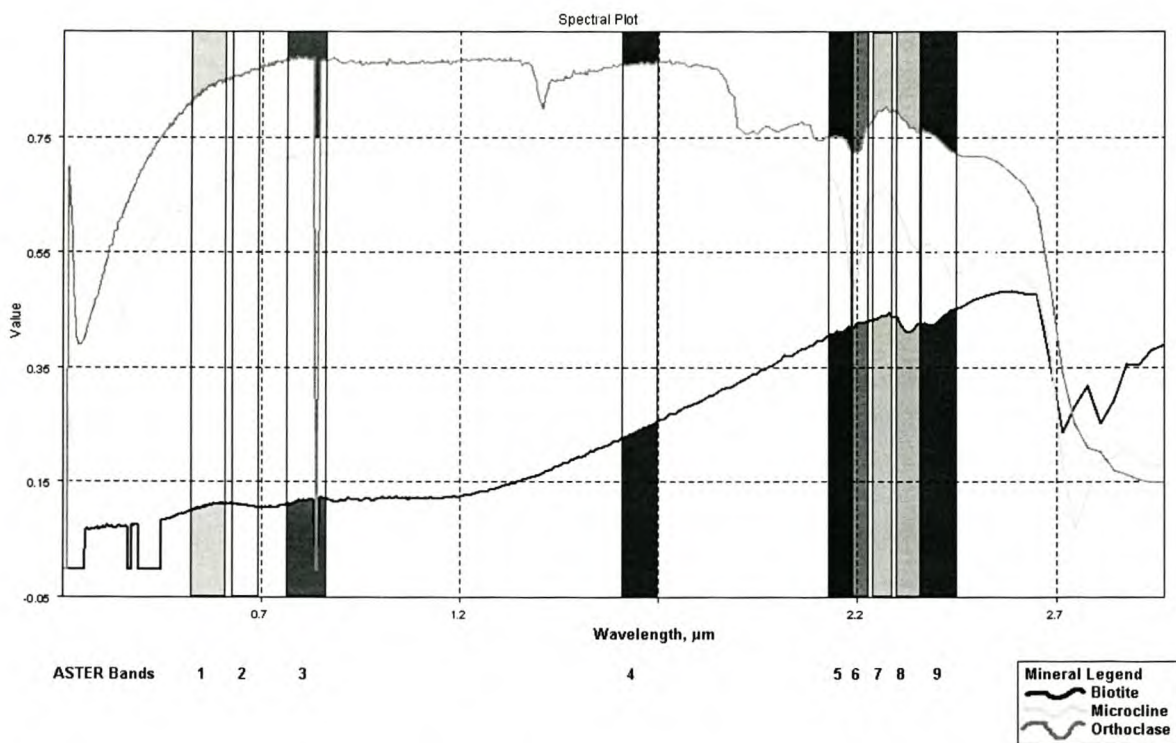


Figure 3e: Spectral signatures of potassic zone minerals positioned on the ASTER bands.

Iron oxide = 4/3

Ferruginous alteration is mapped using the ratio 4/3. The simple ratio is derived from the spectral signatures of iron-bearing minerals such as jarosite, hematite and limonite. The

spectral curves indicate iron has an absorption feature in band 3 and is highly reflective in band 4. A division of band 4 over 3 therefore tends to accentuate the occurrence of iron-bearing minerals. A study of the spectral curves will indicate that iron will also show values with ratios of B8/B7 and B5/B7, but these ratios have been avoided deliberately in the derivation since calcite will also respond to the ratios. A 4/3 ratio will differentiate the iron-bearing minerals from the calcite, since calcite has a relatively flat spectral response from band 1 to 4. The iron oxide image ratio is subjected to the software defoliant technique to remove spectral interference from clay minerals in section 3.3.2. The overall result for the iron ratio image is shown on 3.8.

Spectral signatures for ferrigenous minerals superimposed on the ASTER bands

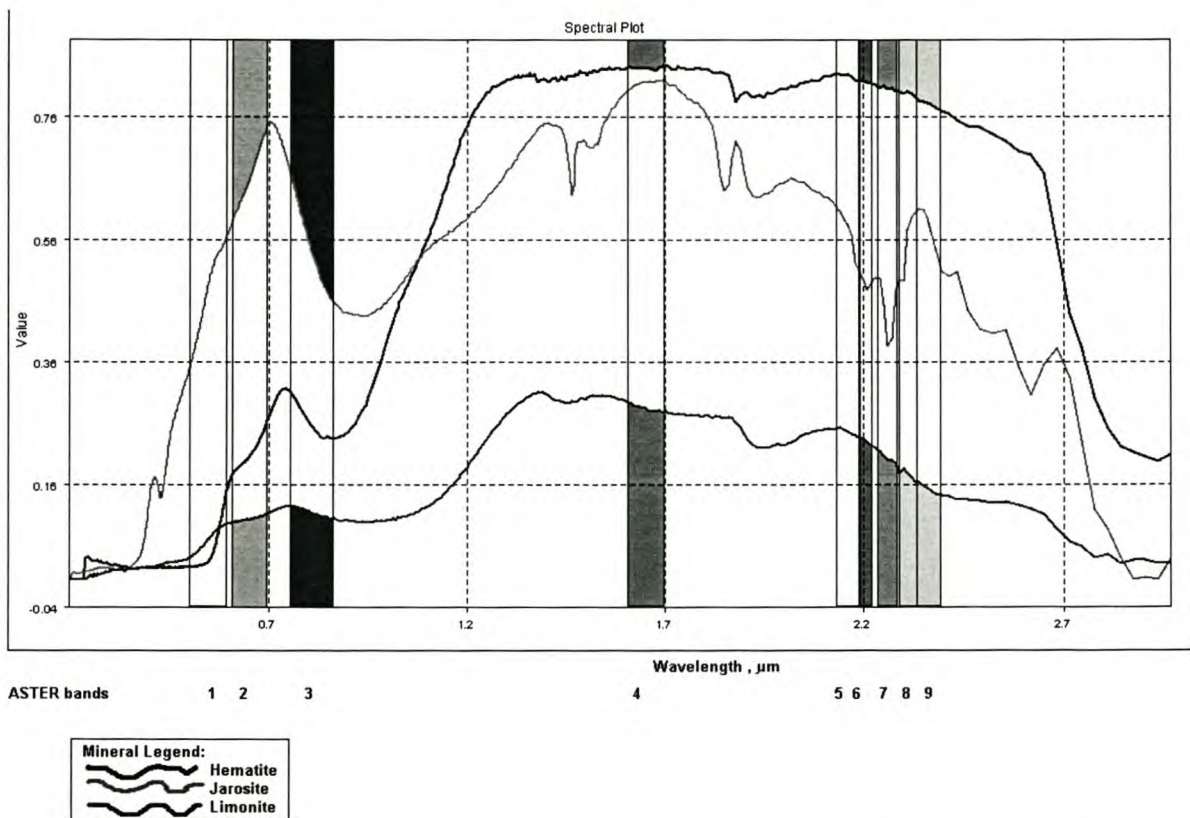


Figure 3f: Spectral signatures of ferrigenous minerals positioned on the ASTER bands.

### 3.3.2 Application of the software defoliant technique for analysis of band ratios

The software defoliant technique is a variant of a directed principal component analysis, which is done on two band ratios. This image-enhancement technique is done to further improve the results of band ratios, which often experience spectral interference from other materials. The selection of input ratio images is based on the fact that one band ratio contains information related to the other component of interest. For example, the spectral responses of hydroxyl clay minerals such kaolinite may experience interference from the spectral response of iron oxides, which are also highly reflective in band 4. The second band ratio contains

information about the spectrally interfering component. Input band ratios should be computed from unstretched data which must then be equalized (Fraser & Green, 1987). The Principal Component (PC) that has loadings of similar signs on both input band ratios images indicates the variance due to similarities in the spectral responses of the interfering component and the component of interest. The other PC, whose loadings are of different signs on either of the two input band ratio images, indicates contributions unique to each of the components. Positive loadings indicate target minerals that show out as bright pixels, while negative loadings imply dark pixels in the component of interest.

The software defoliant technique is applied to the 4/3 iron oxide ratio, the 7/3 biotite ratio and the 4/1 quartz ratio to minimize the spectral interference from kaolinite bearing clay minerals with a 4/6 band ratio.

Table 3.1 Directed principal component analysis of the quartz and kaolinite band ratios for quartz detection by the software defoliant technique.

Principal component	Eigenvector	
	Quartz Ratio : 4/1	Kaolinite Ratio : 4/6
PC1	<b>0.997</b>	<b>-0.072</b>
PC2	0.072	0.997

The results for the directed Principal Component Analysis for the detection of quartz using band ratios 4:1 and 4:6 are shown in Table 3.1. The kaolinite component PC 2 has positive loading in both input ratio images. The high positive eigenvector loading in PC 1 on the quartz ratio suggests that the quartz is mapped as bright pixels in the PC 1 mineral image (Figure 3.8).

Table 3.2 Directed Principal Component Analysis of the biotite and kaolinite band ratios for potassic-biotite alteration detection by the software defoliant technique.

Principal component	Eigenvector	
	Biotite Ratio : 7/3	Kaolinite Ratio: 4/6
PC1	<b>0.984</b>	<b>-0.177</b>
PC2	0.177	0.984

The results for the directed Principal Component Analysis for the detection of biotite using band ratios 7:3 and 4:6 are shown in Table 3.2. The kaolinite component PC 2 has positive

loading in both input ratio images. The high positive eigenvector loading in PC 1 on the biotite ratio suggests that the biotite is mapped as bright pixels in the PC 1 mineral image (Figure 3.9).

Table 3.3 Directed Principal Component Analysis of the iron oxide and kaolinite band ratios for ferrigenous alteration detection by the software defoliant technique.

Principal component	Eigenvector	
	Iron oxide Ratio : 4/3	Kaolinite Ratio :4/6
PC 1	0.169	0.986
PC 2	<b>0.986</b>	<b>-0.169</b>

The results for the directed principal component analysis for the detection of iron oxide using band ratios 4:3 and 4:6 are shown in Table 3.3. The kaolinite component PC 2 has positive loading in both input ratio images. The high positive eigenvector loading in PC 2 on the iron oxide ratio suggests that the iron oxide is mapped as bright pixels in the PC 2 mineral image in Figure 3.10.

### 3.4 Log residual technique

The log residual algorithm calibrates or models the observed radiance value for each image cell as a product of the surface reflectance, topographic factor and an illumination factor (Green & Craig, 1985). In automatic log residuals the pixels are first normalized to the same total energy; this removes or minimises albedo variations and topographic effects. The bands are then subjected to a transformation, which takes place in two steps; firstly the algorithm generates a band-to-band addition of the ASTER data and then it applies the log residual formula to the bands. This technique results in a transformed set of image bands, which is assumed to depict the lithologies of the exposed surface more accurately.

The modified log residual proposed by Lyon (1987) was implemented in this study and involves five steps:

- (a) Conversion of image to log basis
- (b) Calculation of the average of each band in step 1 (above);
- (c) Calculation of the average of each pixel;
- (d) Subtraction of the band average (step b) and the pixel average (step c) from the converted image (step a);
- (e) Calculation of the exponential of step d (above).

### **3.4.1 Selection of bands for the log residual technique**

The log residual technique was applied to all the six SWIR bands. The selection of the six SWIR bands is based on the study of the spectral characteristics of the targeted minerals, which are clays, chlorites, epidote, carbonates and sulphates minerals. These minerals have distinctive diagnostic features in this region. All clays have a high reflectance in band 4 and diagnostic absorptive features in bands 5 and 6, whilst chlorites and carbonates have diagnostic absorptive features in band 8. These spectral features make it possible to give a distinct and discriminatory colour variation between the lithologies. The VNIR bands were not used in this process, because problems may be incurred with additive atmospheric effects. The TIR bands were not selected for this application, since there may be linear emissivity temperature relationships of the different minerals/lithologies.

### **3.4.2 Log residual results**

The results for the log residual technique are shown below. The results show a colourful image which indicates the concentration of clay alteration in the study area. Clays are bright red, orange and pink to yellow. The results indicate the overall clays in the area and are not specific in distinguishing the different clay minerals, but are very useful in determining the distribution of low-grade and high-grade alteration zoning. The results are also useful for general lithological mapping and can be calibrated with a reference geological map.

### **3.5 Crosta Technique (Feature-orientated Principal Component Analysis).**

Principal components analysis (PCA) is a multivariate statistical data compression technique that allows redundant or correlated data to be compacted into fewer bands, which results in a reduction in the dimensionality of the data (Crosta & Rabelo, 1993). The PCA is applied to the ASTER bands in order to extract specific diagnostic spectral responses that uniquely identify key end member minerals for used to map hydrothermal alteration zones (Crosta *et al.* 2003 ). The output bands from a PCA are non-correlated and independent, and are often more interpretable than the original data. The first principal component accounts for as much of the variability in the data as possible, and each succeeding component accounts for as much of the remaining variability as possible. The technique involves the selection of uncorrelated linear combinations (eigenvector loadings) of variables in such a way that each successively extracted linear combination called the principal component (PC) has a smaller variance (Jensen, 2000).

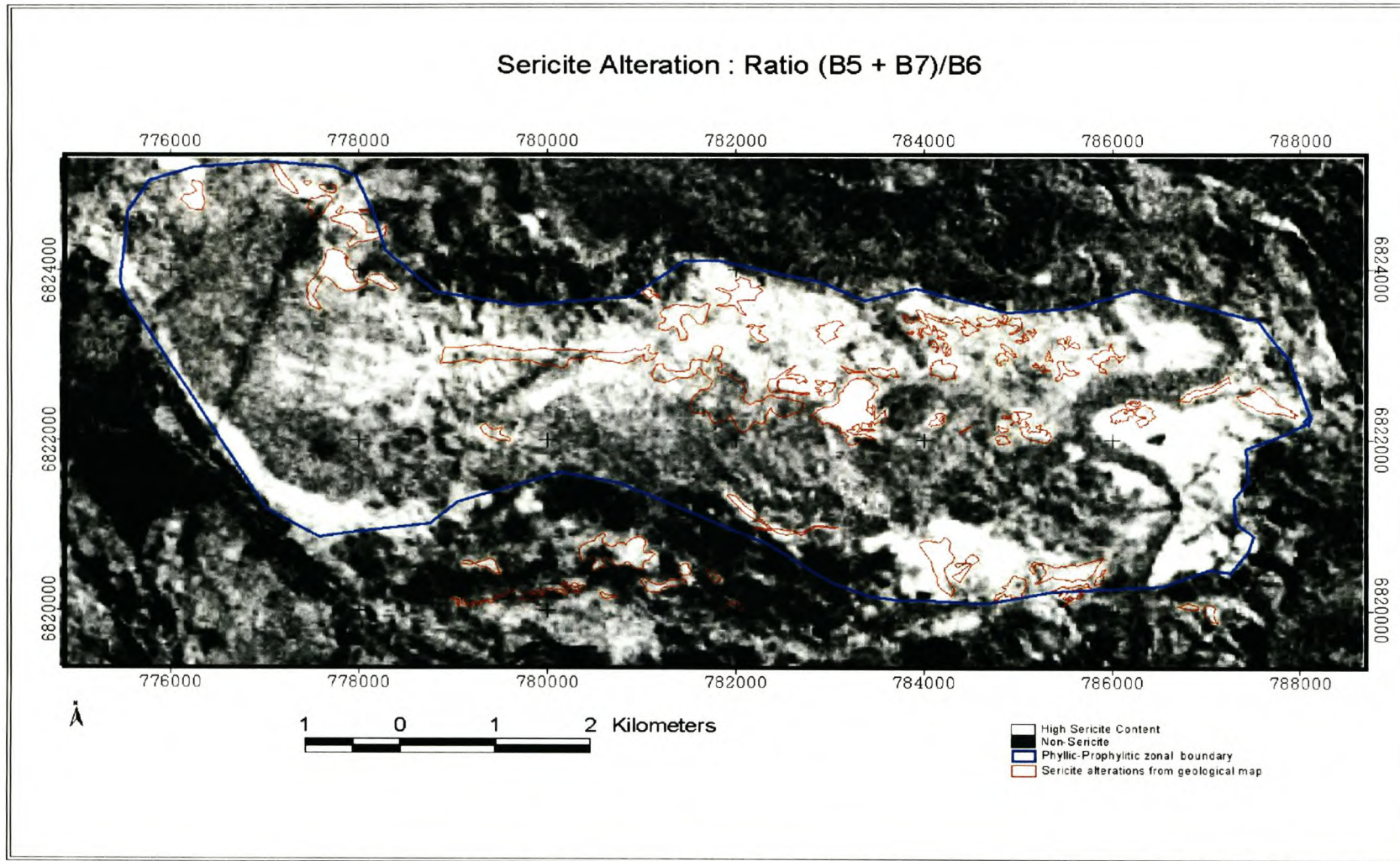


Figure 3.4: Sericite alteration ratio.

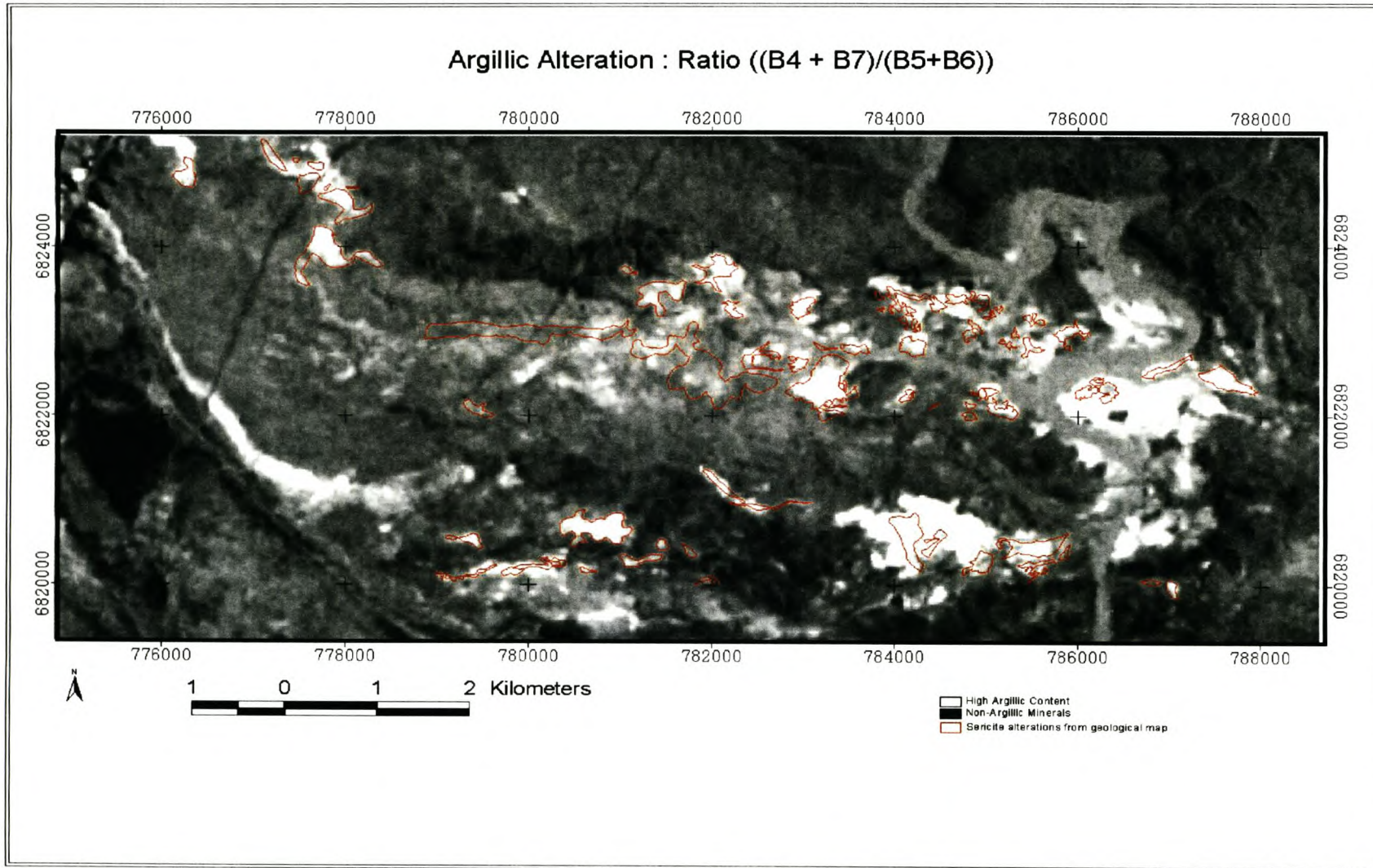


Figure 3.5: Argillic alteration ratio.

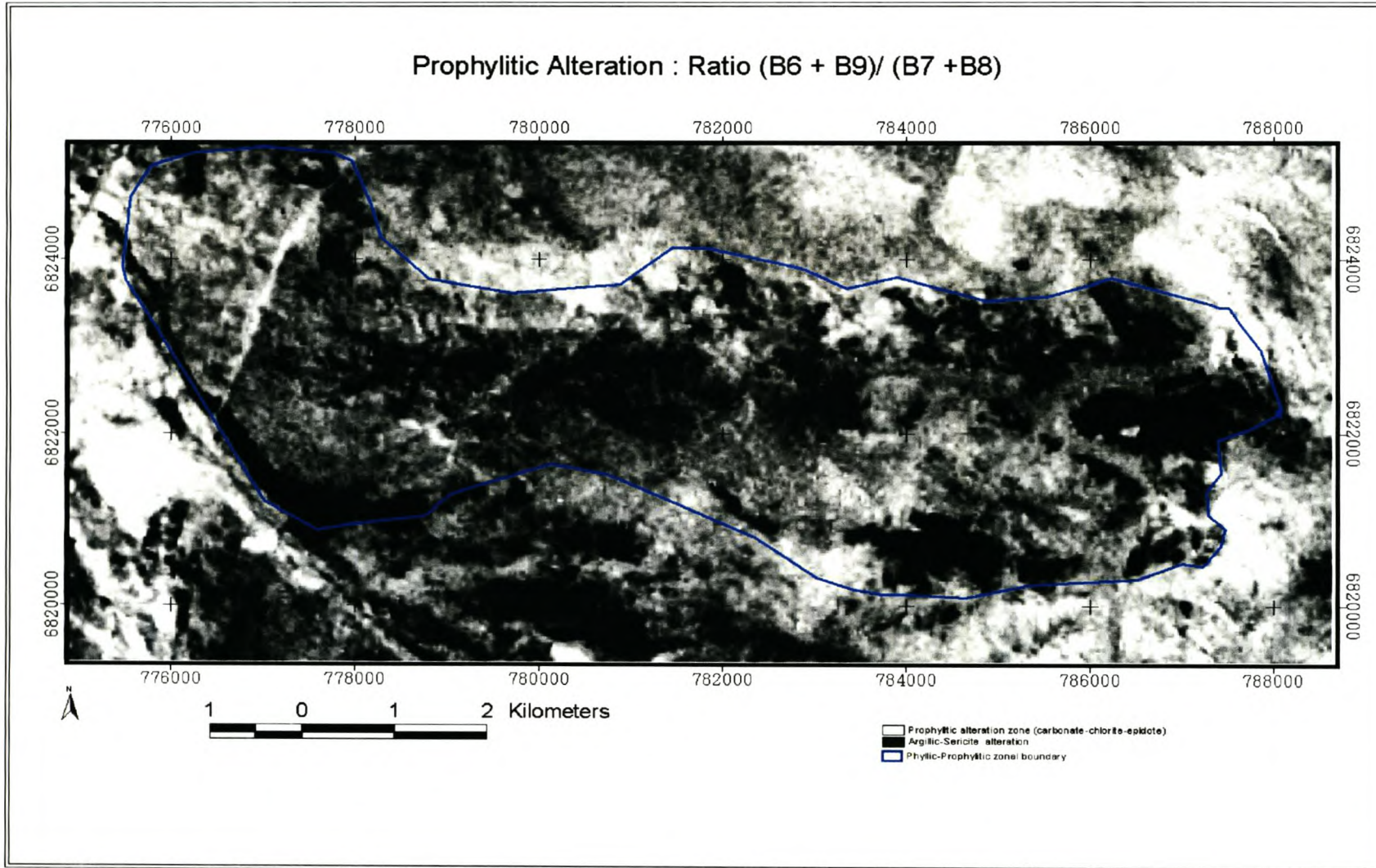


Figure 3.6 Prophylic alteration ratio.

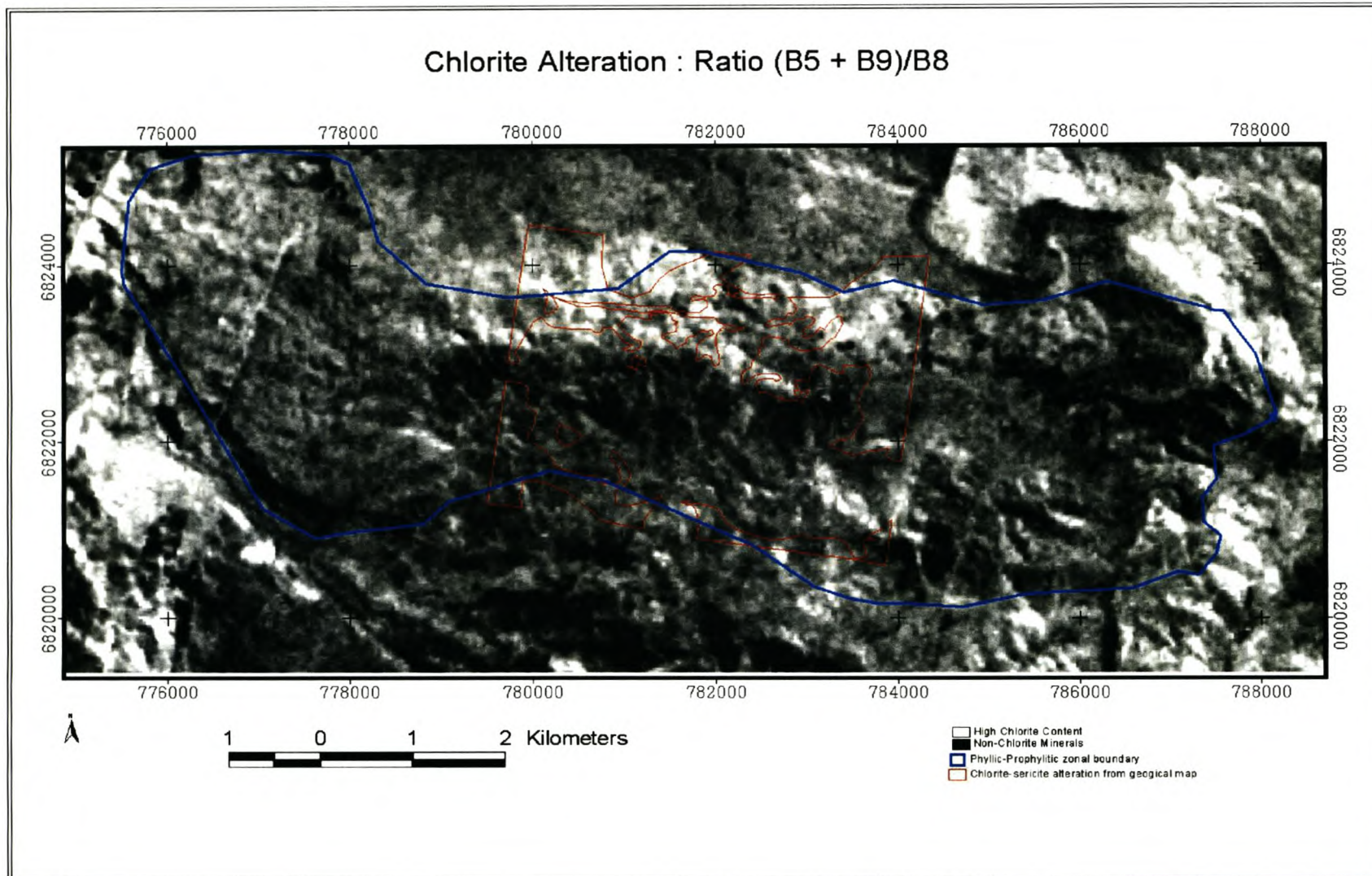


Figure 3.7: Chlorite alteration ratio.

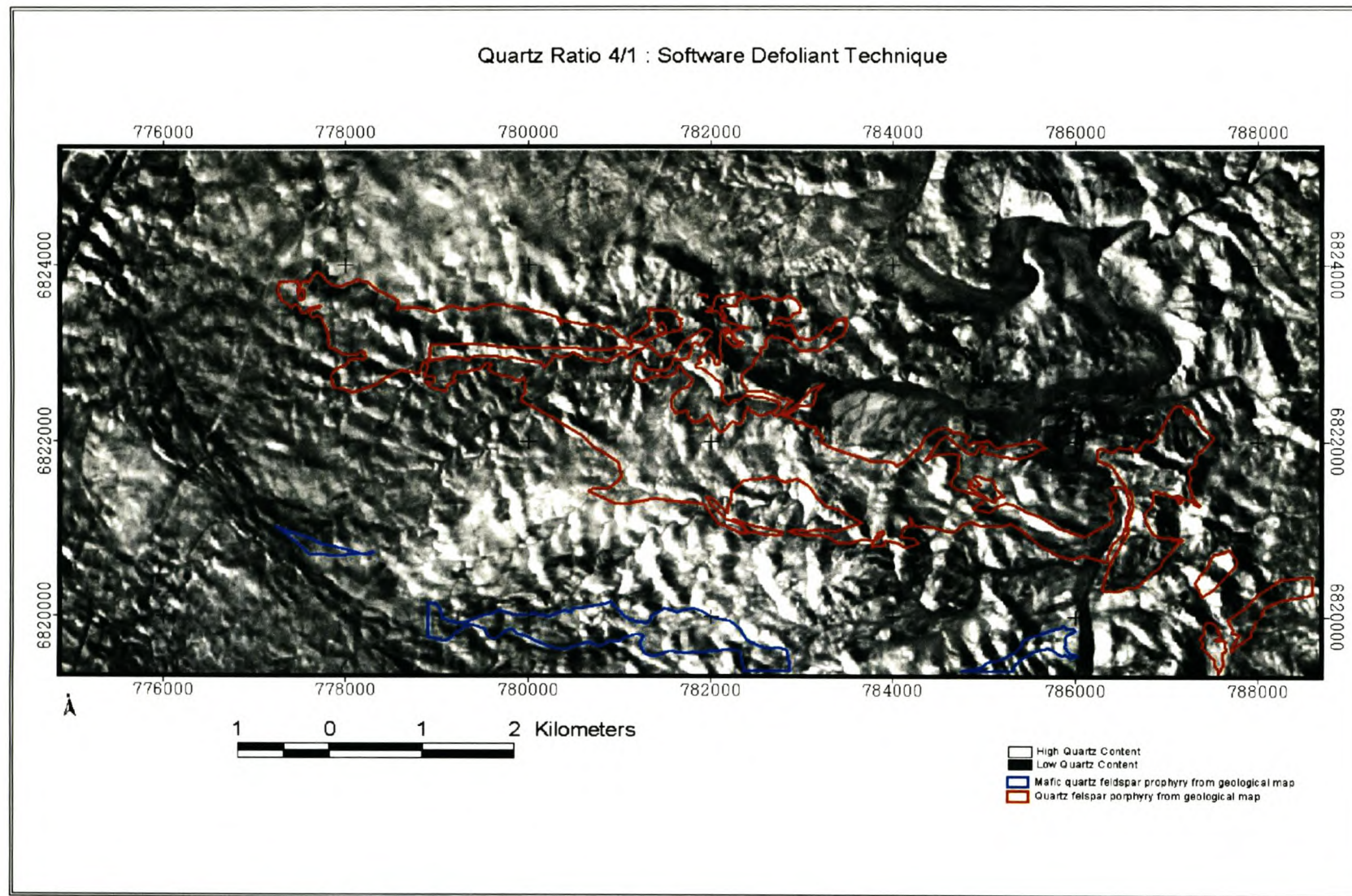


Figure 3.8: Quartz ratio subjected to the software defoliant technique.

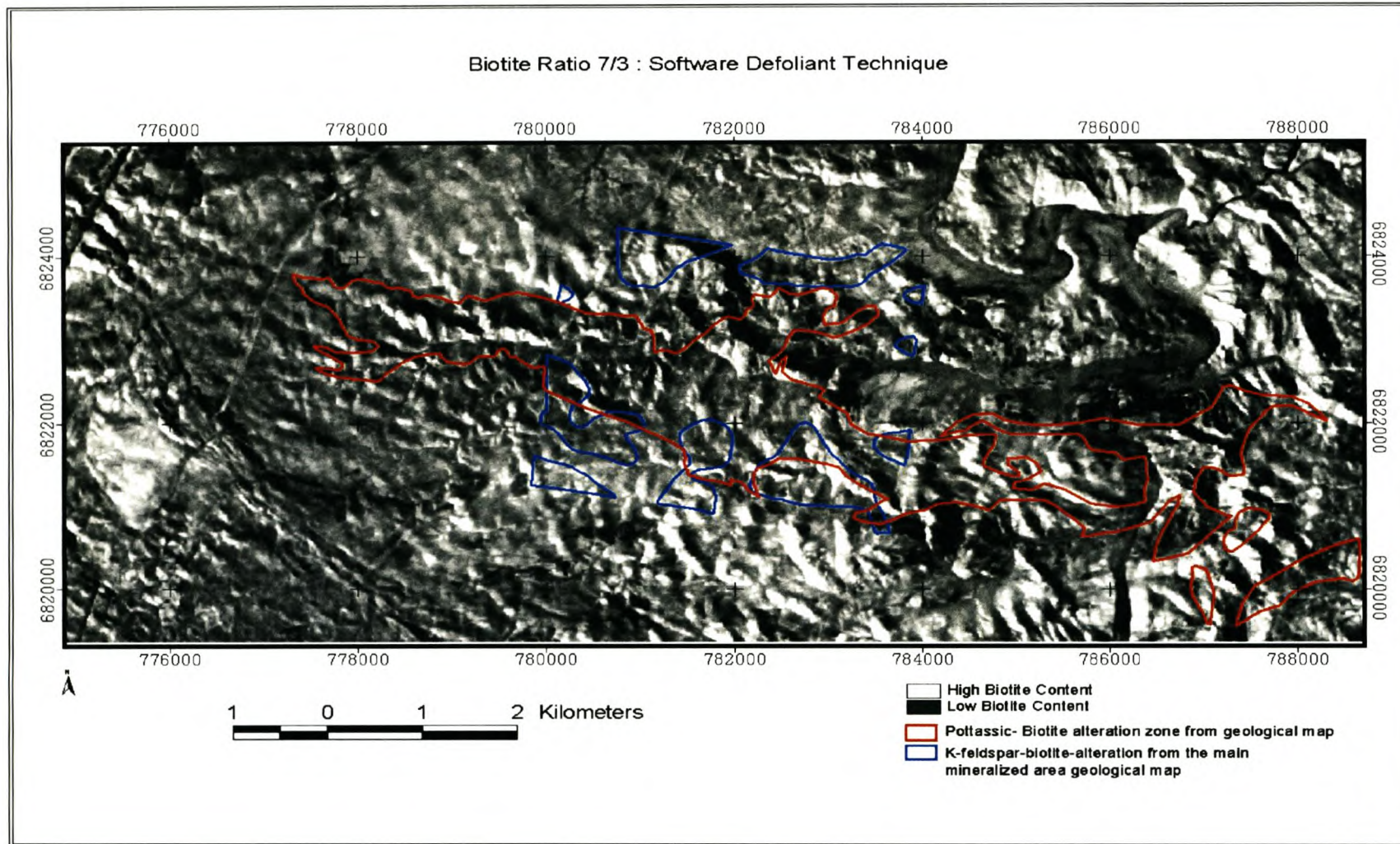


Figure 3.9: Biotite ratio subjected to the software defoliant technique.

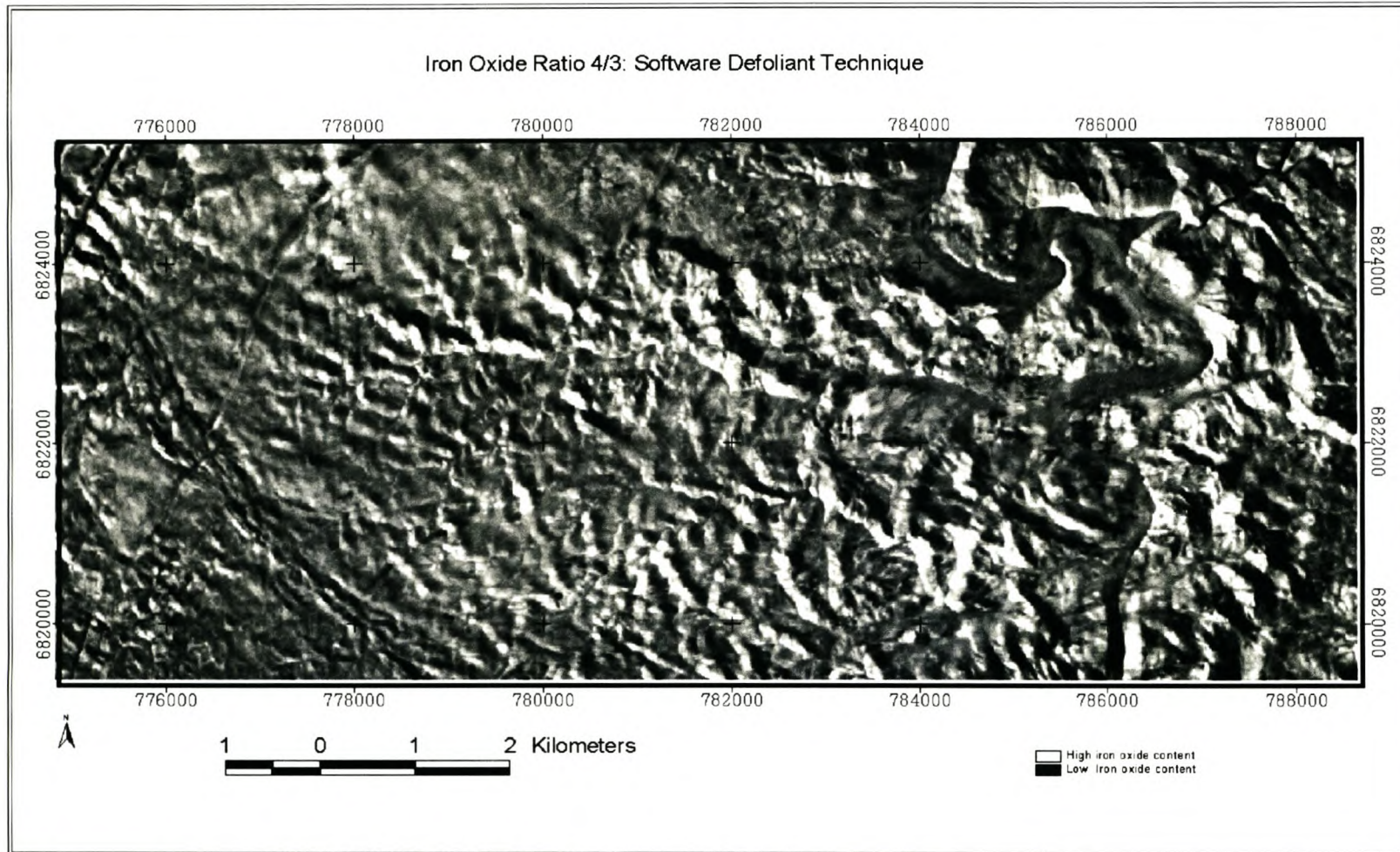


Figure 3.10: Iron oxide ratio subjected to the software defoliant technique.

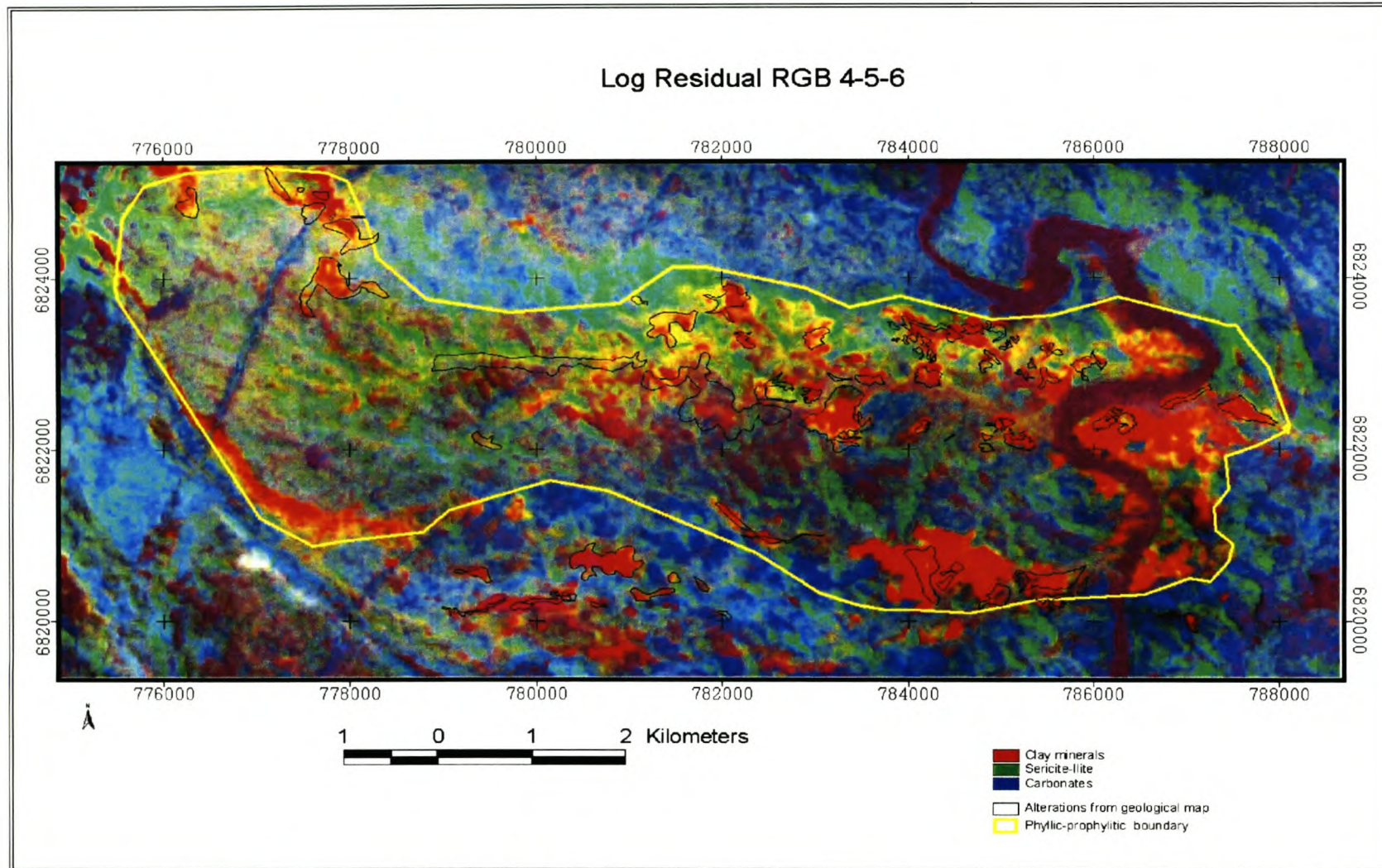


Figure 3.11: Log residual image for general alteration mapping.

In geological remote sensing the statistical variance of multispectral images is related to the spectral responses of the surficial mineralogy and the PCA technique is used to suppress irradiance effects that characterize the bands, thus favourably enhancing the spectral reflectance features of the minerals. A modification of the Principal Component Analysis called the feature-orientated principal component selection (FPCS) establishes the relationship between the spectral responses of the target minerals and the numerical values extracted from the eigenvector matrix used to calculate the principal component (PC) images. The PC which contains the spectral information of the target is determined using this relationship and one is able to determine the digital numbers (DNs) of pixels containing the target minerals whether they have high (bright) or low (dark) values (Tangestani & Moore, 2000).

The Crosta technique is a modification of the feature-orientated principal component analysis developed by Loughlin (1991). Specific bands sets are selected before applying PCA separately to them to ensure that certain materials would be mapped and the spectral information from the target minerals are mapped into a single PC. The subsets of bands are selected on the basis of the spectral characteristic of the mineral end member to be mapped in the VNIR and SWIR portions of the spectrum (Crosta *et al.*, 2003). The reduction in the number of input bands is done to avoid spectral interferences from other materials; this in turn enhances the chances of defining a unique PC for a specific mineral class.

### **3.5.1 Band selection and criterion for the identification of PCs carrying the target mineral**

The subset of bands is selected on the basis of the spectral characteristic of the mineral end member to be mapped in the VNIR and SWIR portions of the spectrum. In this research the selection of bands was based on identification of two diagnostic reflective features and two diagnostic absorptive features for each end member subjected to PCA for a subset of four bands and a similar criterion is applied for a subset of six bands, where bands in three diagnostic reflective features and three absorptive features are selected. The premise of such selection is to ensure band spectral contrast, which makes identification of the PC carrying the spectral information for the target mineral easy. Loughlin (1991) proposes that the PC that contains the target spectral information shows the highest eigenvector loadings, but should have opposite signs (+ or -), which indicates the eigenvector loadings will be from diagnostic reflective and absorptive bands. PC 1 accounts for more than 90% of the variance and maps

albedo, and is therefore not considered in the selection of the PC containing the targeted spectral information.

### **3.5.2 Application and selection of end members to be subjected to the Crosta technique**

Biotite has been chosen to represent the potassic-feldspar biotite core due to its diagnostic spectral features. Orthoclase has a flat spectral signature, which makes it unsuitable for this purpose. Bands 1-3-7-8 were selected as the subset to be subjected to the PCA. This is because biotite is highly reflective in bands 1 and 7 and absorbs strongly in bands 3 and 8.

Chlorite is selected on the basis that it is indicative of the prophyllitic zone if found in larger concentrations. Bands 2-5-8-9 have been selected as subset to be subjected to a PCA. This is because chlorite is strongly absorbing in bands 8 and 2, highly reflective in band 5 and has reflective features in band 9, which contrasts with the deep diagnostic absorptive feature in band 8. Band 4 has deliberately been eliminated to avoid mapping hydroxyl minerals. Chlorite has similar spectral characteristics to epidote, which is also mostly found in the prophyllitic zone. This implies that the PC which carries chlorite, will also contain proportions of epidote. Chlorite and epidote are found in abundance in the prophyllitic zone.

Carbonates are also major constituents of the prophyllitic zones and are comprised mainly of calcites and dolomites. Calcite and dolomite have slight spectral variation, although they have a similar diagnostic absorptive feature in band 8 and high reflectance in band 6. Bands 4-6-8-9 have been selected to map out calcites, where bands 4-6-9 are all reflective peaks and only band 8 has an absorptive feature. A subset of 5-6-7-8 was selected to map out dolomite using the Crosta technique. The total carbonate composition was computed by subjecting the two selected PCs containing calcite and dolomite to a pairwise principal component analysis and selecting the one PC with the total carbonate composition.

Hydroxyl-bearing minerals such as kaolinite, montmorillonite, illite and alunite are abundant in the phyllic, argillic and potassic zones. Targeting hydroxyl-bearing minerals will therefore highlight alteration zones in general. A study of the spectra for the hydroxyl-bearing mineral species indicates that all the minerals are highly reflective in band 4 and all are absorbing in band 9. Six bands are selected on this basis to map out the hydroxyl-bearing minerals. Bands 1-2-4-5-7-9 were subjected to principal component analysis. Elimination of band 8 from the selection eliminates the carbonates and chlorites, which have diagnostic spectral features in that band. The PC the contains most of the hydroxyl mineral should have high eigenvector

loadings in band 4 and 9, which are of opposite signs since these two bands have similar features for all hydroxyl minerals.

Sericite has been selected to the representative end member for the phyllic alteration. Sericite-illite-smectite-muscovite group minerals are spectrally similar and difficult to discriminate. Bands 3-5-6-7 were selected to map sericite. Bands 5 and 7 are highly reflective, whilst sericite shows absorption in bands 6 and 3. Band 4 has been deliberately avoided, since it is highly reflective for all hydroxyl minerals.

Kaolinite has been selected to map out the argillic alteration and will be representative of all the kaolinite group members such as dickite. The argillic alteration zone are kaolinite rich, but it is crucial to note that kaolinite is pervasive from the potassic zone, argillic zone and phyllic zone, and will therefore act as indicator of possible hydrothermal alteration in general. Bands 1-4-6-7 were selected to map kaolinite. Kaolinite has high reflectance features in bands 4 and 7 and is strongly absorptive in bands 6 and 1.

Alunite has been selected to map out argillic alteration. Bands 1-3-5-7 have been selected as subset to be subjected to principal component transformation. Bands 3 and 7 are highly reflective and bands 1 and 5 are strongly absorbing.

Illite is stable in the argillic zone and it is spectrally similar to sericite and its selection is meant to assist in the mapping of the Al-OH-bearing mineral species (muscovite-illite-Al smectite). Bands 1-3-5-6 are the illite subset subjected to principal component analysis. Bands 5 and 1 and have absorptive features in bands 6 and 3.

Kaolinite and smectite can be mapped together using selective bands 3-4-6-7, which are then subjected to principal component analysis. Bands 3 and 6 have absorptive features for kaolin/smectite and bands 4 and 7 are highly reflective.

Ferrigenous minerals such as hematite, goethite and jarosite are indicators of alteration and develop over porphyry copper deposits. At the Haib copper prospect the presence of ferrigenous alteration has been attested. Bands 2-3-7-8 were selected as subset to be subjected to principal component analysis. The rationale is based on the fact that iron is highly reflective in bands 2 and 8; band 4, where it has its highest reflectance, is deliberately avoided

to prevent the inclusion of hydroxyl minerals, which also have high reflectance in this band. Band 3 has a diagnostic absorptive feature, whilst band 7 also indicates some absorption.

### 3.5.3 Crosta Techniques results

The results for the Crosta technique are discussed in this section. The eigenvector statistics are tabulated and the PCs carrying the target minerals are selected. Selected PC images are displayed in layouts.

Table 3.4: Eigenvector statistics for mapping hydroxyl-bearing minerals

	PC1	PC2	PC3	PC4	PC5	PC6
Band 1	0.245	-0.573	0.102	-0.142	-0.746	-0.154
Band 2	0.312	-0.707	0.063	0.129	0.603	0.133
Band 4	0.622	0.182	-0.727	-0.023	-0.074	0.211
Band 6	0.391	0.244	0.512	0.575	-0.182	0.402
Band 7	0.407	0.189	0.128	0.174	0.149	-0.854
Band 9	0.369	0.206	0.422	-0.776	0.138	0.151
Eigenvalue (%)	66.73	24.96	6.51	0.95	0.63	0.22

PC 3 indicates pixels that are likely to contain hydroxyl-bearing minerals represented by low (dark) reflectance values. This PC 3 has been selected because it has a high negative loading in band 4 of -0.727 and a high positive loading in band 6 of 0.512. Higher loadings in PC 5 contained in bands 1 and 2 are due to albedo and topographic effects. PC1 and PC 2 contains 91.7 % of the information from all bands, which is mostly on albedo and topographic effects. The PC shown in Figure 3.12 has been negated to show the anomalous concentrations of hydroxyl bearing clay minerals.

Table 3.5: Eigenvector statistics for mapping ferrigeous alteration minerals.

	PC 1	PC 2	PC 3	PC 4
Band 2	0.637	-0.230	0.719	-0.158
Band 3	0.698	-0.232	-0.662	0.142
Band 7	0.236	-0.686	-0.137	-0.674
Band 8	0.226	0.650	0.163	0.707
Eigenvalue (%)	82.71	15.38	1.65	0.26

PC 3 indicates pixels that are likely to contain ferruginous alteration such as jarosite, hematite and goethite, which will be represented as bright pixels. This PC has been selected because it carries a high positive loading in band 2 of 0.719 and a high negative loading of -0.662 in band 3. PC 3 will be able to contrast iron oxide minerals well because of their high reflectance in band 2 and strong absorption in band 3. The high loadings in PC 4 found in band 7 and 8 are due to calcite. Figure 3.13 shows the PC carrying ferruginous alteration minerals.

Table 3.6: Eigenvector statistics for mapping sericite-muscovite.

	PC 1	PC 2	PC 3	PC 4
Band 3	0.454	-0.889	0.058	0.004
Band 5	0.500	0.242	-0.162	-0.815
Band 6	0.529	0.320	0.737	0.273
Band 7	0.513	0.221	-0.654	0.510
Eigenvalue (%)	68.77	29.55	1.14	0.54

PC 3 indicates the pixels that contain sericite-muscovite, which are represented as bright pixels. The selection of PC 3 is based on the fact that sericite-muscovite is highly reflective in band 7 and strongly absorptive in band 6, which implies PC 3 will be able to contrast these two bands well, since it has a high positive loading in band 6 of 0.737 and a high negative loading in band 7 of -0.654. PC 4, which also has high loadings, carries information for a different mineral from sericite, since sericite is highly reflective in both bands 5 and 7 yet PC4 contrasts these bands by giving them opposite signs (- and +). Figure 3.14 shows PC 3 in bright pixels.

Table 3.7: Eigenvector statistics for mapping chlorite-epidote.

	PC 1	PC 2	PC 3	PC 4
Band 2	0.417	-0.908	0.022	0.034
Band 5	0.524	0.236	-0.737	0.355
Band 8	0.522	0.210	0.041	-0.826
Band 9	0.527	0.275	0.675	0.437
Eigenvalue (%)	69.15	28.02	1.90	0.94

PC 4 is more likely to contain chlorite and epidote based on a high negative loading in band 8 of -0.826 and a moderate to high positive loading in band 9 of 0.437 will be able to distinguish between chlorite and epidote effectively. A spectral study of the features of

chlorite and epidote indicates that these minerals have a diagnostic strong absorptive feature in band 8 and a moderate to high reflectance in band 9, which is testified by the values obtained from the PCA. Chlorite and epidote will show up as dark pixels and have been negated to display them as bright pixels in Figure 3.15.

Table 3.8: Eigenvector statistics for mapping calcite.

	PC 1	PC 2	PC 3	PC 4
Band 4	0.671	-0.714	0.100	0.170
Band 6	0.442	0.524	-0.727	0.027
Band 8	0.422	0.155	0.339	-0.825
Band 9	0.417	0.437	0.589	0.538
Eigenvalue (%)	87.80	10.15	1.49	0.56

PC 4 has been selected to show anomalous concentrations of calcite based on the fact that it contains the highest contrasting eigenvector loadings in band 8 of -0.825 and 0.538 in band 9. Calcite, which has a diagnostic strong absorption feature in band 8 and a high reflectance in band 9, will be distinguished effectively in PC 4. Calcite will be represented by dark pixels and has been negated to display it as bright pixels in Figure 3.16.

Table 3.9: Eigenvector statistics for mapping biotite:-potassic zone indicator.

	PC 1	PC 2	PC 3	PC 4
Band 1	0.535	-0.255	0.805	0.029
Band 3	0.743	0.311	-0.592	-0.018
Band 7	0.290	0.665	-0.007	0.688
Band 8	0.279	0.629	-0.040	0.725
Eigenvalue (%)	69.34	28.43	1.86	0.37

PC 3 was selected to indicate the anomalous amounts of biotite, which is used in this study as the indicator for the potassic-biotite rich core. The basis of selection of PC 3 is derived from the fact that this PC has the highest negative eigenvector loading in band 1 of 0.805 with a high positive loading in band 3 of 0.592. Biotite has a deep absorptive feature in band 3 and reflectance in band 1, which gives PC 3 a good contrast, which will be able to emphasize biotite. Biotite is shown in Figure 3.17 as very bright pixels.

Table 3.10: Eigenvector statistics for mapping illite-sericite.

	PC 1	PC 2	PC 3	PC 4
Band 1	0.280	0.604	0.071	-0.743
Band 3	0.272	0.695	-0.076	0.661
Band 5	0.540	-0.237	0.805	0.066
Band 6	0.745	-0.309	-0.585	0.086
Eigenvalue (%)	65.82	31.62	1.79	0.77

PC 3 contains anomalous illite concentrations; the basis of the selection is the high eigenvector loading of +0.805 in band 5 and high negative loading in band 6. Illite is highly reflective in band 5 and has a strong diagnostic absorption feature in band 6, which means loadings in these bands contained in PC 3 will effectively contrast and highlight the presence of illite. High loads in PC 4 contained in band 1 and 3 can be attributed to differences between the visible and very near infrared region as well as iron oxide enrichments. The PC 3 for illite is shown in Figure 3.18 as bright pixels.

Table 3.11: Eigenvector statistics for mapping alunite-argillic alteration zone.

	PC 1	PC 2	PC 3	PC 4
Band 1	0.536	-0.251	0.801	0.087
Band 3	0.743	-0.312	-0.587	-0.076
Band 5	0.274	0.646	0.095	-0.706
Band 7	0.292	0.649	-0.067	0.699
Eigenvalue (%)	66.02	31.09	1.86	1.03

PC 4 contains alunite concentrations due to the high opposite eigenvector loadings in bands 5 (-0.706) and 7 (+0.699). Alunite has a high diagnostic absorptive feature in band 5 and is highly reflective in band 7, which makes PC 4 suitable for showing the anomalous concentrations of alunite. High eigenvector loadings in PC 3 in bands 1 and 3 can be attributed to the differences between the visible and very near infrared regions. PC 4 containing alunite is shown in Figure 3.19 as bright pixels.

Table 3.12: Eigenvector statistics for mapping kaolinite-indicator argillic alteration zone.

	PC 1	PC 2	PC 3	PC 4
Band 1	0.196	-0.964	0.177	-0.006
Band 4	-0.733	0.033	-0.641	-0.224
Band 6	0.450	0.224	0.703	-0.504
Band 7	0.470	0.137	0.254	0.834
Eigenvalue (%)	75.63	16.30	7.69	0.38

PC 3 contains anomalous kaolinite concentrations; the selection of PC 3 is based on its high opposing eigenvector loadings in band 4 (-0.641), where kaolinite is highly reflective, and in band 6 (+0.703), where one of its doublet diagnostic absorptive features is centred. This PC will therefore be able to contrast and accentuate the anomalous concentrations of kaolinite. Kaolinite concentrations are shown in Figure 3.20 as bright pixels.

Table 3.13: Eigenvector statistics for mapping kaolin-smectite.

	PC 1	PC 2	PC 3	PC 4
Band 3	0.367	-0.922	0.122	-0.014
Band 4	0.702	0.197	-0.648	-0.221
Band 6	0.418	0.267	0.706	-0.505
Band 7	0.444	0.199	0.259	0.834
Eigenvalue (%)	69.98	23.06	6.63	0.33

PC 3 contains anomalous concentrations of kaolin-smectite; the selection of this principal component is based on the high opposing eigenvector loadings in band 4 (-0.648) and band 6 (+0.706). Kaolin-smectite, like kaolinite, is highly reflective in band 4 and strongly absorbing in band 6. PC 3 will be able to exhibit this spectral contrast between bands 4 and 6 effectively and hence highlight an abundance of kaolin-smectite. PC 3 shows kaolin-smectite as bright pixels in Figure 3.21.

### 3.5.4 Discussion of the Crosta Technique results

The results produced by the Crosta are relatively easy to interpret in that anomalous concentrations of each mineral category are represented by the brightest pixels on each image (after negation in some cases). There is no need to consult the eigenvector matrices after the images have been created to understand and interpret these images. If all the bands are utilized as input for the principal component analysis, reference to the eigenvector matrices will always be necessary. Images produced by the Crosta technique have another advantage in

that they can be added together to see the combined effect of two mineral end members in which pixels with anomalous concentrations of both minerals occur as bright pixels. A pairwise PCA can also achieve the same result. Colour composite can be utilized to visualise the mineral zonations according to individual preferences. Colour composites have been applied the mineral abundance images generated by the Crosta technique to establish the spatial association of the mineralized zones.

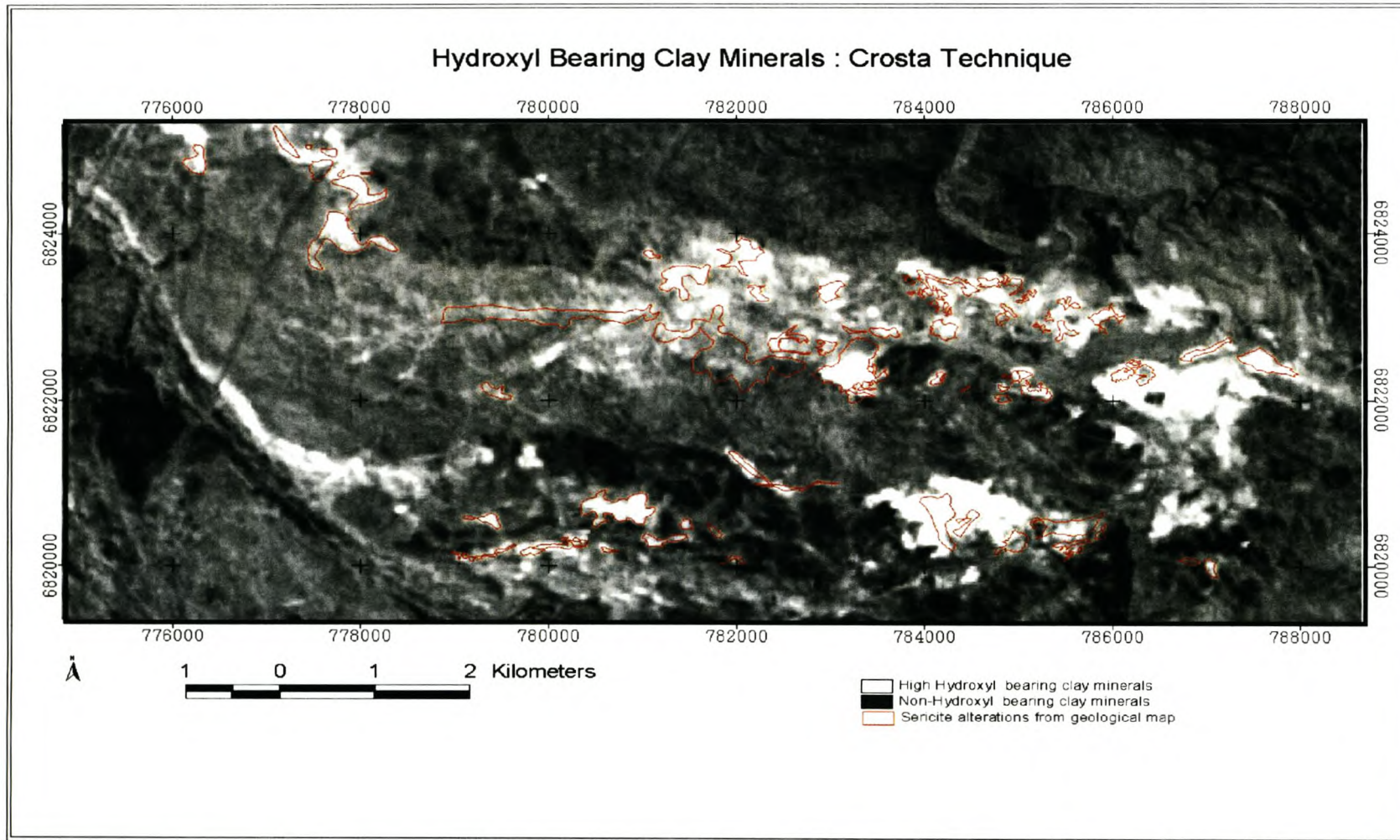


Figure 3.12: Hydroxyl bearing clay mineral: Crosta Technique.

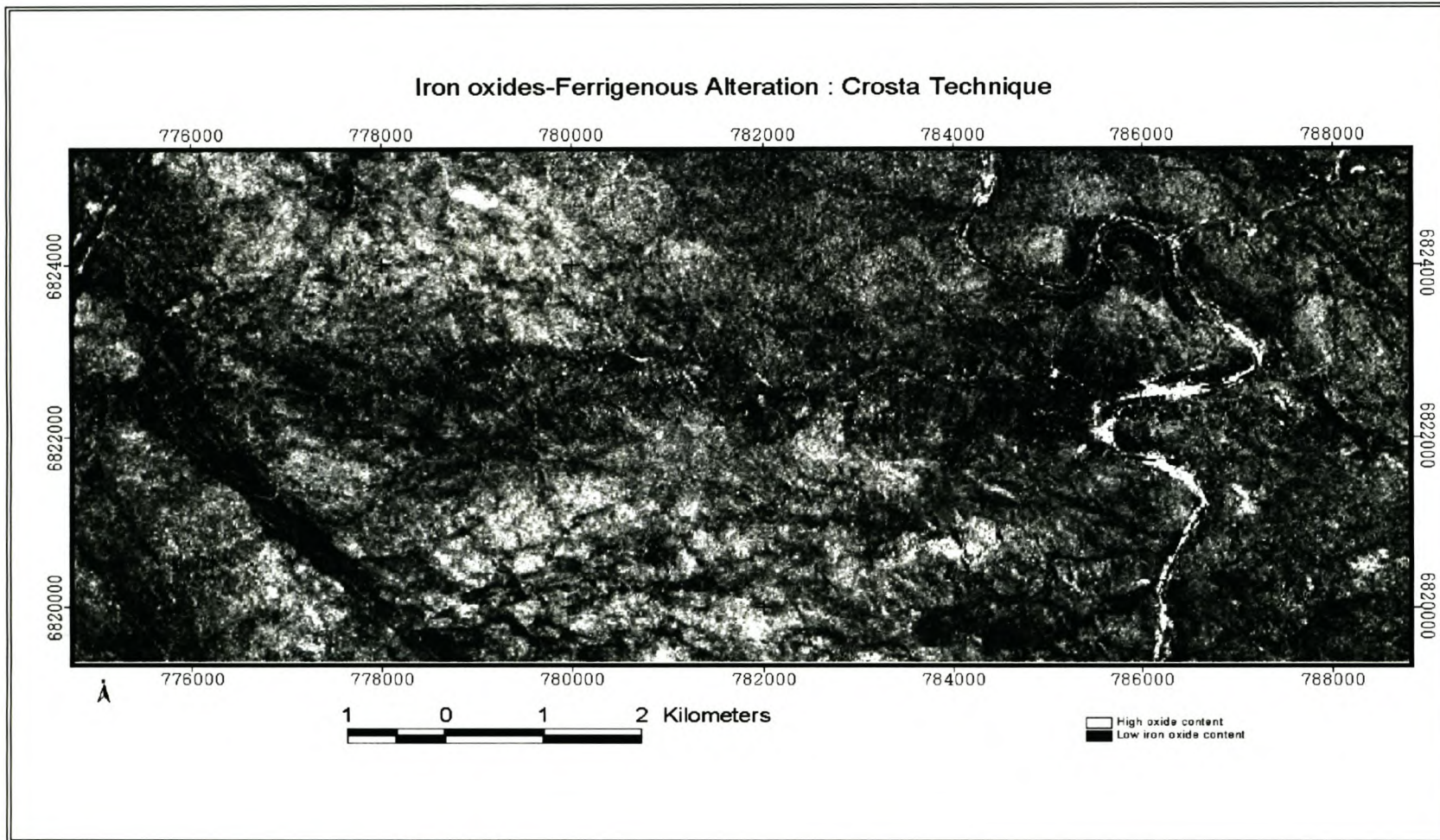


Figure 3.13 Iron oxides-Ferruginous alteration: Crosta Technique.

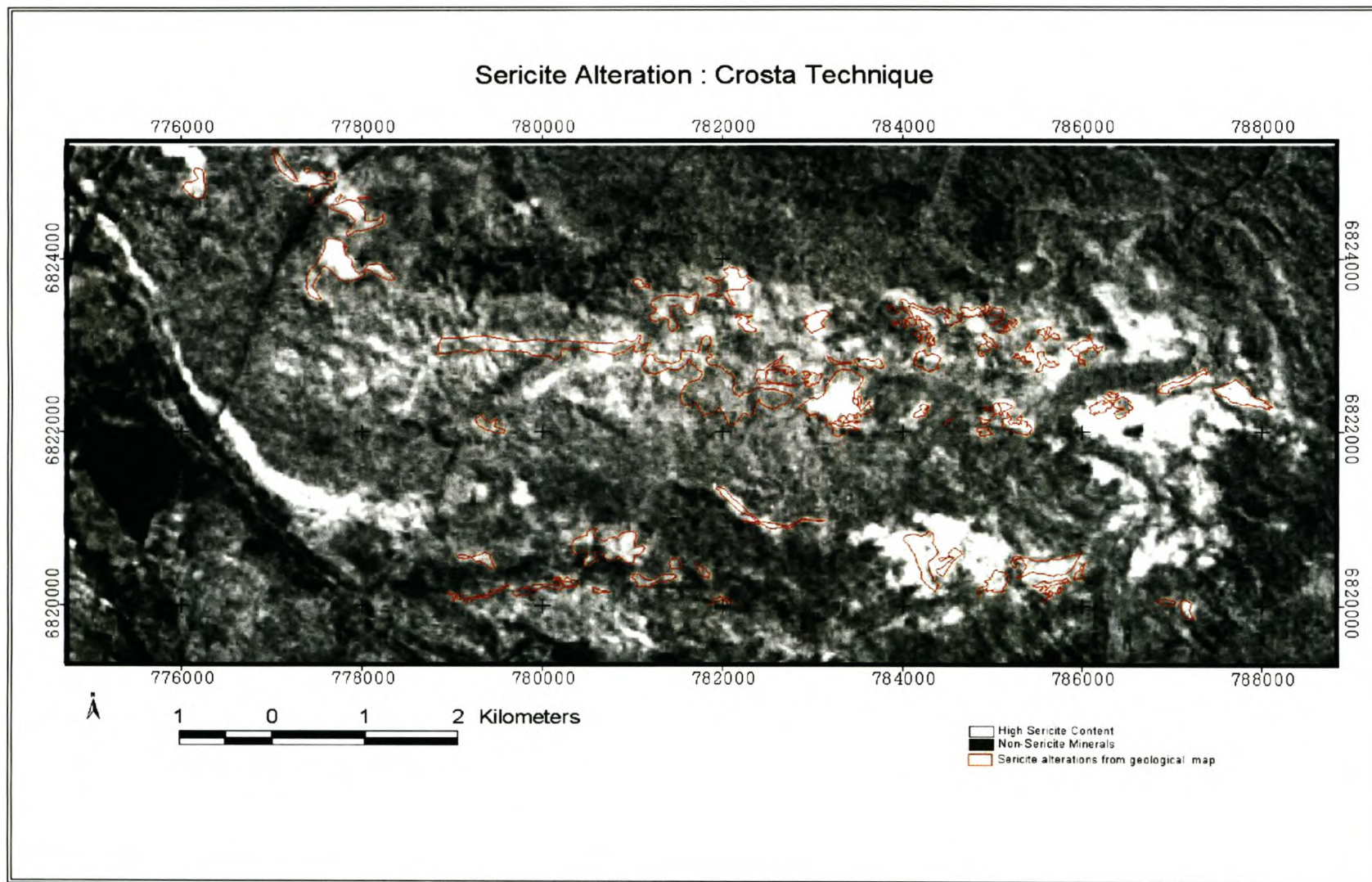


Figure 3.14: Sericite alteration: Crosta Technique.

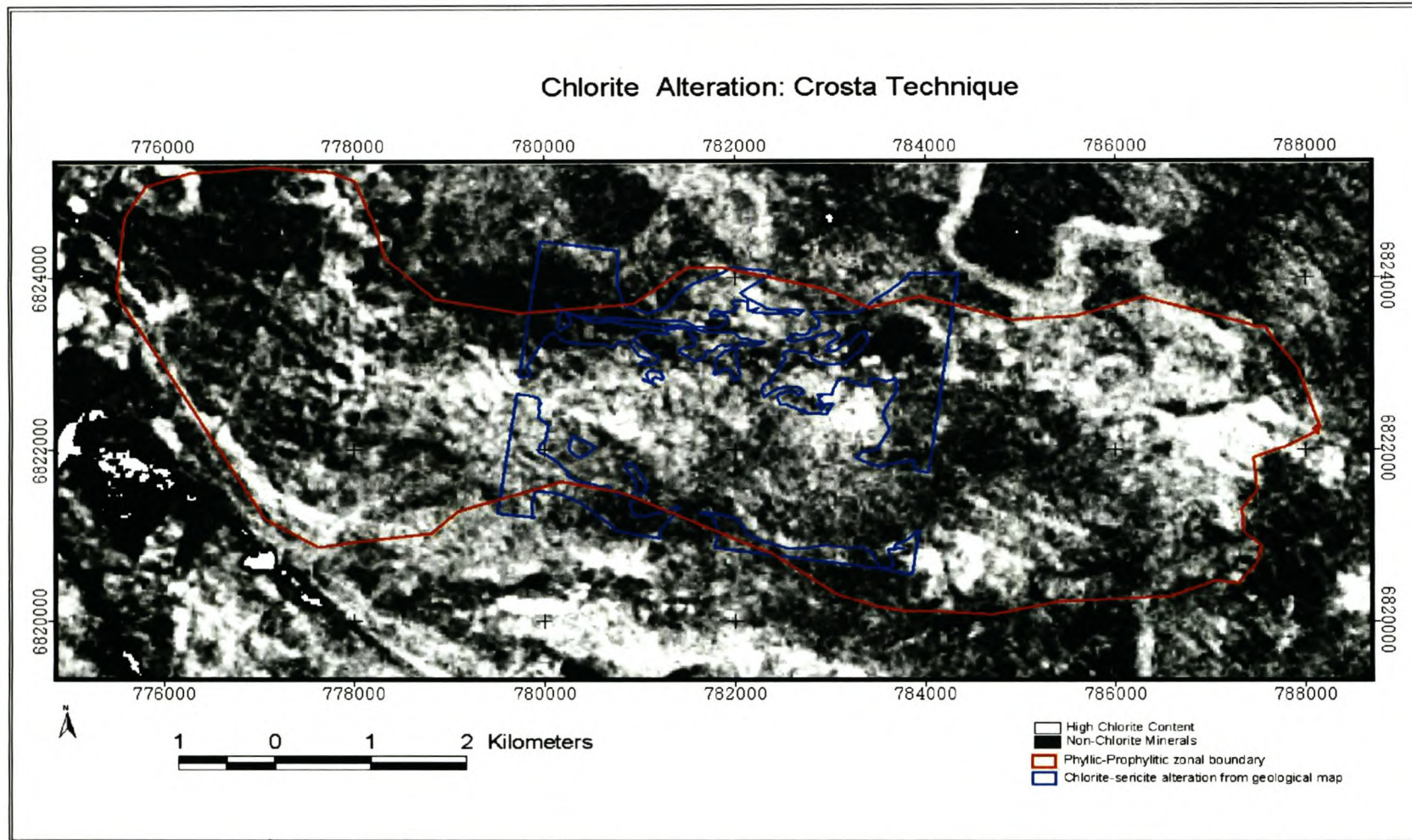


Figure 3.15: Chlorite alteration: Crosta Technique.

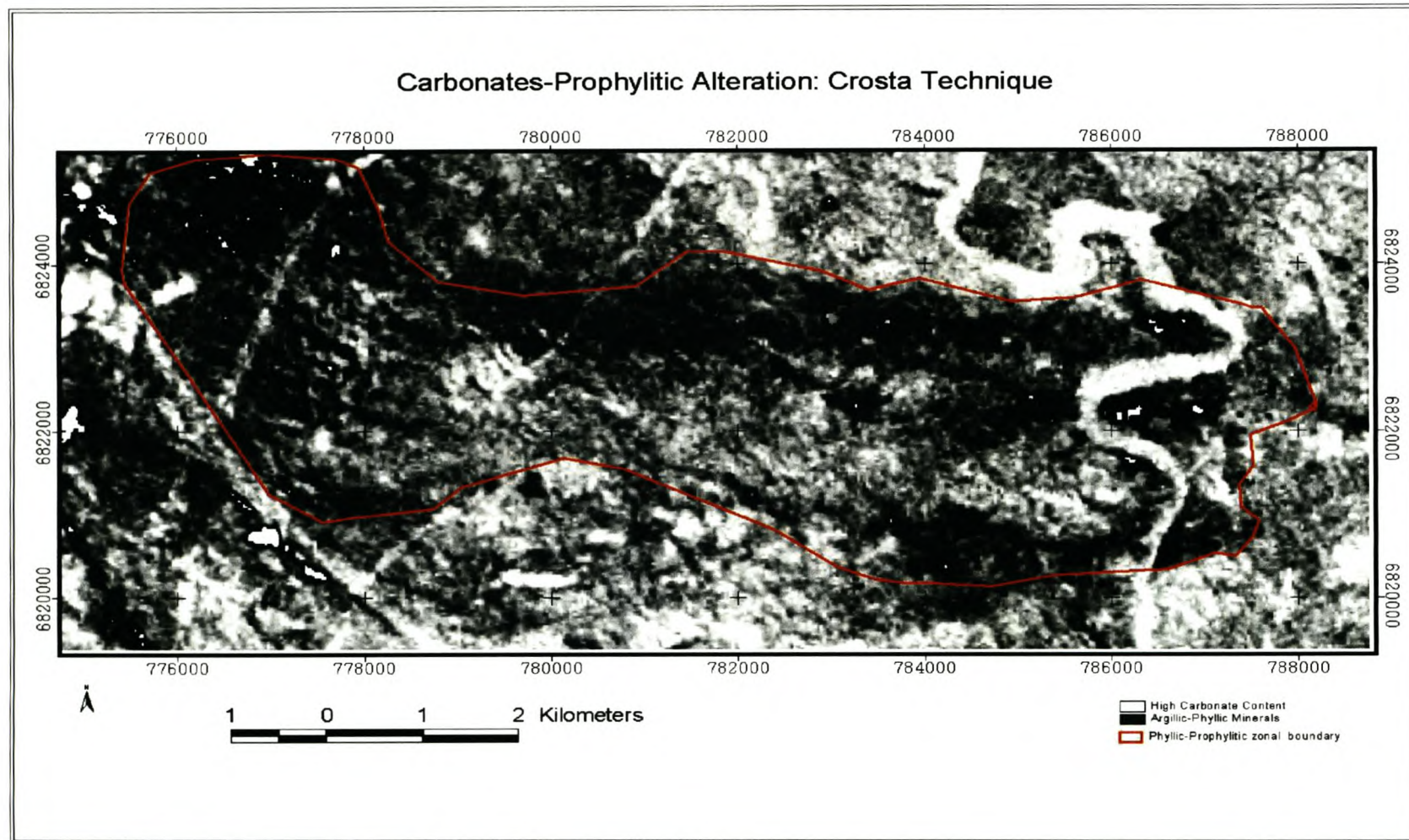


Figure 3.16 Calcite (carbonate): Crosta Technique.

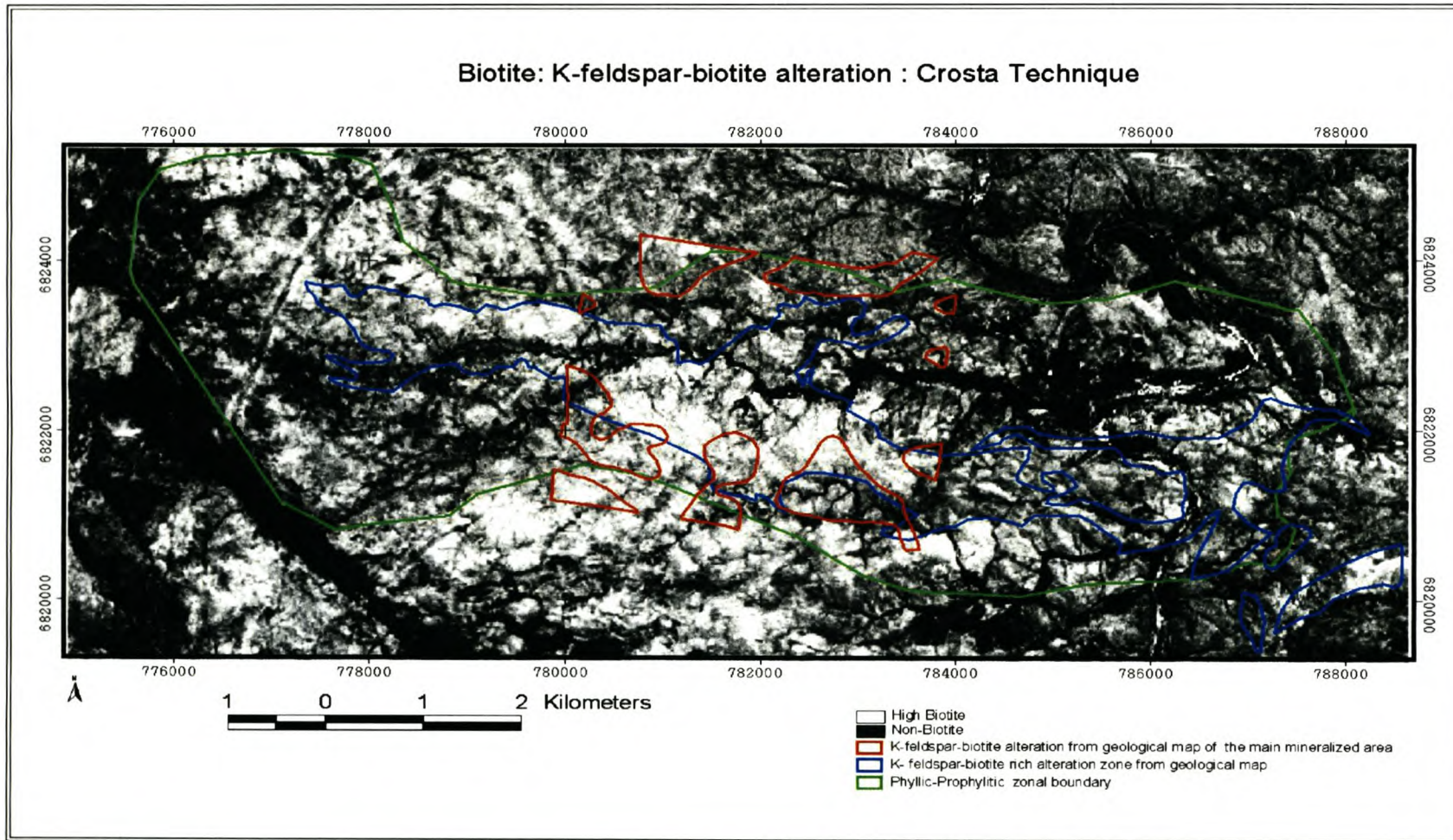


Figure 3.17: Biotite: Crosta Technique.

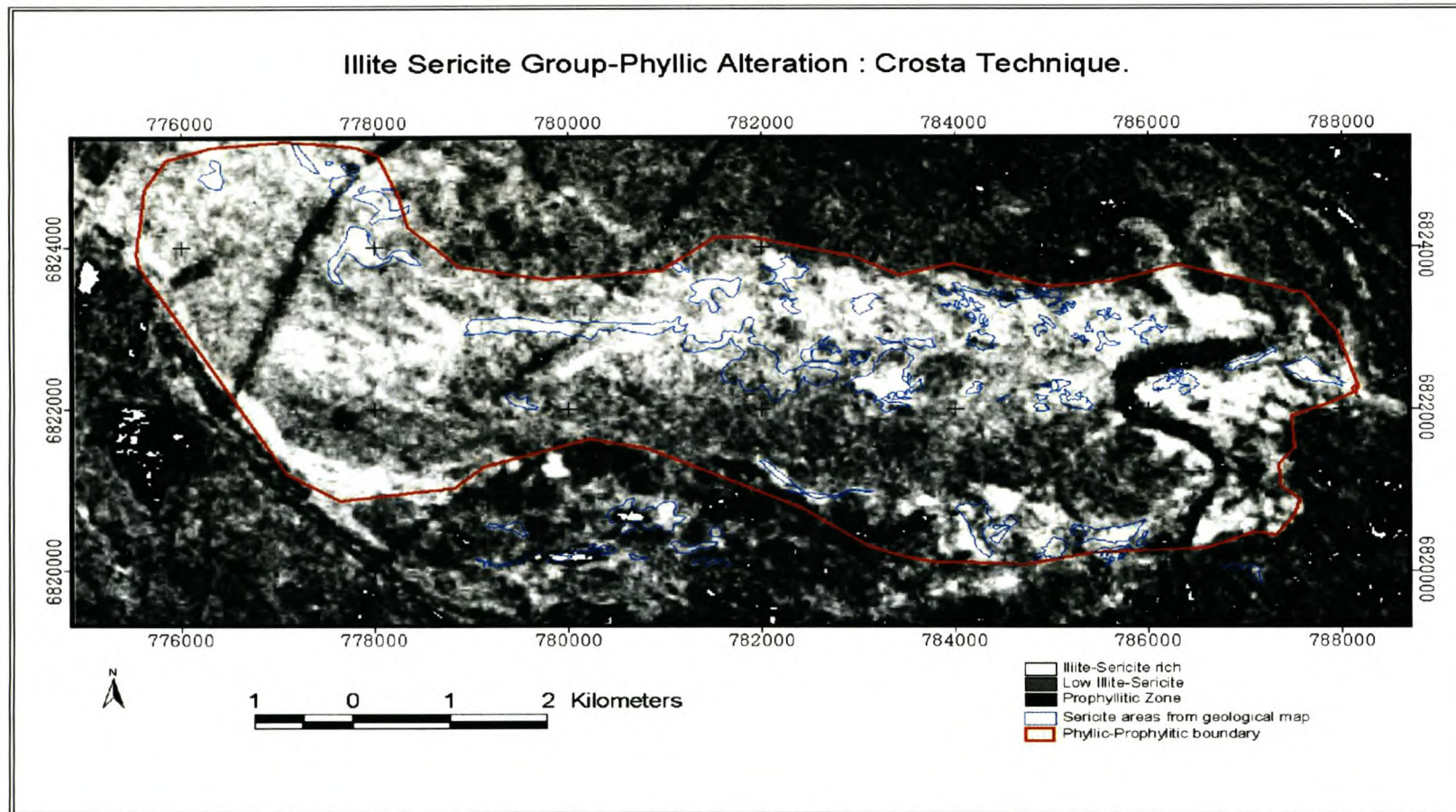


Figure 3.18 Illite-sericite group: Crosta Technique.

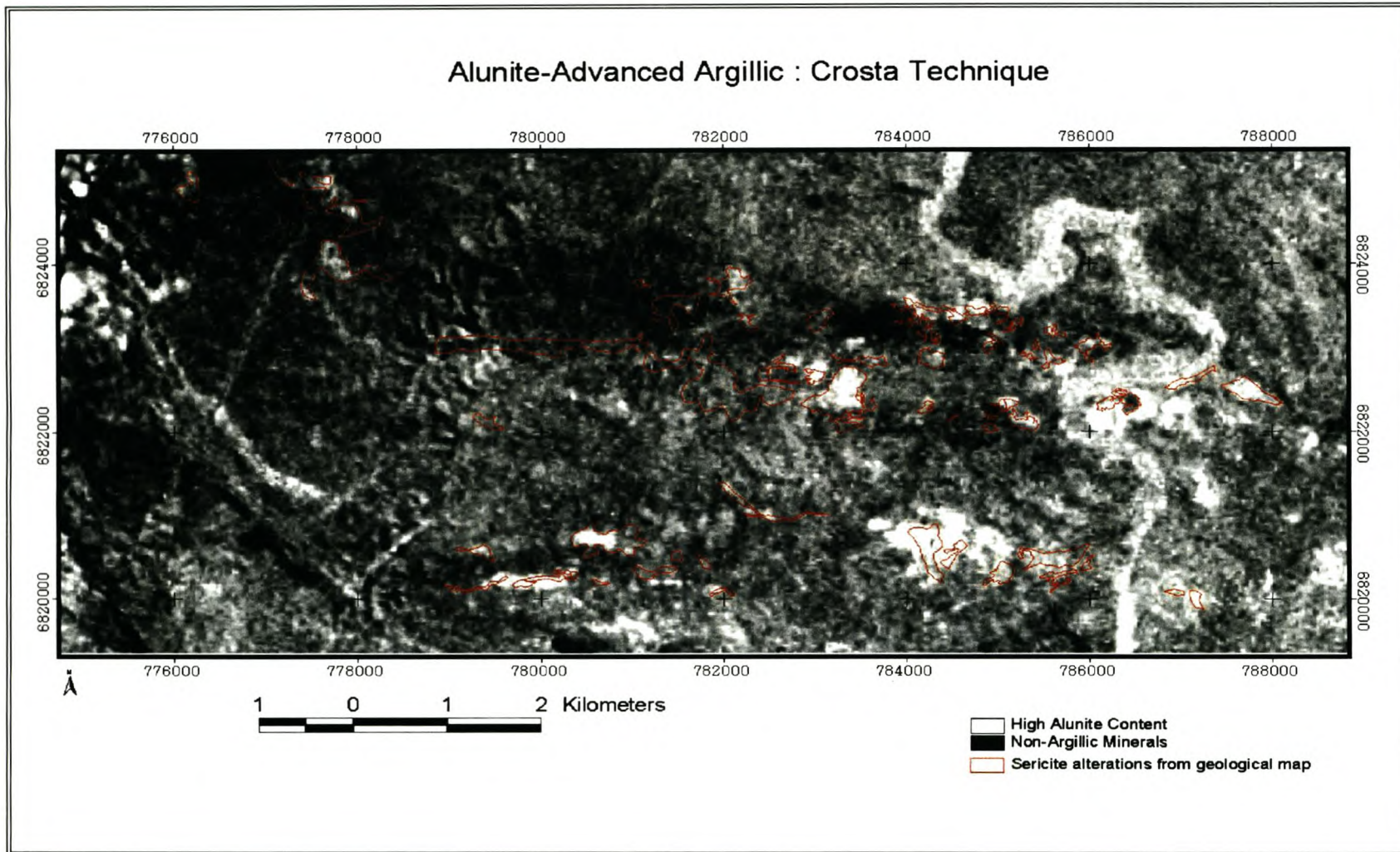


Figure 3.19: Alunite: Crosta Technique.

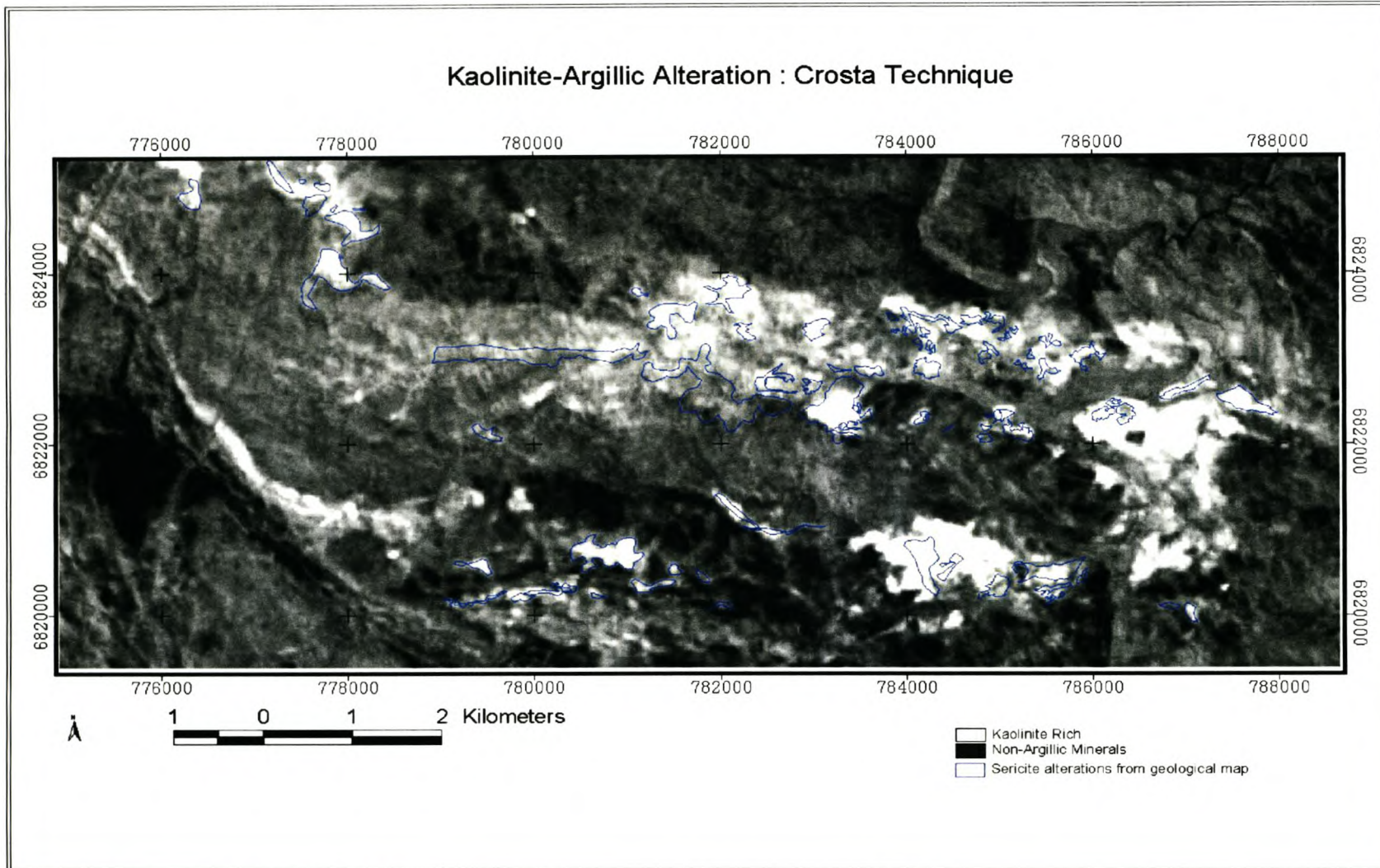


Figure 3.20: Kaolinite: Crosta Technique

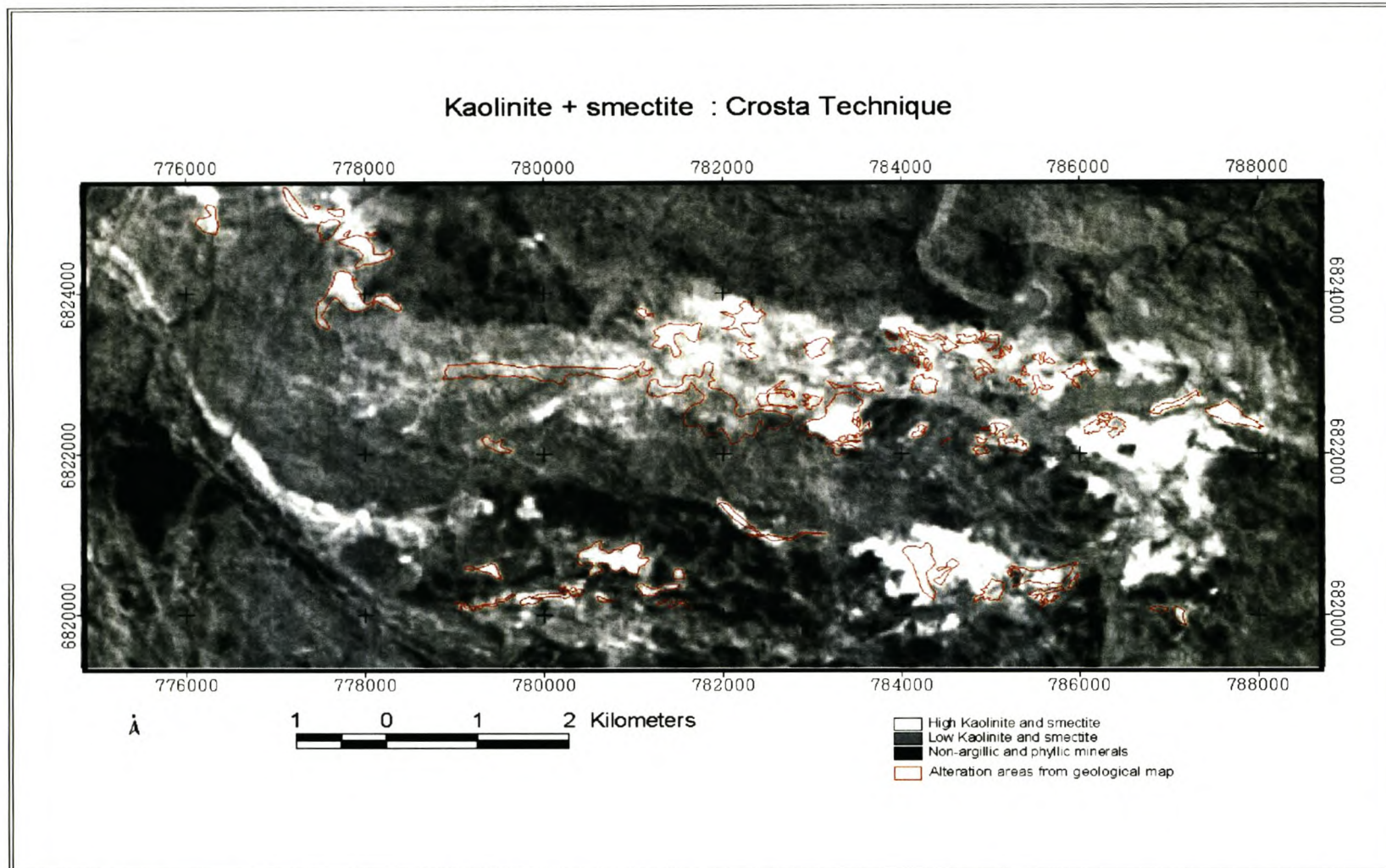


Figure 3.21: Kaolinite-smectite: Crosta Technique.

### 3.6 Spectral Linear Unmixing

The spectral Linear Unmixing method applies a suite of end member spectra to assess the spectral composition of each image cell (Smith, 2001). It is a deconvolution technique that aims at estimating the surface fractions of a number of spectral end members together, responsible for the observed mixed spectral signature of a pixel. A linear combination of spectral end members is chosen to decompose the mixed reflectance spectra of each pixel,  $R_i$ , into fractions  $f_j$  of its end members  $j$  in the  $n_i$  bands,  $Re_{ij}$ , using the equation below.

$$R_i = \sum_{j=1}^n f_j Re_{ij} + e_i \text{ and } 0 \leq \sum_{j=1}^n f_j \leq 1$$

where each of the  $n$  image end members has a residual error  $e_i$ , which is approximated by the difference between the measured end modelled digital number (DN) in band  $i$ . An equal solution is found from this equation by minimizing the residual error,  $e_i$ , in a least squares solution (van der Meer, 2002). The spectral unmixing model requires a number of spectrally pure end members to be defined, which cannot exceed the number of image bands minus one to allow a unique solution to be found that minimizes the noise or error in the model. Furthermore, constraining factors are that the fractions sum to unity and that the fractions of the individual end members vary from 0 to 100% (van der Meer, 2002).

A set of end members should describe all the spectral variability of all pixels, produce results and be of significance to the objectives of the spectral mapping. The actual selection of end members can be achieved in two ways:

1. From a spectral (laboratory or field) library;
2. From the purest pixels in the image.

#### 3.6.1 Application and selection of minerals for spectral linear unmixing

Selection of end members from the spectral libraries is generally denoted as “known”, while those from the purest pixels in the image are known as derived end-members (van der Meer, 2002). The first method is applicable to reflectance datasets and was selected for this study. The selection of mineral end members in this research is based on the selection of known end members whose existence has been proved through detailed geo-chemical and geo-physical methods in the previous exploration done by Rio Tinto and other published research on the Haib copper prospect. Mineral end members were selected from the USGS spectral libraries and automatically resampled to the ASTER central band wavelengths before the execution of the spectral linear unmixing process. Standard libraries provide the purest form of the end member, which is crucial for the success of this method. Biotite and microcline are chosen to

model the potassic zone, while muscovite and illite were selected to represent sericite in the phyllic zone due to their spectral similarities. Illite, however, will also present argillic zones. Kaolinite was selected to present the argillic zone and epidote-chlorite-calcite the phyllic zone. Pyrite spectral signature was chosen to show the amount of sulphide mineralization. The results from the spectral linear unmixing are presented below.

### 3.6.2 Results for spectral linear unmixing

The darkest pixels indicate areas which have the best match, whilst bright pixels contain materials that are not included in the end member set. To facilitate visualisation and display as false colour composites, the images are negated to ensure they occur as bright pixels. The results for spectral linear unmixing are displayed as false colour composites, which assists in establishing the spatial relationship between minerals and reduces the number of the mineral abundance images to be displayed. Argillic alteration is shown in Figure 3.22. Figure 3.23 shows the sericite alteration. The spatial association between orthoclase-sericite and calcite is shown in Figure 3.24. Figure 3.25 shows the distribution of alteration assemblages in the main mineralized zone. The potassic-phyllic-prophylic alteration zones are simulated in Figures 4.5 and 4.6.

### 3.7 Structural feature extraction

In determining the presence of hydrothermal alteration deposits, it is crucial to determine the presence of structures such as fractures, faults and shears. Fracturing and faulting occur during events of tectonism and intrusion, and hydrothermal fluids then precipitate and crystallize along the fracture zones. Fracture systems also provide conduits and plumbing systems for the hydrothermal mineralization and alteration solutions (Minnit, 1986).

The automatic detection of lineaments is essential in order to establish the spatial associations between fractures and mineralization. Fractures and shears were extracted using the Sobel edge detection gradient filter. Gradient filters are used to enhance edges in all directions (Carrere, 1989). Edges on the image are determined as abrupt changes in grey level from one pixel to another. This is achieved by filtering the image in two orthogonal directions, that is the vertical and horizontal directions, and combining the results in a vector calculation. Edge detection in this application implies detecting a line, which in this study could mean a fracture, fault or brecciation zone. The length of the composite vector gives the magnitude of the local image gradient and the direction of the local gradient is given by the angle between the composite vector and the co-ordinate axis (Carrere, 1989).

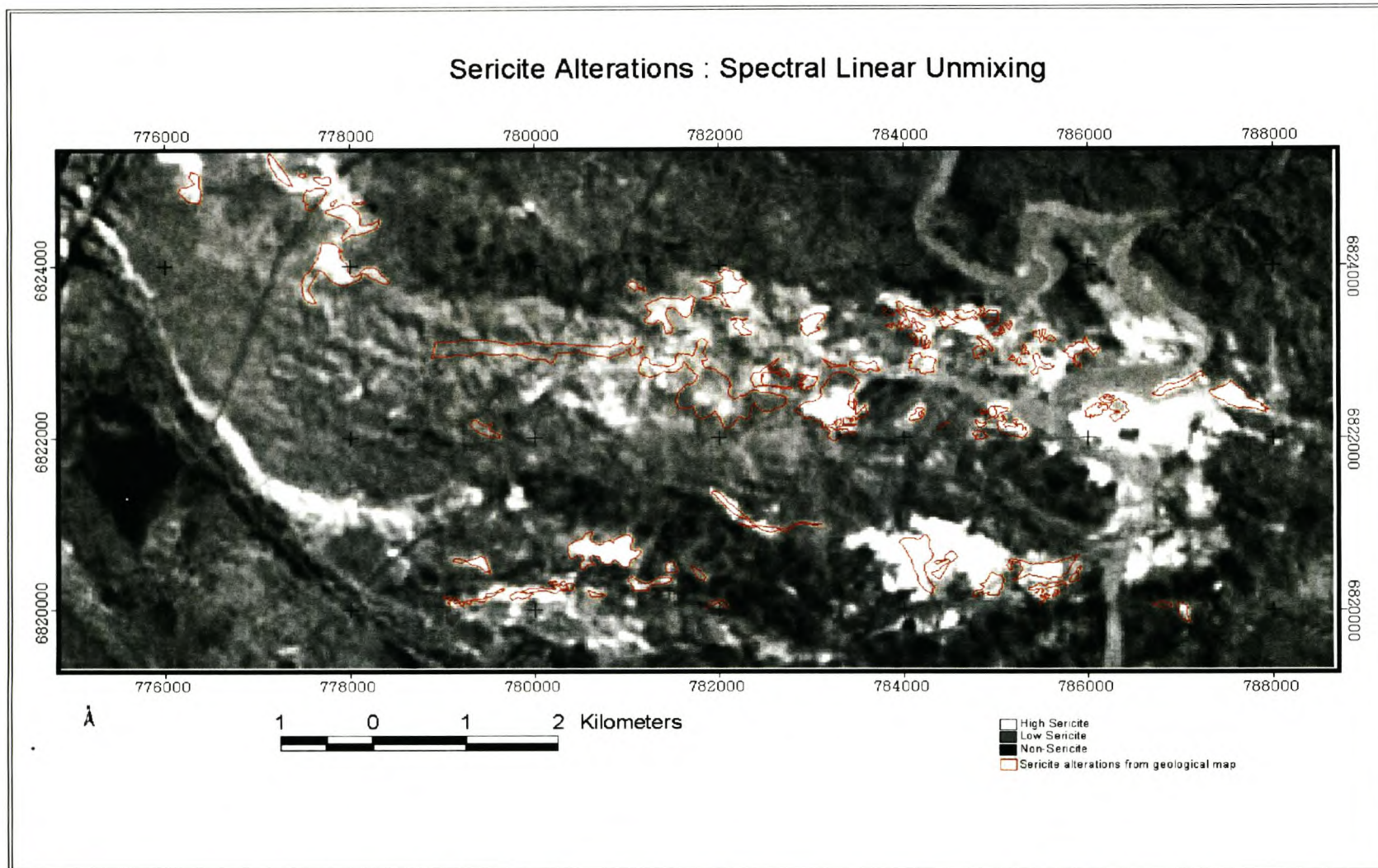


Figure 3.22: Sericite alteration: Spectral linear unmixing.

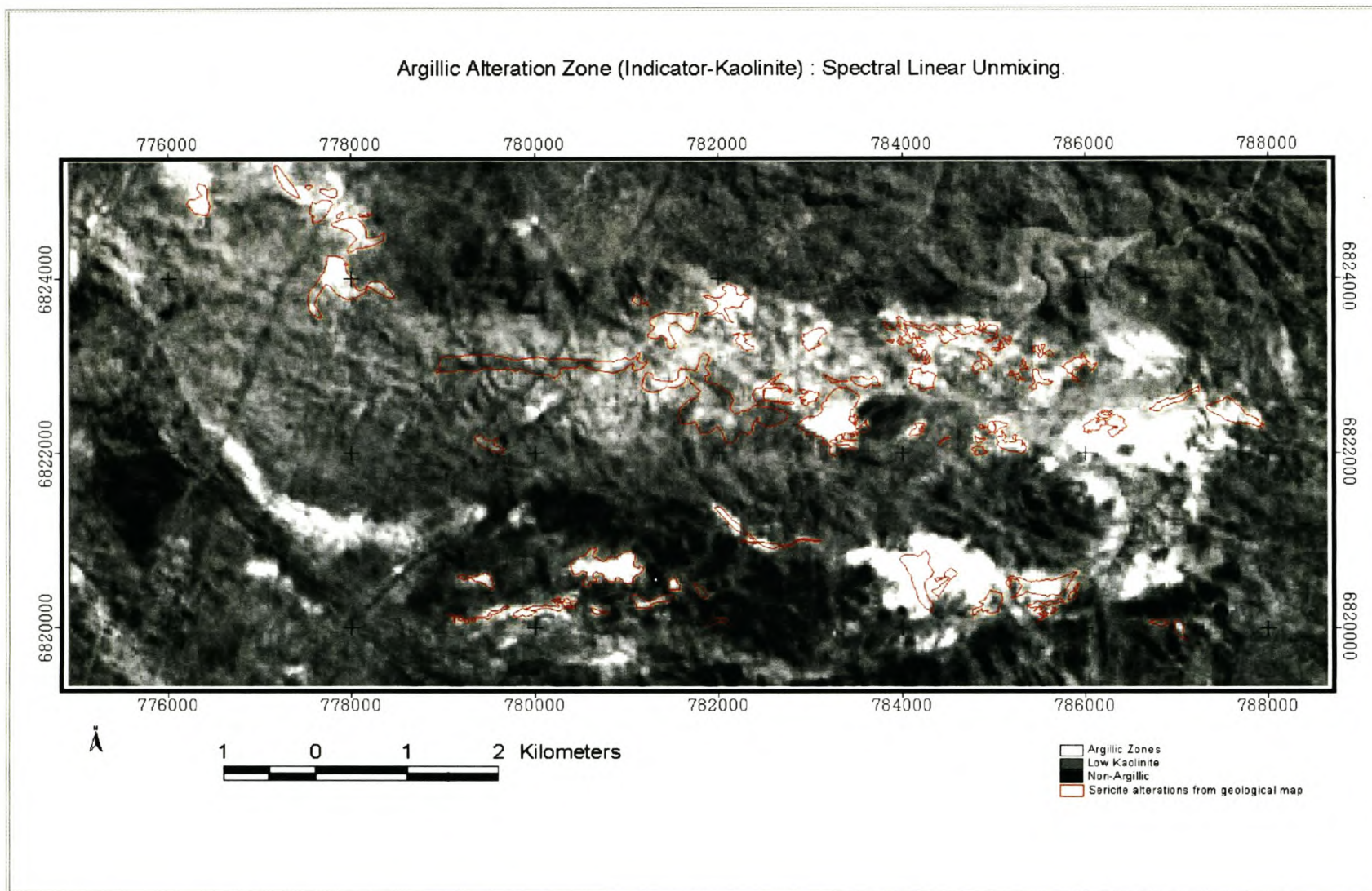


Figure 3.23: Argillic alteration (Indicator kaolinite): Spectral linear unmixing.

### 3.7 Structural feature extraction

In this study the ASTER VNIR bands were selected for Sobel filtering in order to map out the fractures and faults. The reason for selecting the VNIR bands over the SWIR and TIR is due to the higher spatial resolution of the VNIR bands, which have pixel sizes of 15 m compared to 30 m for SWIR, and 90 m for TIR. The increased spatial resolution of the VNIR bands make them suitable for this application, since smaller fractures can be detected. Surface reflectance also tends to be higher in the VNIR region, which makes subtle changes in the grey level from one pixel to the other more detectable. The results of the Sobel filtering were then subjected to a principal component transformation in order to compress all the structural information into one component. The first principal component image was selected and contains most of the structural information, since more than 90% of the information is compressed into this component. To facilitate visualisation of the extracted fractures and faults the selected component containing structural features is mapped into a colour composite with two other images, which map specific alteration zones. This scenario will enable one to visually analyse the relationship between the fracture system and hydrothermal mineralized zones.

The technique used for feature extraction was successful; the presence and amount of fracturing can be established to very high levels of detail through the application of ASTER. A visual and overlay inspection of the fractures derived from the ASTER image compared well with the structural map in terms of fracture density and orientation. The results from ASTER showed detail and refinement.

Analysis of the spatial relationships between the alteration zones and the fractures indicate that alteration zones tend to coincide with regions of high fracturing. This indication suggests and attests to the previous proposals that mineralization precipitated in the highly fractures zones. A visual inspection of the relationship between fracturing and mineralization also indicates that some regions of intense fracturing are not mineralized, which gives a suggestion that they acted as conduits along which the hydrothermal solutions moved before precipitation. A spatial association which was done by combining the mineralized zones and the extracted fractures using a RGB composite suggests the mineralization at the Haib is fracture controlled.

### **3.8 Conclusion**

All the image enhancement techniques applied this chapter were successful and showed varying levels of detail. The results correspond well to the published geological maps. Fractures extracted by Sobel filtering were in agreement with previously mapped results in terms of general orientation and intensity of fracturing. The spatial association of the extracted fractures with the regions of alteration suggests the mineralization at the Haib is fracture controlled. Chapter 4 gives a descriptive comparison of the techniques used in Chapter 3 and tests the ability of the techniques to simulate the Lowell-Guilbert Model.

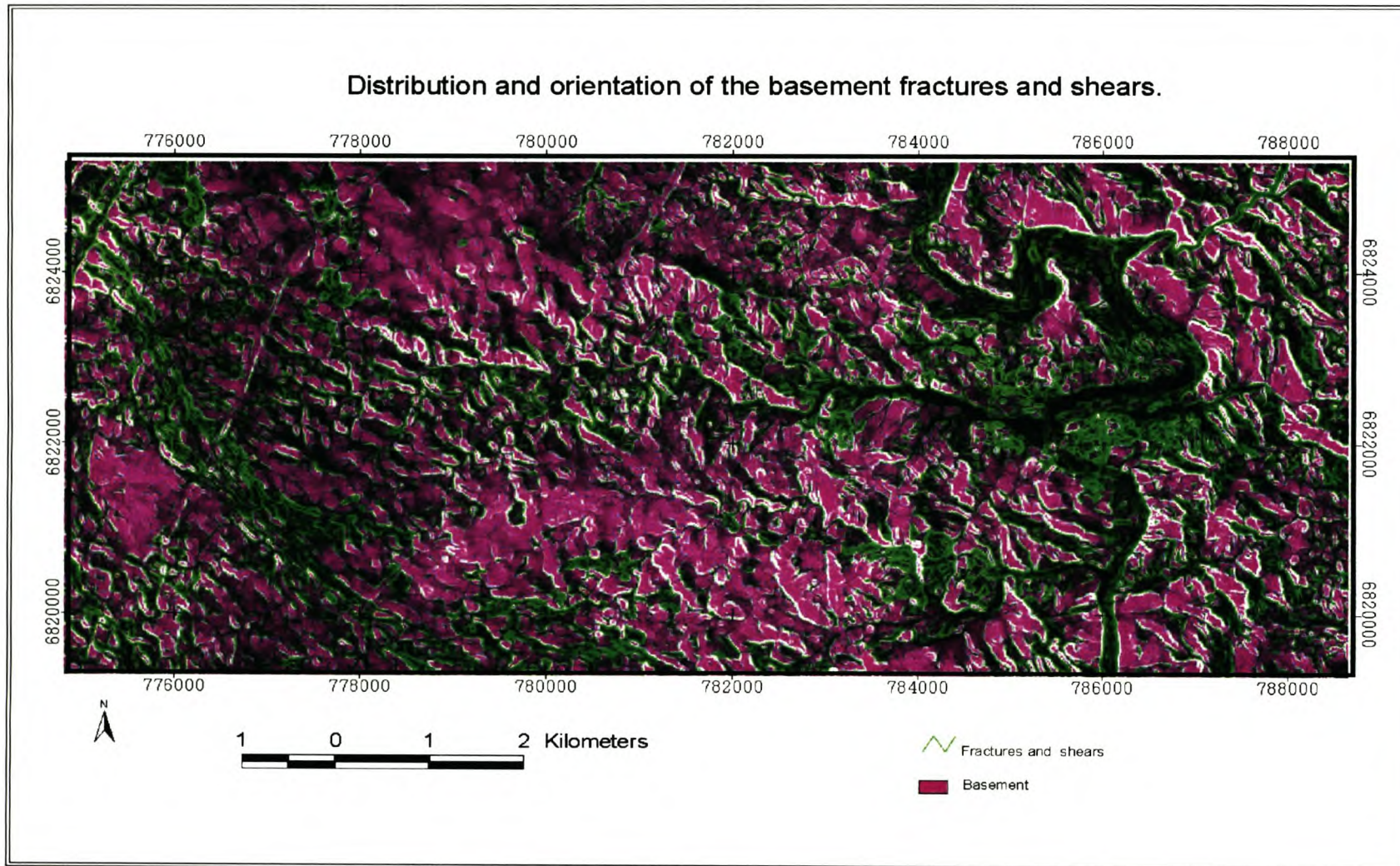


Figure 3.24: Distribution and orientation of basement fractures and shears: Extracted by Sobel Filtering.

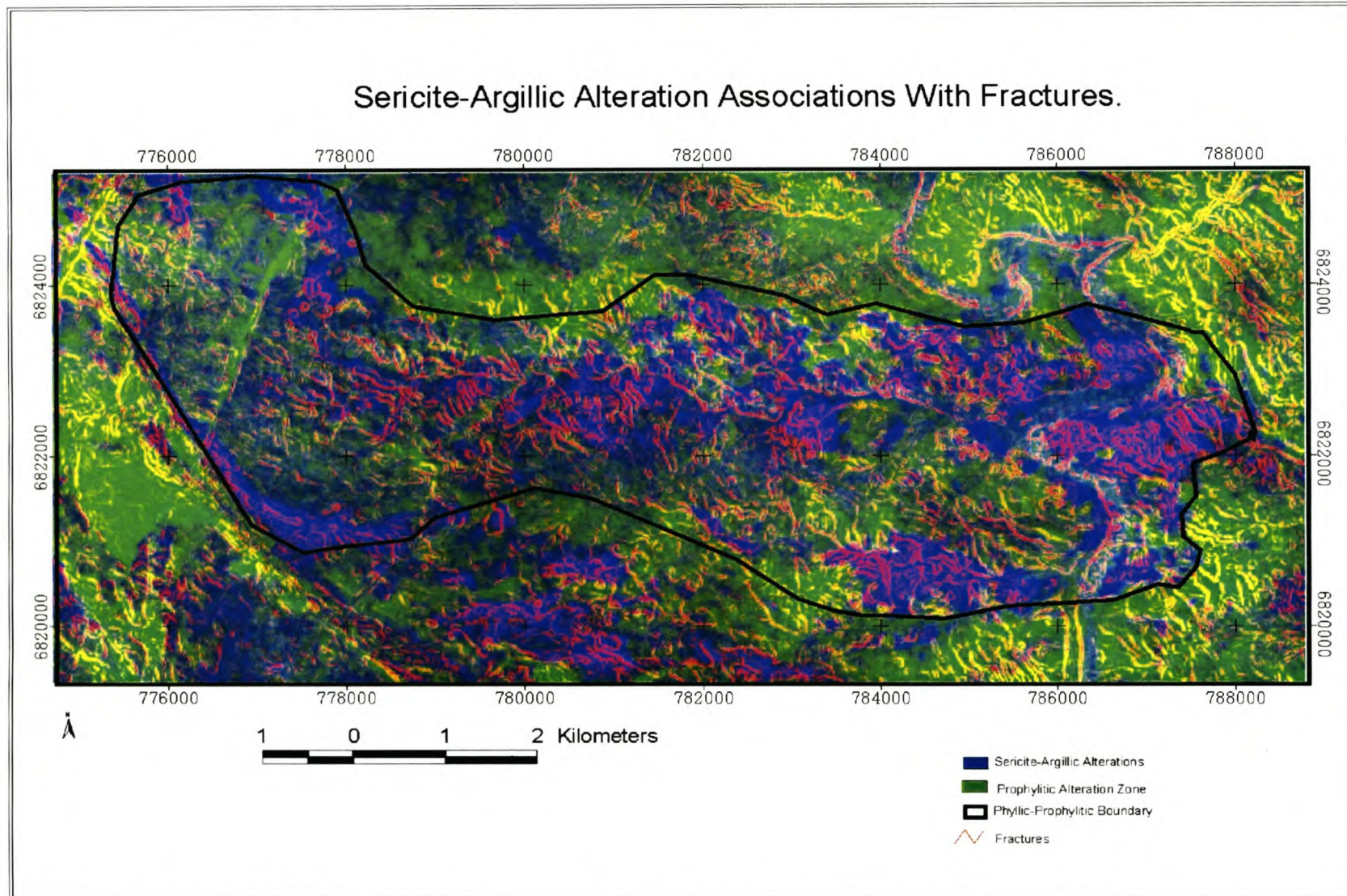


Figure 3.25: Sericite-Argillic alteration spatial association with fractures.

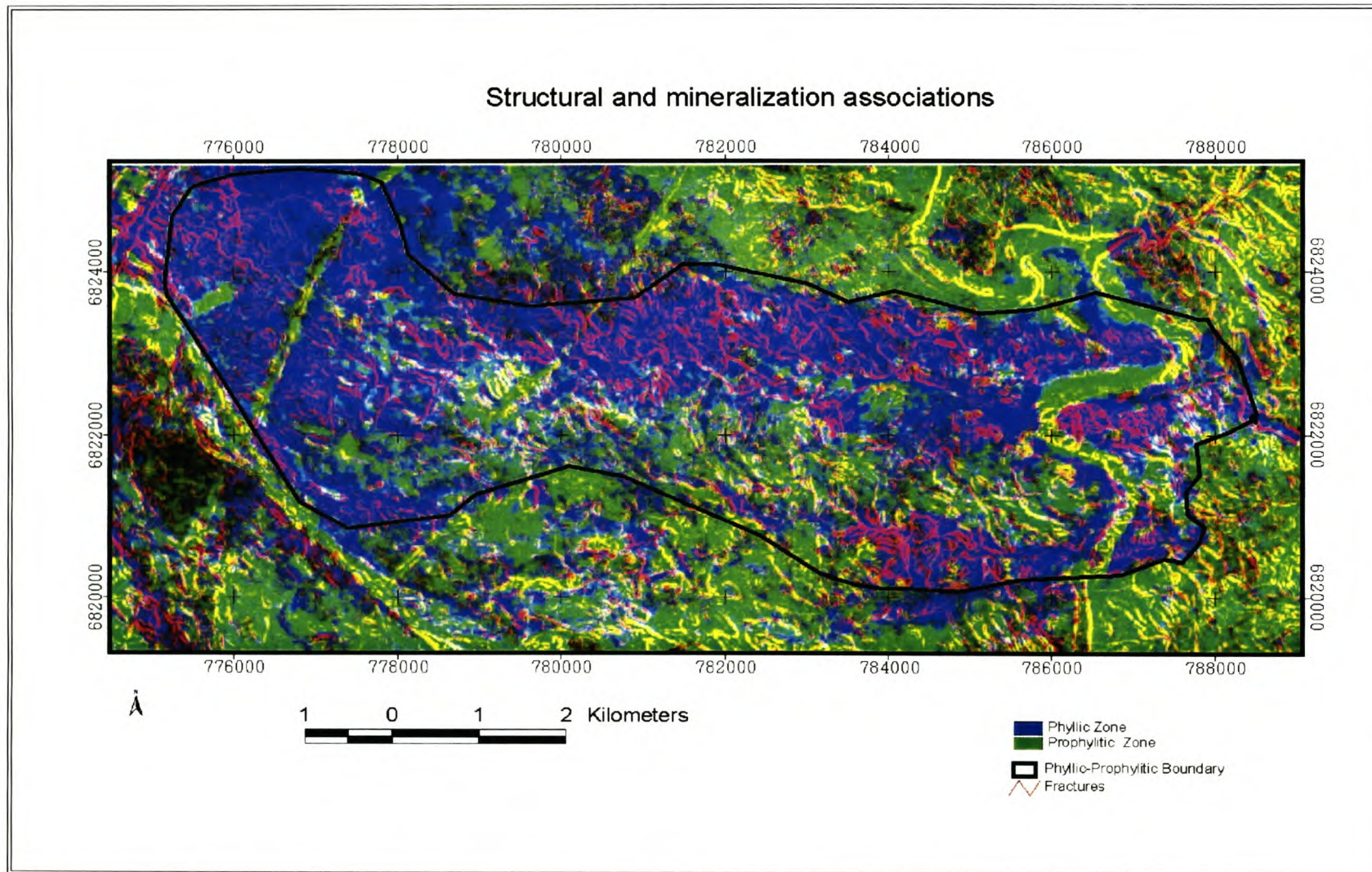


Figure 3.26: Structural and phyllic mineralization spatial association.

## **CHAPTER 4 COMPARISON OF TECHNIQUES AND DISTRIBUTION OF SIMULATED ALTERATION ZONES.**

### **4.0 Introduction**

The mapping techniques applied in this study are compared to each in terms of their success to map alteration zones. This chapter also evaluates the success achieved by the techniques in simulating the Lowel-Guilbert model. The simulated distribution of alteration assemblages in the main mineralized zone is also evaluated, followed by the spatial association of sericite zones with pyrite mineralization. The level of accuracy of the techniques is evaluated using the overlay method.

### **4.1 Comparison of techniques used to map hydrothermal alteration deposits**

All the methods applied in this research indicated they can be used successfully to map hydrothermal alteration deposits but to varying levels of detail and accuracy. The level of sophistication for each of the methods is also varied. Each of the techniques used in this research requires an understanding of the spectral features of the minerals being targeted. The level to which the spectral characteristics of the minerals are fully utilized was directly proportional to the accuracy to which specific end members can be mapped. The choice of technique to be used for mapping hydrothermal alteration deposits is therefore dependent on the level of detail required and whether one seeks to do a qualitative analysis or quantitative analysis. Standard false colour composite displays, band depth mapping and ratioing are qualitative techniques. The Log residual technique involves a qualitative analysis as a final step, although the band computation involves an advanced mathematical transformation. Spectral linear unmixing and the Crosta techniques are quantitative methods.

Standard false colour composites produced good results, which highlighted the alteration areas that were in agreement with the published geological map. RGB band combination provides an easy way to highlight areas of alteration without much tedious spectral analysis. This method requires one to know the highly reflective peaks of the targeted pixels that will stand out as bright pixels. This method, however, suppresses the diagnostic absorptive features, which occur on the image as dark cells. Standard RGB band combinations cannot separately discriminate hydroxyl bearing minerals, which are all highly reflective in band 4. For example, in the 4-6-8 composite, clays, iron oxides and calcites have a high reflective feature in band 4, which implies they are all mapped into the red band. Calcite also has another reflective feature in band 6, which implies in this band combination that calcite occurs in shades of yellow because of the mixture of red and green, and as green, which limits

the detail to which the standard colour composites can be applied. Albedo and topographic effects are a drawback in the use of standard band combinations. The initial selection of bands for use in a composite is not an easy task, since some bands tend to be correlated. Methods that assist in the selection of bands, such as the Optimum Index Factor, use band correlation techniques without emphasis on the material composition of bands, which limits their use for detail mapping. Standard RGB combinations are, however, still useful when one needs to have a general impression of the hydrothermal alteration zones before embarking on more detailed and advanced mapping techniques. The results for standard RGB band combination can also be further improved by normalization, which removes albedo and topographic effects, and makes image more comparable to results from more advanced spectral mapping techniques such as Spectral Linear Unmixing.

Relative band depth mapping uses the band depth or simply the diagnostic absorptive features of the target minerals instead of the highly reflective features used in the standard colour composite displays. The principle does not vary much for the standard colour composite technique, the focus of the method is to make use of the diagnostic absorptive features, which in the case of hydrothermal alteration mineralogy are more discriminative since the ASTER bands 5, 6 and 8 are centered on kaolinites, which have a doublet absorptive feature in band 5 and 6; the muscovite-illite-smectite group has absorption features centred in band 6, whilst band 8 is centred on the carbonate, chlorite and epidote absorptive features. Negation of bands 5, 6 and 8 will therefore show the specific minerals with absorptive features as bright pixels. Results from this method are highly successful. The distinction between the phyllic zone and prophylic zone modelled using this method compared favourably with those from the published geological maps. The use of diagnostic absorptive features, which uniquely define mineral end members in hydrothermal alteration mapping, provides an easy method for accurately mapping kaolinite group minerals, the muscovite-illite-smectite group and carbonates, chlorites and epidote. The level of specificity in terms of uniquely mapping alteration mineralogy according to alteration zones and mineral species has in general increased compared to the standard colour composite technique, which makes use of reflective features where most of the minerals tend to share the same reflective peaks yet they may be of a different species and come from a different alteration zone.

Band ratioing produced good results that accentuated the specific minerals and alteration zonations clearly. Band ratioing results indicated the applicability of this method to map out a number of minerals that constitute an alteration zone as a single unit in one ratio. The high

success level of the band ratioing method is attributed largely to the utility of both the absorptive and reflective features of the targeted minerals. Simple ratioing is useful, however more refined result is obtained by using compound ratios which uses more than two to define the spectral characteristic of the mineral more uniquely and accentuate the target mineral more, which is the goal of any ratioing. In most cases it was necessary to do band addition before ratioing, which significantly improved the results. The level of mapping refinement therefore tends to be better by using ratios as compared to standard band combinations. Ratios also provide another advantage in that they can also be subjected to a false colour composite display in order to establish the spatial relationships between alteration assemblages. The results from band ratioing can be further improved by the application of the software defoliant technique to minimize spectral interferences from other minerals. In this study the spatial relationships between alteration zones could be established to a relatively high degree of accuracy, which is not possible with standard colour band composites. Band ratioing involves a simple arithmetical procedure but produces good results, which compares favourably with the published geological maps. The effects of albedo and topography were also cancelled out by the use of ratios, which are relatively constant for all bands. Ratioing proved to be a simple way of mapping out individual alteration minerals that is more advantageous compared to the standard colour composites where making distinctions between individual minerals is difficult. Groups of mineral end members indicative of the different alteration zonations can also be mapped at a glance and produced on a single image, which is not possible with spectral pixel unmixing. Ratioing utilizes both the reflective and absorptive features, which surpasses band depth mapping, which only utilizes the absorptive features and hence produces more detailed results.

The log residual technique produced very good results that favourably compared with the alteration from the published geological map of the Haib. Although the log residual method has a more advanced mathematical algorithm compared to standard band combinations, band depth mapping and ratioing, image-processing software provide an automatic algorithm to generate a log residual image. A log residual image indicates all the clay absorption areas clearly in red, orange and pink, and the intensity of the redness indicates a proportional increase in the intensity of alteration. The log residual technique may then possibly be the most ideal of the techniques to study the variation in the intensity of alteration, which is not possible with other techniques. Log residuals are, however, not specific in discriminating the different clay types; all of the clays are mapped as red to pink. Log residual results are good for general lithological mapping and can be calibrated with a standard published geological

map. Log residual results also indicate that topographic effects and albedo were cancelled out, which is usually present in RGB band composites.

Feature-orientated principal component analysis (Crosta techniques) provides a statistical treatment of the selected image bands. Results from the Crosta technique indicate a very high level of accuracy, which compares favourably with published geological maps. The eigenvector loadings form the basis for selecting the PC containing the target mineral which occur on the image as bright pixels, but this is sometimes after negation. The selected PC highlights the target minerals and suppresses the unwanted detail as dark pixels. The level of detail obtained when mapping individual mineral end members is very high and deliberately eliminates most minerals that could have been highlighted due similar spectral responses. This application has allowed pure end members to be mapped fairly accurately. The technique uses more bands to map one target mineral than the standard RGB band composites. This refines the level to which the mineral can be mapped accurately. This statistical approach has allowed compositional information to be mapped into one band. Use of the Crosta technique removes the weakness of a qualitative analysis, where there might be variations in the manner in which individuals analyse the information as in standard RGB composites. Results from the Crosta technique compare well with more advanced methods such as spectral linear unmixing. The processing and analyses of results in terms of selecting the PC with the target mineral is relatively simple. Once the PC image has been selected, one does not need to use the eigenvector matrix again, which is necessary when one subjects all the bands to principal component transformation. The Crosta technique provides another advantage in that the selected PCs can be added together to identify zones where anomalous concentrations of both minerals occur. This can also be achieved by a pairwise PCA, where one of the PCs with the combined concentration of both mineral end members is selected. The Crosta technique is highly recommended in the mapping of hydrothermal alteration zones due to its ability to map mineral detail to a high level of accuracy, robustness and ease of use and analysis. Results obtained from the Crosta technique can act as a guide to a more detailed mineral exploration using geochemical and geophysical methods.

Spectral linear unmixing proved to be effective in mapping out alteration mineralogy with great precision. The accuracy of this method is largely attributed to the greater use of spectral features, since the entire mineral spectrum is subjected to the analysis. More bands are also involved in the analysis, which improves accuracies. Ratioing, standard colour composites, band depth mapping and the Crosta technique selects specific bands to map out the mineral

end members, which sometimes limits their ability to uniquely define individual minerals. The co-occurrence of sulphides such as pyrites with sericite has been unveiled by the application of the spectral linear unmixing, which was able to detect the presence of pyrites. Spectral linear unmixing, however, demands one to understand linear equations which are solved in order to input the right number of end members based on the numbers of bands used, which is more advanced compared to the other mapping techniques used in this research.

Sobel filtering proved to be an effective technique for structural feature extraction such as fracture systems and faults. This technique greatly assisted in establishing the spatial associations between mineralization and fracturing.

#### **4.2 The Lowell-Guilbert Model**

Significant success was achieved in trying to model the alteration zones proposed by the Lowell-Guilbert (1970) model on a regional scale. The distinction between the phyllic zone and the prophylic zone could to a large extent be distinguished clearly. A definitive potassic core boundary with the phyllic zone as proposed in the Lowell-Guilbert model could not be clearly demarcated in all the techniques which attempted to model this zone precisely in this study. This is largely attributed to the development of this alteration zone at depth, which limits its detection by satellite technology in general. The difficulty in spectral detection of the potassic zone may also be attributed to the overprinting of this zone by sericite (phyllic) alteration assemblages, which are superimposed on the earlier potassic alteration during the late phase of alteration and mineralization. The argillic facies, which strongly expressed themselves in all the techniques employed in this research, are also superimposed on the Haib porphyry stock, adjacent to the phyllic alteration zone. The argillic zone was formed by the low-temperature hydrothermal fluids during the very late stage of alteration and mineralization (Minnit, 1986). High concentrations of biotite, however, characterized the central regions of the phyllic zone, which could be attributed to the pervasive nature of biotite in both the potassic-feldspar-biotite-rich core and the phyllic zone. Orthoclase, which could possibly mark out this boundary more distinctively, however, has a relatively flat spectral signature, which limits its application in modelling of the potassic zone using multispectral remote sensing. Exposure of the potassic zone by erosion processes also account for the high concentration of biotite and microcline in the centrality of the phyllic zone, although a continuous boundary between potassic and phyllic alteration could not be delineated. The

attempt to model alteration zoning largely supports findings from the previous detailed mineral explorations in this prospect.

Band depth mapping, ratioing and the Crosta technique successfully mapped out the phyllic zone from the prophylic. Displaying the phyllic ratio, propylitic ratio and the potassic ratio in false colour composite enabled all three hydrothermal mineralized zones to be analysed in a single view and their spatial relationships determined. The use of at least two mineral end members to define a zone proved effective in marking the alteration zonations. Results from the Crosta technique need be combined into a single component as in the case of carbonates and chlorites, which occur in greater concentrations in the prophylic zones and are used as indicator end members for this zone. Display of the indicator minerals for each alteration assisted in mapping the regional distribution of alteration assemblages in terms of zones as proposed in the Lowell-Guilbert model. Figure 4.1 shows the results of the modelling the alteration zones using the Crosta technique. Figure 4.2 shows the pervasive nature of biotite, which cannot be used to effectively distinguish the potassic-feldspar-biotite rich zone from the phyllic zone. Biotite, which is shown in red, occurs throughout the image.

Band depth mapping proved to be effective in delineating the phyllic zone from the propylitic zone despite its simplicity. Figure 4.3 shows the results for band depth mapping.

Standard band colour combinations could not effectively map out the alteration mineral zonations on a regional scale due to their limited specificity in uniquely defining end member minerals used as indicators for a particular zone. Ratios proved to be an effective means of distinguishing the phyllic zone from the prophylic alteration zone, the potassic zone could not be effectively discriminated from the phyllic zone. Figure 4.4 shows the result.

Spectral linear unmixing maps single end members accurately, but its ability to define a group of minerals in a zonation at the same time is limited. Spectral linear unmixing showed superior accuracy in mapping each single end member. Figures 4.5 and 4.6 show the spectral linear unmixing results for mapping alteration zones using biotite and orthoclase respectively to map the potassic-biotite alteration zone.

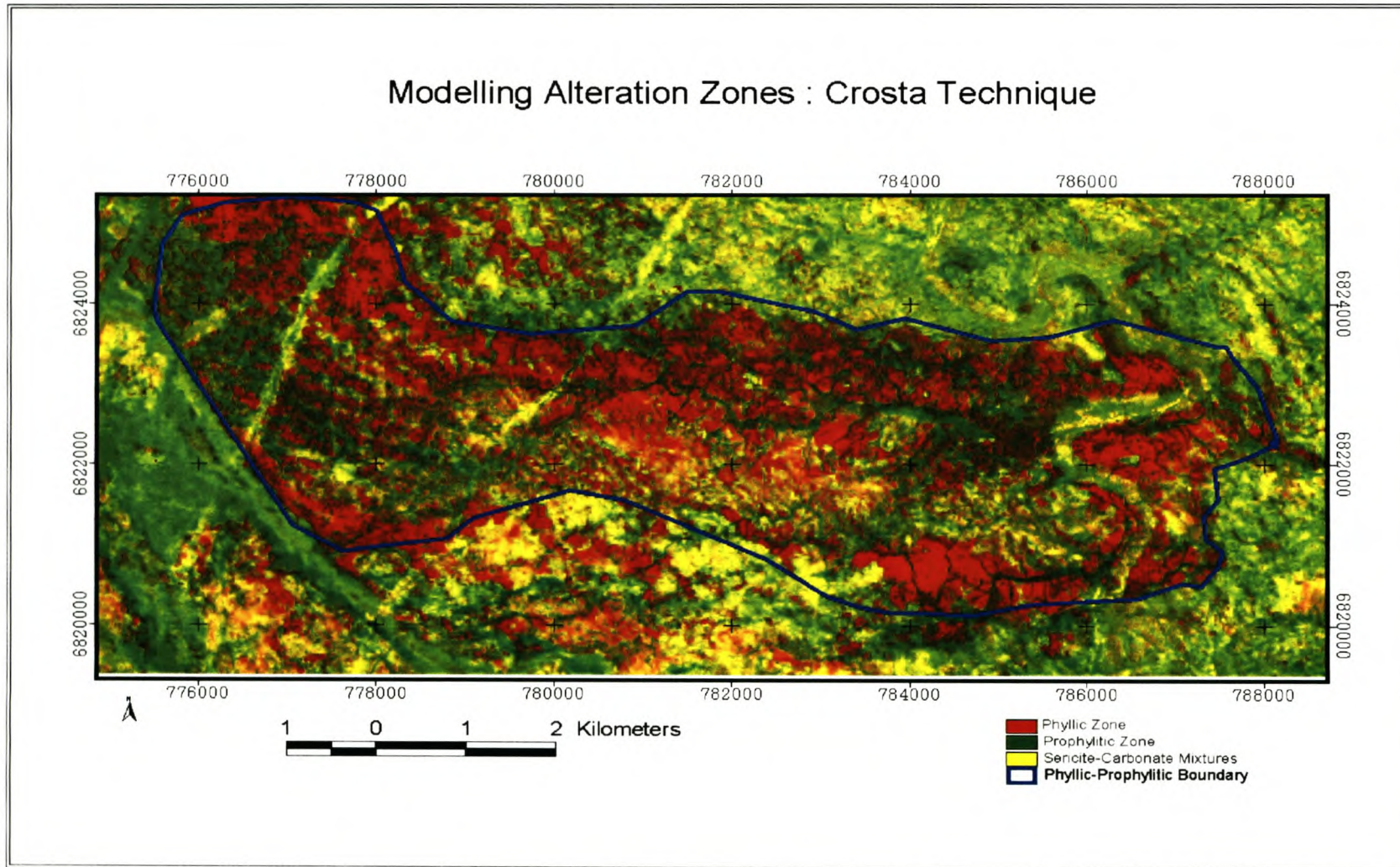


Figure 4.1: Modelling the phyllic-propylitic alteration zones: Crosta Technique.

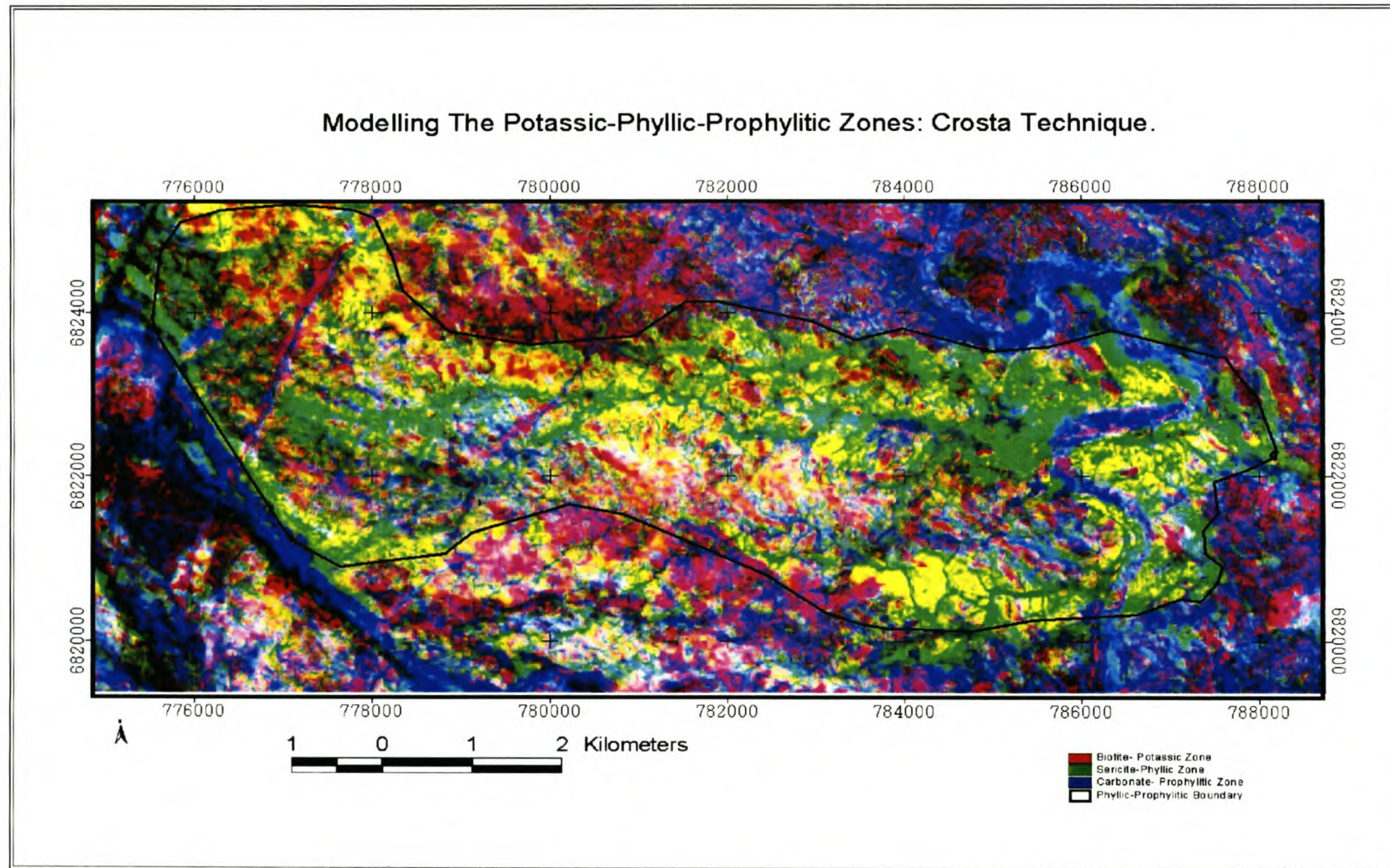


Figure 4.2: Modelling the potassic-phyllic-prophylic zones: Crosta Technique.

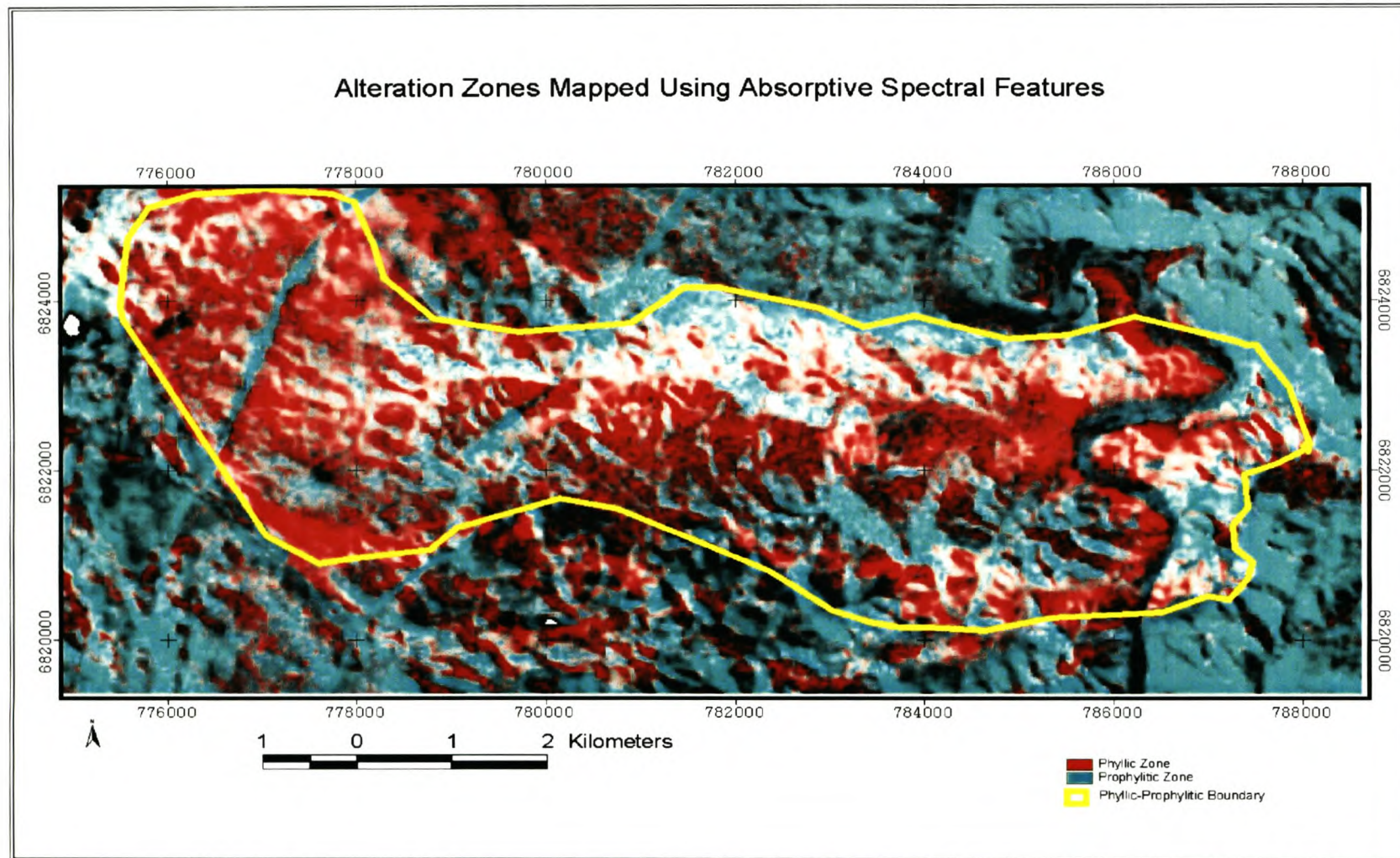


Figure 4.3 Modelling the phyllic-propylitic alteration zones: Absorptive feature mapping.

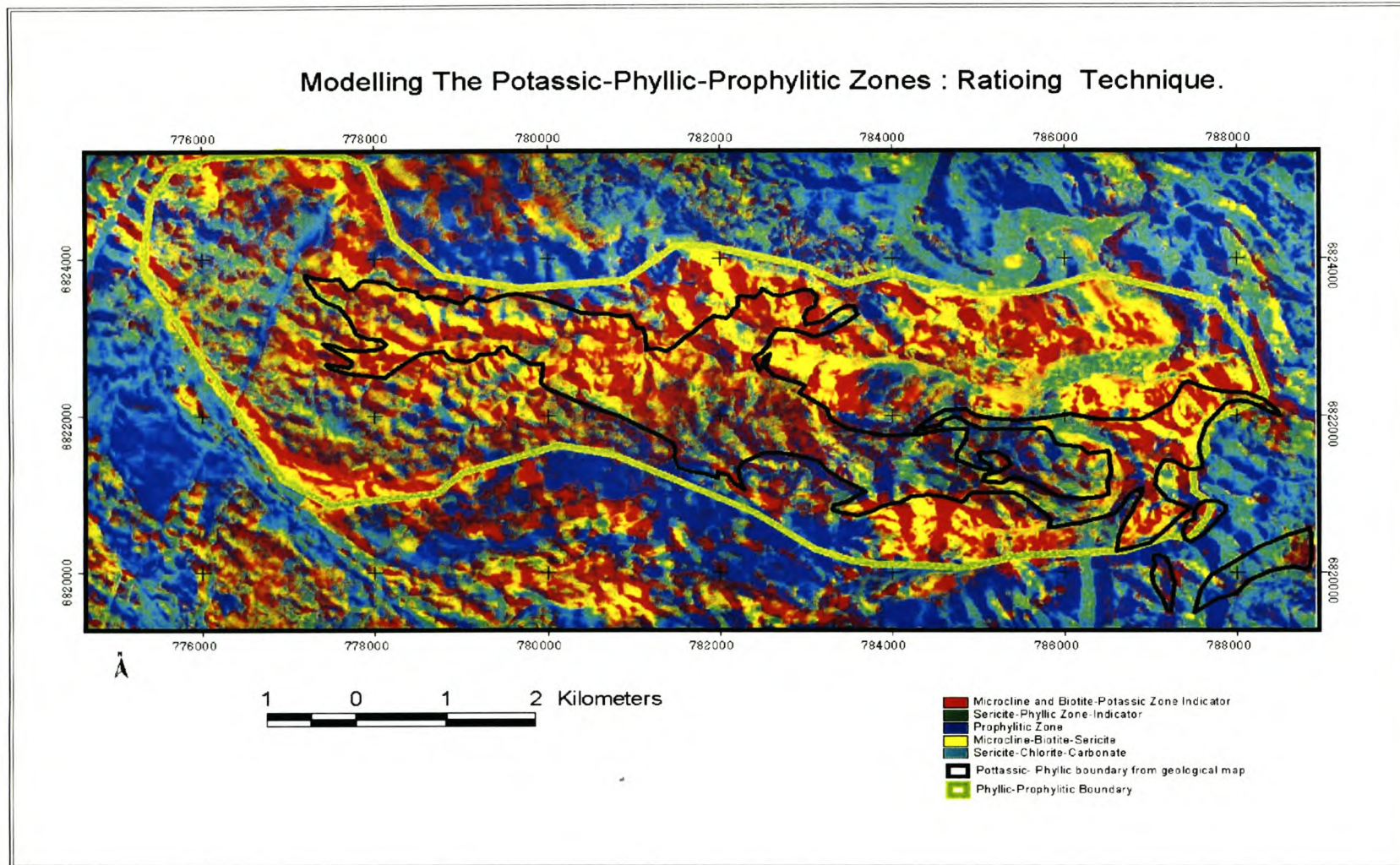


Figure 4.4: Modelling the potassic-phylic-prophylic alteration zone: Ratioing Technique.

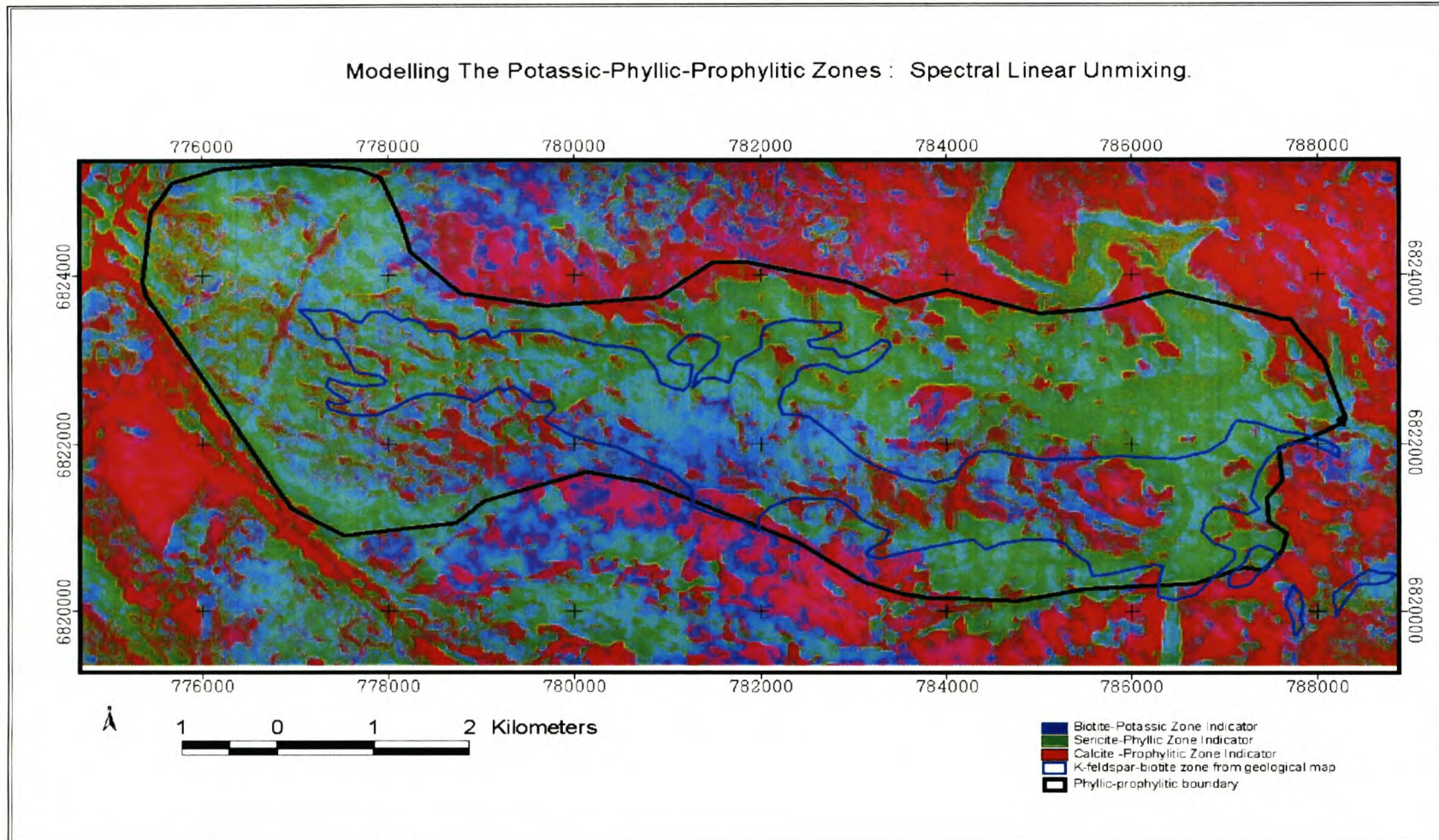


Figure 4.5: Modelling the potassic-phyllitic-prophylic zones using biotite as potassic zone indicator: Spectral Linear Unmixing.

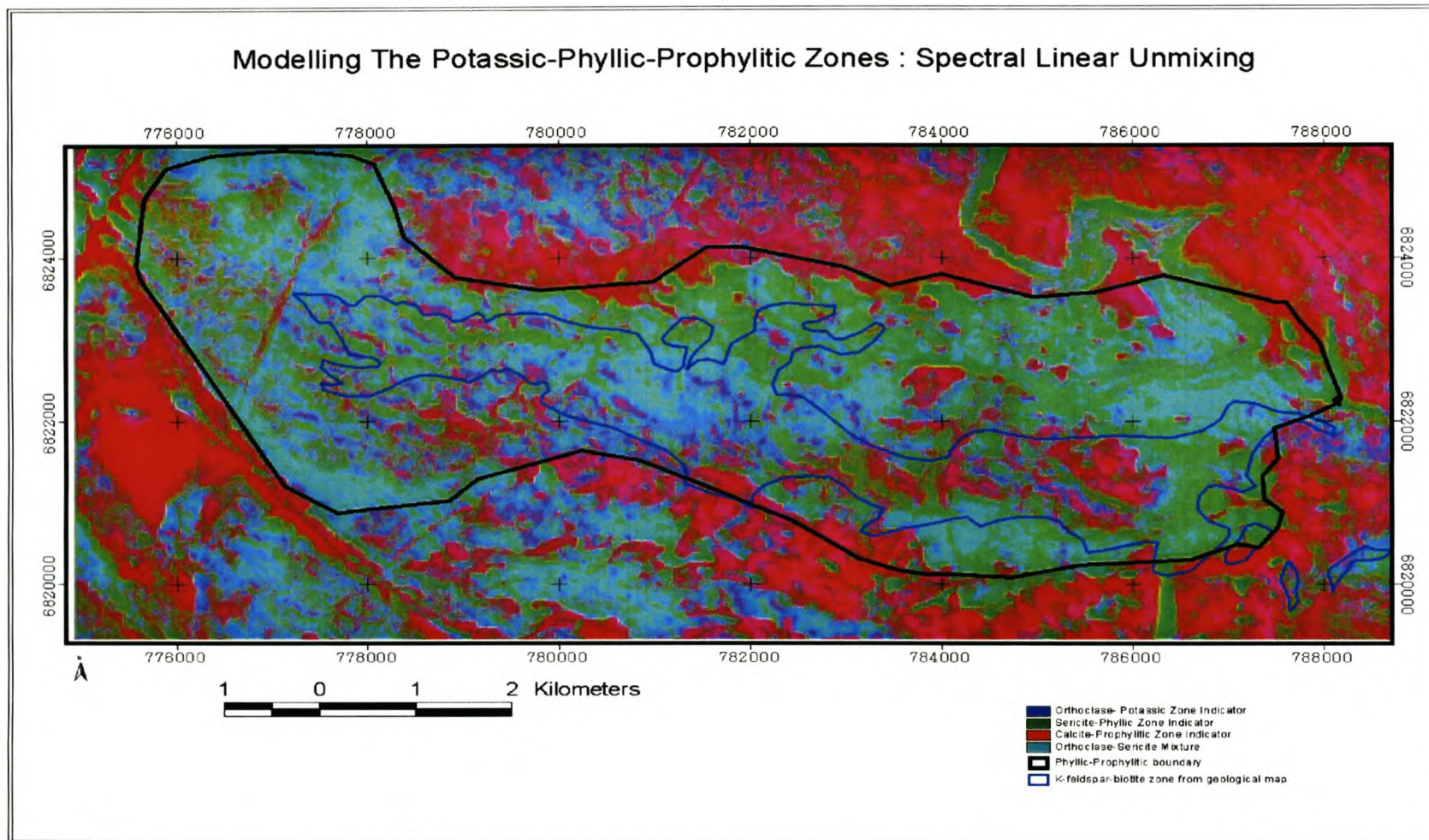


Figure 4.6: Modelling the potassic-phyllitic-prophyllitic zones using orthoclase as potassic zone indicator: Spectral Linear Unmixing.

The application of ASTER proved the presence of the phyllic and propylitic zones at the Haib copper prospect to a large extent. The potassic-phyllic boundary could not, however, be accurately captured due to the development of the potassic-feldspar-biotite rich core at depth. The biotite and microcline end members, which were used as indicator minerals for the potassic-biotite rich core, are also pervasive in the phyllic zone, which makes establishing a definitive boundary between these two zones difficult.

#### **4.3 Distribution of alteration assemblages in the main mineralized zone**

The surface spatial distribution of alteration assemblages in the vicinity of the main mineralized zone was determined by the application of the ratioing and spectral linear unmixing. The results for the ratioing and spectral linear unmixing methods are similar and largely correlate to the results from the previous exploration by Rio Tinto. Figure 4.5 shows results from the ratioing method, whilst Figure 4.6 shows the output from the spectral linear unmixing technique.

#### **4.4 Association of sericite alteration with sulphide mineralization.**

A spatial association of sericite alteration areas with pyrite mineralization indicates the co-occurrence of sericite with sulphides. The co-occurrence of sericite and pyrite was established by means of a RGB composite, where pyrite was assigned to red, sericite green and the extracted fracture system in blue. The results highlight the co-occurrence of pyrites and sericite in yellow, the yellow colour is a result of the red and green mixture from pyrite and sericite respectively. This result confirms the geological understanding of the association of sericite or clay alteration in general with sulphide mineralization, which provides the premise on why sericite or clay alterations are associated with economic mineralization.

#### **4.5 Accuracy assessments**

For the qualitative evaluation of the classification, the ASTER results were visually compared to the geological maps to verify the degree of agreement by overlaying the digitized altered zone from the geological map. The results indicate a high degree of spatial intersection and to a large extent indicate a high level of accuracy. This method of assessing accuracy is based on line intersect sampling, which estimates the length of cover class boundaries on a map that coincide with the true boundaries of the cover classes on the ground. A ratio of coincident boundary to total boundary is proposed as a measure of mapping accuracy and this ratio is called the boundary error. Although this technique has been developed for vector maps, it is equally applicable to raster maps (Skidmore, 2002).

#### **4.6 Conclusion**

A comparison of the techniques used in this study indicates that each of the techniques can be applied successfully depending on the level of detail required. The accuracy of the mapping is directly proportional to the level to which the spectral characteristics of the mineral are utilized, and whether one intends to do a quantitative analysis or a qualitative analysis. Significant success was achieved in simulating the Lowell-Guilbert model on a regional scale and results largely correspond with previous detailed mineral exploration on the Haib copper prospect. The results of the generated surface distribution of alteration assemblages in the main mineralized zone correlated well with those mapped by Rio Tinto. The co-occurrence of sericite and pyrite was proved by combining pyrite, sericite and fractures in a RGB composite display. The overall conclusions in this research and recommendations are detailed in the next chapter.

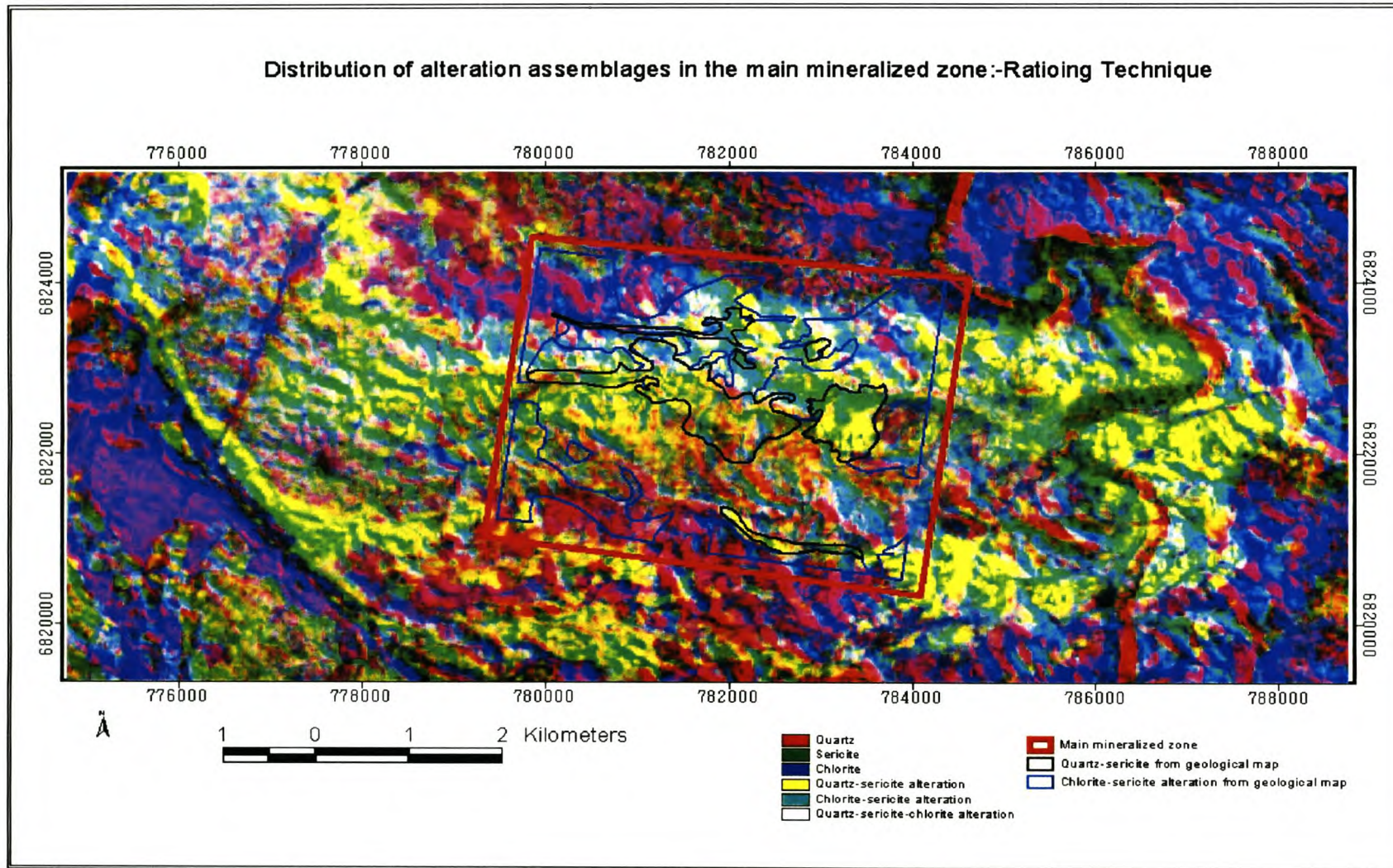


Figure 4.7: Surface distribution of alteration assemblages in the main mineralized zone: Ratioing Technique.

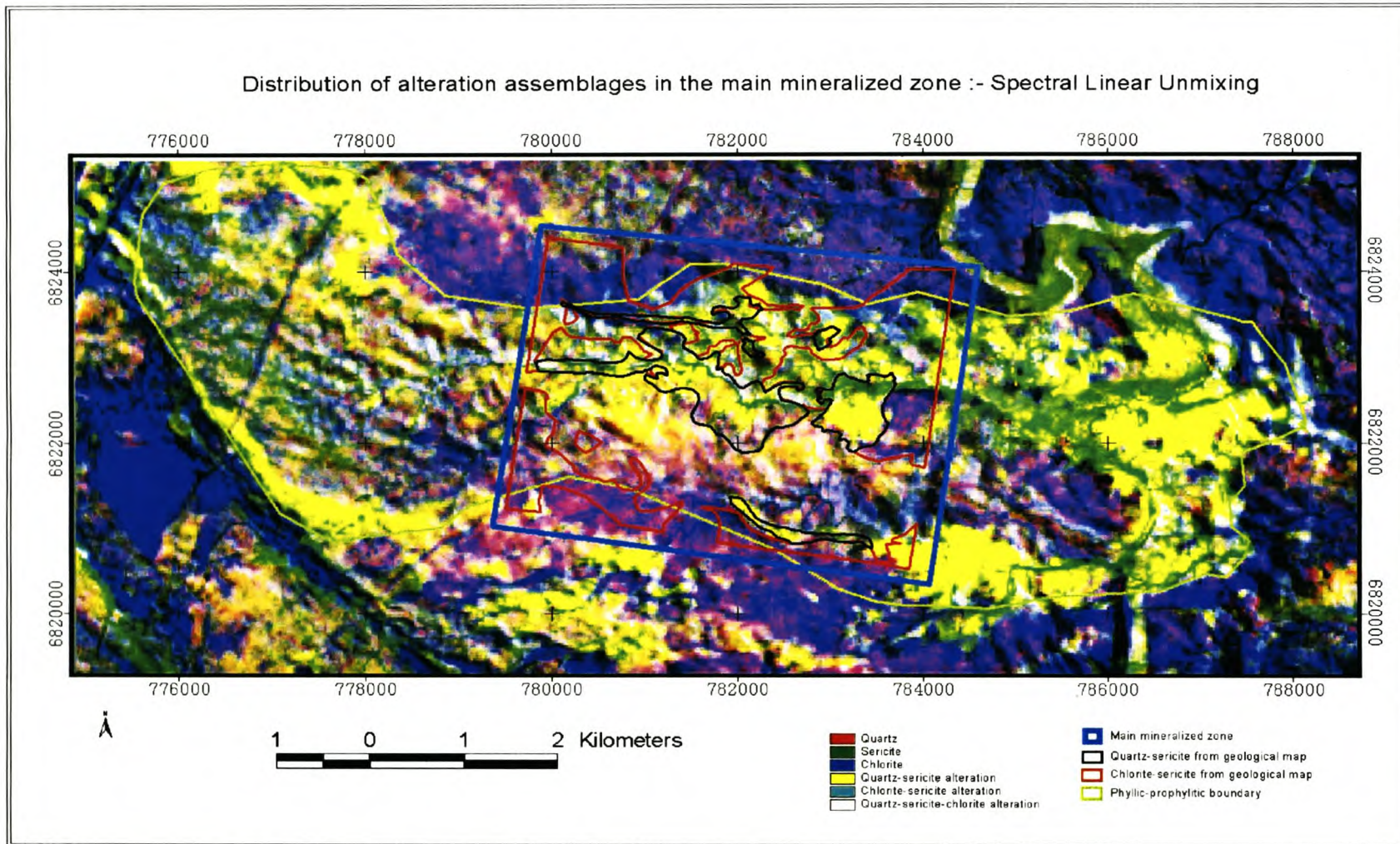


Figure 4.8: Surface distribution of alteration assemblages in the main mineralized zone: Spectral Linear Unmixing.

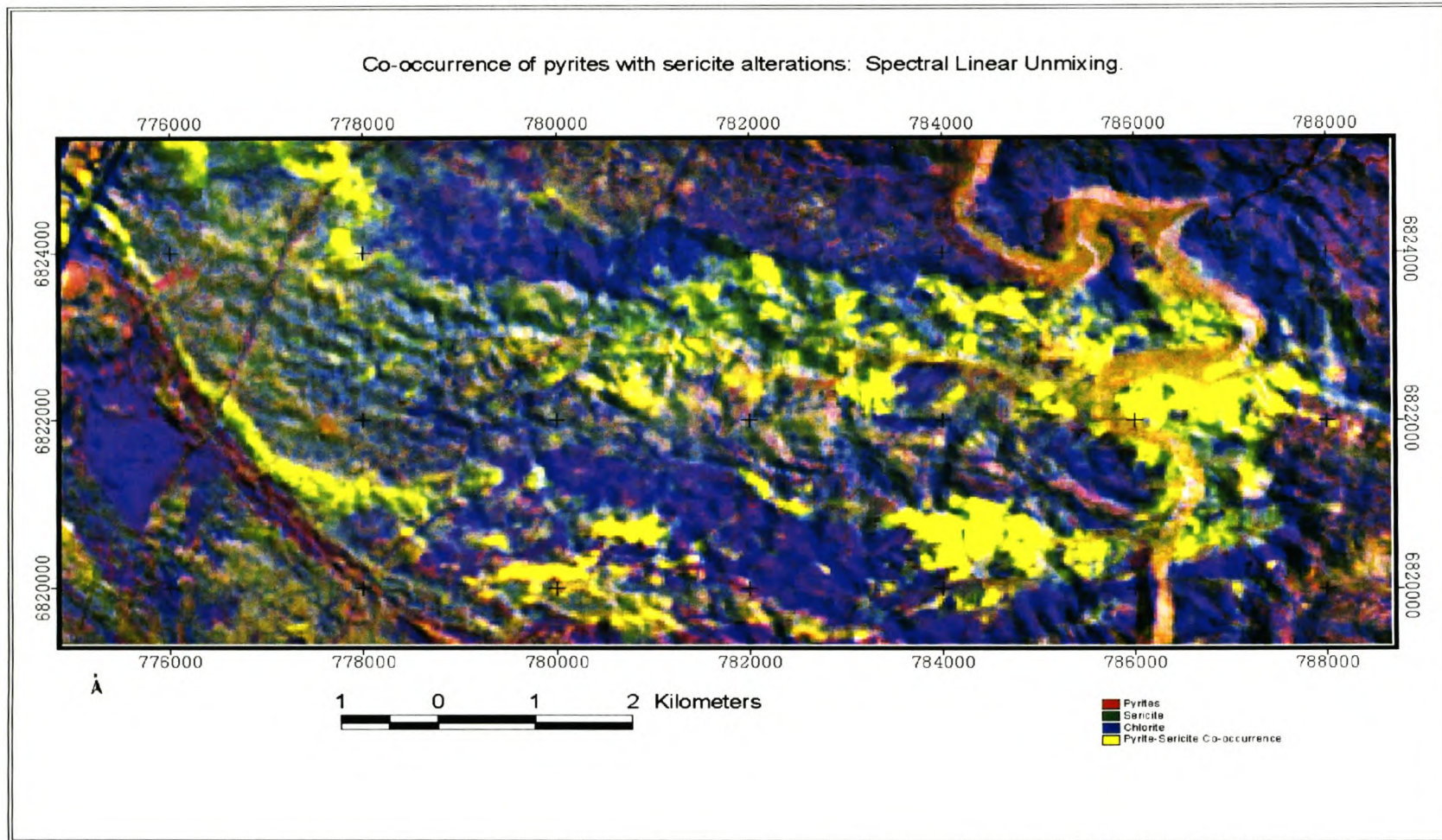


Figure 4.9 Spatial co-occurrence of pyrites with sericite alterations: Spectral Linear Unmixing.

## CHAPTER 5 CONCLUSIONS AND RECOMMENDATIONS.

### 5.0 Introduction

This chapter gives a summary of the conclusions drawn from this study and makes recommendations for future research.

### 5.1 Conclusions

The results from this study indicate that ASTER is an effective tool for reconnaissance hydrothermal alteration mapping, since the results obtained by applying various analytical techniques to the imagery are to a large extent comparable with those from published geological maps, where more detailed geochemical and geophysical surveys have been done. Results from this research indicate a great deal of information can be obtained from ASTER without any detailed prior knowledge of the geology of the area. The high level of success obtained in this research is largely attributed to ASTER's increased spectral resolutions, with bands strategically positioned on diagnostic spectral features for minerals associated with hydrothermal alteration deposits. High success rates in the techniques used for mapping the hydrothermal alterations zones may also be attributed to the ideal arid environment which characterizes the Haib copper prospect, which makes it favourable for remote sensing applications related to mineral exploration due to good surface exposure of outcrops. The software defoliant technique can be used to minimize the interferences of other minerals.

A spatial association of fractures extracted by Sobel filtering with the areas of hydrothermal alteration suggests the mineralization at the Haib copper prospect is fracture controlled. The sericite zone also coincides with areas with pyrite mineralization, which indicates the association of sericite with sulphide mineralization.

The presence of a phyllic, argillic and prophylic zone has also been established by the application of band ratioing, band depth mapping and the Crosta technique. High concentrations of biotite could be noted within the phyllic zone, which suggests the presence of a potassic feldspar-biotite-rich core, but this zone could not be mapped out distinctively. Previous detailed mineral exploration by Rio Tinto indicates the lack of a definitive potassic-biotite core on the surface, as suggested by the Lowell-Guilbert model, which limits its detection by satellite technology in general. The boundaries between the phyllic zone and prophylic zone could be determined by ASTER through the application of ratioing, Crosta and spectral linear unmixing techniques, which attempted to model out the alteration zones.

A comparison of the different techniques for mapping hydrothermal alteration applied in this study indicate that the choice of method should be based mainly on the level of detail required. If mapping of specific mineral end members is the goal, then band ratioing, the Crosta technique and spectral linear pixel unmixing are more appropriate for this application. The use of standard band combinations is ideal for less detailed mineral mapping purposes and to give a general overview of possible mineral composition, since this method of mineral detection is subjected to a lot of spectral responses from other materials. Diagnostic absorptive features proved to be useful in uniquely differentiating specific mineral species related to alteration mineralogy. The intensity of alteration within a zone could be analysed with the use of log residuals, which are non-specific in terms of differentiation of the different clay minerals. The colour variations in log residuals make it suitable for general lithological mapping and the results could be calibrated against a standard.

The spatial resolution of 30 m for ASTER in the SWIR region results in a mixed pixel effect, which makes distinguishing end member minerals difficult. ASTER was also not able to distinguish certain groups of minerals such the muscovite-illite-smectite group and the kaolinite group.

The results from the Crosta technique, band ratioing and pixel unmixing indicate that these methods provide a potential means of refining and updating the existing geological maps of the area and could also be used as guide maps in more detailed mineral exploration.

## **5.2 Recommendations**

This reconnaissance study proves the ability of ASTER to provide a rapid and efficient method for mapping hydrothermal alteration mineralogy.

The results from this study suggest a significant mineral potential at the Haib prospect from a remote sensing perspective, which has been supported by previous more detailed geochemical and geophysical surveys that verify the exact mineral potential of the area. It is therefore suggested that similar techniques may be applied elsewhere without detailed knowledge of the mineral deposits. The results from the study were evaluated using a visual overlay analysis, a statistical evaluation to quantify the accuracy of the mapping could not be done due to restrictions in the length of the thesis. It is therefore suggested that future studies should mathematically evaluate the accuracies achieved in such a study using predictive models such

as the weights-of-evidence method. Future research should focus on developing diagnostic mixture modelling techniques that simulate the argillic-phyllitic facies transition for finding the best end member combination that can easily delineate this alteration boundary. Developments in computer analysis of spatial features should lead to refinements in procedures for geological mapping that require less human intervention. More research should focus on automatic extraction of the enhanced altered zones, since currently one is required to delineate the altered zones by visual interpretation, which might result in inaccuracies and low work efficiency to meet the demands of geological exploration.

**REFERENCES**

- Ashley RP & Abrams MJ 1980. Alteration mapping using multispectral images-  
Cuprite Mining District, Esmeralda County, Nevada: *U.S Geological Survey  
Open-File Report 19*: 80-367.
- ASTER 2003. Advanced Spaceborne Thermal Emission and Reflection Radiometer.  
[Online]. Available: <http://asterweb.jpl.nasa.gov/instrument/band.htm>  
[11.05.2004]
- Blanchard R 1968. Interpretation of leached outcrops: *Nevada Bureau of Mines  
Bulletin 66*:96.
- Blignault HJ 1977. Structural-metamorphic imprint on part of the Namaqua Mobile  
belt in South West Africa: *Bulletin. Precambrian Research Unit, University of  
Cape Town 23*:197.
- Blodget HW, Gunther FJ & Podwysoki MH 1978. Discrimination of rock classes  
and alteration products of Southwestern Saudi Arabia with computer-enhanced  
Landsat data: *U.S. National Aeronautic and Space Administration Technical  
Paper 1327*:34.
- Carrere V 1989. Development of multiple source data processing for structural  
analysis at a regional scale. *Image processing '89, Sparks, Nevada , 23 May  
1989. American Society of Photogrammetry and Remote Sensing*: 239.
- Chavez PS, Graydon LB & Sowers LB 1982. Statistical method for selecting Landsat  
MSS ratios. *Journal of Applied Photographic Engineering 8*,1: 23-30.
- Chavez PS, Guptill SC & Howell JA 1984. Image processing techniques for Thematic  
Mapper Data. *American Society of Photogrammetry*: 728-743.

- Clark RN 1999. Spectroscopy of rocks and minerals. In Rencz AN (ed), *Remote sensing for earth sciences: Manual of remote sensing*, pp 3-58. New York: John Wiley and Sons.
- Crosta AP, De Souza CR, Filho CR, Azevedo F & Brodie C 2003. Target key alteration minerals in epithermal deposits Patagonia, Argentinian, using ASTER imagery and Principal Component Analysis. *International Journal of Remote Sensing* 24, 21:4233-4240.
- Crosta AP & Rabelo A 1993. Assessing Landsat TM for hydrothermal alteration mapping in central-western Brazil. In Proceedings, 9<sup>th</sup> Thematic Conference on Geologic Remote Sensing, Pasadena, 2, pp. 1053-1061. Environmental Research Institute of Michigan, Pasadena.
- Coumoul A, Abdulhay G. & Roubichou P 1989. Results of gold exploration in the Wadi Bidah District: Shaib at Tair Prospect. *BRGM-OF-09-9*, Directorate General of Mineral Resources, Ministry of Petroleum and Mineral Resources, Jeddah, Saudi Arabia .
- Drury SA 2001. *Image interpretation in geology*. Chapman and Hall: London.
- Eiswerth BA. & Rowan LC 1993. Analyses of Landsat Thematic Mapper images of study areas located in Western Bolivia, Northern Chile, and Southern Peru. *United States Geological Survey TC-88-02-32-5: 19-44*.
- Gibson PJ & Power CH 2000. *Introduction to digital image processing and applications*. London: Routledge.
- Green AA & Craig MA 1985. Analysis of aircraft spectrometer data with logarithmic residuals. Proceedings of the Airborne Imaging Spectrometer data Analysis Workshop, April 8010, JPL Publication 85-41: 111-119.

- Griffiths PS, Curtis P A S., Fadul S E A & Scholes P D 1987. Reconnaissance geologic mapping and mineral exploration in Northern Sudan using satellite remote sensing. *Geological Journal* 22: 225-249.
- Guilbert JM. & Park CFJ 1986. *The geology of ore deposits*. New York:W.H Freeman.
- Ferrier G, White K, Griffiths G, Bryant R & Stefouli M 2001. The mapping of hydrothermal alteration zones on the island of Lesbos, Greece using an integrated remote sensing dataset. *International Journal Remote Sensing* 2001:1-16.
- Fraser SJ & Green AA 1987. A software defoliant for geological analysis of band ratios. *International Journal of Remote Sensing* 8: 525-532.
- Hook SJ, Abbott EA, Grove C, Kahle AB & Palluconi FD 1999. Use of multispectral thermal infrared data in geologic studies. In Rencz AN (ed), *Remote sensing for earth sciences: Manual of remote sensing*, pp 59-110. New York: John Wiley and Sons.
- Hunt GR 1977. Spectral signatures of particulate minerals in the visible and near infrared: *Geophysics* 42, 3: 501-513.
- Hunt GR & Ashley RP 1979. Spectra of altered rocks in the visible and near infrared: *Economic Geology* 74, 7: 1613-1629.
- Hunt GR & Salisbury JW 1970. Visible and Near-Infrared spectra of minerals and rocks: Silicate Minerals: *Modern Geology* 1,4 :283-300.
- Hunt GR & Salisbury JW & Lenhoff CJ 1971. Visible Near-Infrared spectra of minerals and rocks:IV.Sulphates and Sulphides: *Modern Geology* 3, 3:1-14.
- Jensen JR 1996. *Introductory digital image processing: A remote sensing perspective. Geographic Information Science*. NewYork: Prentice-Hall.

- Jensen JR 2000. *Remote sensing of the environment: An earth resource perspective. Geographic Information Science*. New York . Prentice-Hall.
- Kaufmann H 1988. Mineral exploration along the Aqaba-Levant structure by use of TM data: Concepts, processing and results. *International Journal of Remote Sensing* 9: 1639-1658.
- Kneeper DH & Simpson SL 1992. Geology and mineral resources of the Altiplano and Cordillera Occidental, Bolivia: *U.S. Geological Survey Bulletin* 1975:46-55.
- Kowalczyk P & Ehling M 1991. Analysis of TM images using the IHS transform and adaptive equalization. Proceedings of the Eighth Thematic Conference on geological remote sensing. Denver, Colorado, April 29-May 2, 1991: 207-214.
- Lillesand TM. & Kiefer RW 2000. *Remote sensing and image interpretation*. New York : John Wiley and Sons.
- Loughlin W 1991. Principal component analysis for alteration mapping. *Photogrammetric Engineering and Remote Sensing*. 57:1163-1169.
- Lowell JD & Guilbert JM 1970. Lateral and vertical alteration mineralization zoning in porphyry ore deposits. *Economic Geology Journal* 65:373-408.
- Lyon RJ 1987. Evaluation of AIS-2 data over hydrothermally altered granitoid rocks. Proceedings of the third AIS data analysis workshop. Jet Propulsion Laboratory Publication 87, 30:107-119.
- Ninominya Y, Matsunaga T, Yamaguchi Y & Oganian K 2000. Comparison of TIR emissivity spectra measured in situ in the laboratory, and derived from TIMS data in Cuprite, Nevada. *International Journal of Remote Sensing* 18, 7: 1571-1582.

- Mather PM 2001. *Computer processing of remotely sensed images. An introduction*. New York: John Wiley and Sons.
- Minnit RCA 1979. The geological setting of the porphyry copper mineralization in the Haib River area, South West Africa. PhD dissertation. Johannesburg: University of Witwatersrand, Department of Geology.
- Minnit RCA 1986. Porphyry copper molybdenum mineralization at Haib river South West Africa/Namibia. In Anhaeusser CR (ed), *Mineral deposits of Southern Africa II*, pp1567-1585 .Geological Society of South Africa.
- Miyatake S 2002. *Regional lineament analysis and alteration mineral mapping for intrusive-related copper exploration in the Myanmar Central volcanic belt*, Metal Mining Agency of Japan.
- Mustard JF & Sunshine JM 1999. Spectral analysis for earth science: Investigations using remote sensing data. In Rencz AN (ed), *Remote sensing for earth sciences: Manual of remote sensing*, pp 251-306. New York: John Wiley and Sons.
- Peters PC 1978. *Exploration and mining geology*. New York: John Wiley and Sons.
- Podwysocki MH & Segal DB 1980. Preliminary digital classification of limonitic rocks, *Frisco 15-minute quadrangle, Utah: U.S. Geological Survey Open-File Report 80:19*.
- Podwysocki MH, Segal DB & Abrams MJ 1982. Use of multispectral scanner images for assessment of hydrothermal alteration in the Marysvale, Utah, Mining Area: *U.S. Geological Survey Open File Report 82, 675:29*.
- Ramadan TM, Abdelsalam MG. & Stern RJ 2001. Mapping gold-bearing massive sulfide deposits in the neoproterozoic allaqi suture, Southeast Egypt with Landsat TM and SIR-C/X-SAR Images. *Photogrammetric Engineering and Remote Sensing* 67, 4: 491-497.

- Reid DL 1977. Geochemistry of Precambrian igneous rocks in the lower Orange River region. *Bulletin. Precambrian Research Unit, University of Cape Town*. 22: 397.
- Richards PB, Robinove CJ, Wiesnet DR, Salomonson VV & Maxwell MS 1983. Recommended satellite imagery capabilities for disaster management: in Proceedings of the Meeting of the International Astronautical Federation, Paris, France, September 1982, Paper 1AF-82-93.
- Rockwell B & Campos-Marquetti R 1989. Quantitative lithologic mapping in spectral ratio feature space: Volcanic, sedimentary, and metamorphic terrains. Paper presented at the 7th Thematic Conference on Remote Sensing for Exploration Geology, Calgary, Alberta, Canada, October 2-6, 1989. na:na
- Rowan LC, Hook SJ, Abrams MJ & Mars JC 2003. Mapping hydrothermal altered rocks at Cuprite, Nevada, using the Advanced Spaceborne Emission and Reflection Radiometer ( ASTER), a new satellite-imaging system: *Economic Geology Journal* 98: 1019-1027.
- Rowan LC & Kahle AB 1982. Evaluation of 0.46- to 2.36 $\mu$ m Multispectral Scanner images of the East Tintic Mining District, Utah, For mapping hydrothermally altered rocks: *Economic Geology Journal* 77, 2 :441-452.
- Rowan LC & Mars JC 2001. Initial lithologic mapping results using Advanced Spaceborne Thermal Emission and Reflection Radiometer (ASTER) Data, *EOS, Transactions, American Geophysical Union, Spring Supplement*, Abstract U31A-05.
- Rowan LC, Wetlaufer PH & Goetz AFH 1974. Discrimination of rock types and detection of hydrothermally altered areas in South-Central Nevada by the computer enhanced ERTS images: *U.S. Geological Survey Professional Paper* 883:35.

- Sabine C 1999. Remote sensing strategies for mineral exploration. In Rencz AN (ed), *Remote sensing for earth sciences: Manual of remote sensing*, pp 375-447. New York: John Wiley and Sons.
- Sabins FF 1997. *Remote Sensing: Principles and Interpretation*. New York. W.H. Freeman and Company.
- Sabins FF 1999. Remote sensing for mineral exploration. *Ore Geology Reviews* 14: 157-183.
- Shibata Y 2002. Application of ASTER data to mineral exploration for Cyprus-Type massive sulphide deposits of Oman ophiolite, *ASTER Science Project Report*.
- Skidmore AK 2002. Accuracy assessment for spatial information. In Stein A, van der Meer F & Gorten B (eds) *Spatial statistics for remote sensing*, pp197-209. Dordrecht: Kluwer Academic Publishers .
- Smith RB 2001. Hyperspectral imaging. Getting started with TNT Mips software. Lincoln: Microimages Plc.
- Soha JM & Schwartz AA 1978. Multispectral histogram normalization contrast enhancement: *Proceedings of the 5<sup>th</sup> Canadian symposium on remote sensing, Victoria, British Columbia*: 86-93.
- Starling T 2003. Alteration overview. *Geological Report*. University of Leeds.
- Tangestani MH & Moore F 2000. Iron oxide and hydroxyl enhancement using the Crosta Method: A case study from the Zagros Belt, Fars Province, Iran. *Journal of Applied Geosciences* 2: 140-145.
- van der Meer F 2002. Image classification through spectral unmixing. In Stein A, van der Meer F & Gorten B (eds) *Spatial statistics for remote sensing*, pp251-306. Dordrecht: Kluwer Academic Publishers .

Yamaguchi Y, Kahle AB, Tsu H, Fujisada H, Sato I, Kudoh M, Watanabe H, Kato M. & Pniel M 2001. ASTER instrument and data product overview. *EOS, Transactions, American Geophysical Union, Spring Meeting Supplement, Abstract U31A-01*, 82(20).